Università Campus Bio-Medico di Roma
School of Engineering

PhD Course in Biomedical Engineering
(XXIII - 2008/2010)

Biomechatronic design of wearable and operational robots for rehabilitation and assistive applications

Fabrizio Sergi

Coordinator
Prof. Giulio Iannello

Supervisor
Prof. Eugenio Guglielmelli

Co-Supervisor
Dr. Dino Accoto

March 2011

Biomechatronic design of wearable and operational robots for rehabilitation and assistive applications

A thesis presented by
Fabrizio Sergi
in partial fulfillment of the requirements for the degree of
Doctor of Philosophy
in Biomedical Engineering

Università Campus Bio-Medico di Roma
School of Engineering

Coordinator
Prof. Giulio Iannello

Supervisor
Prof. Eugenio Guglielmelli

Co-Supervisor
Dr. Dino Accoto

March 2011

Abstract

The development of efficient robotic systems for rehabilitation and assistive purposes requires the synergistic deployment of advanced solutions involving multiple aspects, such as the design of the kinematic structure, of the actuation system and a detailed understanding of the biological basis underlying recovery from neurological injury.

This thesis investigates the application of biomechatronic design methods in two complimentary applications, namely the design of wearable robotic orthoses for gait assistance and the design of an operational robotic device for neurorehabilitation of the upper limbs.

In the context of wearable robotic orthoses for gait assistance, an analysis of recent literature allowed to formulate a research hypothesis, which states that the choice of a non-anthropomorphic kinematic solutions for wearable robots can provide improvements, both from ergonomics and dynamical standpoints. However, the process of kinematic synthesis of non-anthropomorphic wearable robots can be too complex to be solved uniquely by relying on conventional synthesis methods, due to the large number of open design parameters.

In order to address this design problem, this thesis describes a novel methodology, which allows to systematically explore the wide set of solutions provided by non-anthropomorphic wearable robotic orthoses and includes novel tests, specifically devised to solve the problem of enumeration of kinematic structures applied to a specified set of human

segments and joints. Preliminary results, emerging from the implementation of the described methodology for the design of a hip-knee robotic orthosis, are reported to validate the described methodology.

In the context of the design of robotic devices for neurorehabilitation of the upper limbs, the capability of a novel actuation architecture to guarantee a transparent interaction during *patient-in-charge* mode was demonstrated, based on an inverse dynamical model a Macro/Mini manipulator and on the analysis of experiments performed on 14 healthy subjects. However, many details concerning the relations between movement therapy, neural plasticity and recovery of motor function after stroke are still largely unknown: this is a recognized cause of limited efficacy of movement therapy. However, knowledge on this topic can be crucial for the design of a new generation of robotic devices for neurorehabilitation. To this aim, a preliminary study describing a novel integration of kinematic measurement technology with functional Magnetic Resonance Imaging (fMRI) to assess the neural correlates of motor recovery during robot-mediated therapy in chronic stroke is reported. This preliminary study was also functional to validate an experimental setup involving the execution of reaching movements in fMRI environments, providing a set of specifications, which were used for the preliminary design of a novel actuated fMRI-compatible robotic device.

Contents

List of Tables

List of Figures

Chapter 1

Introduction

The past twenty years observed an extension of application domains for robotics, from the originary well structured industrial environments demanding for high accuracy, power and repeatability, to human environments, demanding instead for safety and adaptability to a heterogeneous and unpredictable set of interaction modalities.

In the contemporary social context, significantly influenced by population ageing, machines for physical assistance to humans are sought to have an attractive potential to reduce fatigue and stress, increase human capabilities in terms of force, speed, and precision, and improve in general the quality of life.

Application domains asking for human augmentation and function substitution by robots include also everyday houses and offices, such as robot companions and humanoids service robots. Moreover, the increasingly widespread use of robotic devices for providing assistance or supplying physical rehabilitation therapy to impaired subjects opened the use of robots in semi-structured healthcare environments, paving the way to the future use of robots in domestic unstructured environments.

In this context, researchers worldwide are studying the social factors related to the introduction of robots in human environments and often their attention is focused on the cognitive interaction with machines. However, at an even more preliminary level, the mentioned extension of application scenarios is related to the

mechatronic design of such machines, and in particular to aspects related to the physical interaction between the human and the robotic counterparts.

The analysis of human-robot interaction from a mainly physical level is even more crucial in the case of assistive and rehabilitation robotics, where physical human-robot interaction is not only tolerated, but it is actually the design target. This implies that design choices are driven by a challenging set of design criteria.

First of all, the minimization of moving masses is a primary requisite imposed as safety measure to minimize the risk of injury due to unexpected collisions. But in such scenarios safety is not the only special concern. At a second level, the accomplishment of a motor task is always the result of a shared action between the human and the robotic counterparts. The high variability associated to human physiologic and pathologic performance imposes that robot behavior is demanded to include a high level of adaptability to human contribution. This adaptability can be introduced *intrinsically*, by employing elements with passive compliant properties either in the actuation architecture or in the possible points of contact with human operators; or *actively*, by introducing sophisticated interaction controls, which require the use of exteroceptive sensors and of high bandwidth mechatronic systems. Furthermore, especially in rehabilitation environments, the robotic system is demanded to be transparent to the users' movements, so to minimally perturb the spontaneous and correct execution of motor tasks.

These general criteria, however, can have different implications depending on the particular application field, as detailed below.

This thesis is focused the application of the above-mentioned general paradigms to two complimentary scenarios.

1.1 Thesis overview

The first application scenario and main topic of this thesis involves the design and development of wearable robots for the assistance of human gait.

Chapter 2 provides an overview and a critical analysis of the state of the art of mechatronic devices currently developed for gait assistance. On the basis of such analysis, the objectives of this thesis are defined.

Chapter 3 describes the main original contribution of this thesis: the definition of a methodology, which allows to generalize and to solve in a complete and computationally efficient way the problem of kinematic synthesis of a non anthropomorphic wearable robot for gait assistance. The methodology also includes two novel tests, specifically devised to solve the problem of enumeration of kinematic structures of wearable robots: the HR-isomorphism and the HR-degeneracy tests. The method has been implemented to derive the atlas of independent kinematic solutions, suitable for the kinematic design of a planar wearable robot for the lower limbs and used for a simulation-based co-optimization of the mechanical structure and of the controller of a wearable robot for the lower limbs.

The second part of this thesis also focuses on the biomechatronic design of human-interacting robots, but in a different application scenario, that of robot-mediated neurorehabilitation for the upper extremity.

As described below, a critical requisite peculiar to rehabilitation robots is the property of backdriveability during *patient-in-charge mode*. This additional design target poses many challenges to the mechatronic design of robotic systems for movement rehabilitation therapy.

Chapter 4 of this thesis describes the design of a planar robot, which includes a novel actuation architecture suitable for planar manipulators for movement therapy for rehabilitation after stroke.

Within this context, it is currently accepted that the main reason for the limited efficacy of existing rehabilitation therapy after stroke is related to the limited knowledge of many of the details on the relations between movement therapy, neural plasticity and recovery of motor function after stroke. This poses substantial difficulties in the definition of a "golden standard" for movement therapy and limits the amount of specifications provided by rigorous scientific facts to the design of rehabilitation robots. However, the conjunction of robotics technology and brain imaging techniques is potentially a powerful tool to systematically investigate and separate the factors influencing the process of recovery of motor function.

Chapter 5 describes a pilot study conducted to validate the design of an fMRI compatible registration device and to investigate the neural correlates of motor re-

covery through robot-mediated rehabilitation therapy after stroke. This preliminary study was also successful to validate an experimental setup involving the execution of reaching movements in fMRI environments, providing a set of specifications which guided the preliminary mechatronic design of a novel robotic manipulandum, described in the second part of the same chapter.

Chapter 2

pHRI and wearable robotic orthoses for the lower limbs

Physical Human-Robot Interaction (pHRI) is a very important attribute in the design of robots operating in human environments. This attribute becomes crucial in the case of wearable robots, which are person-oriented systems worn by human operators to extend, complement, substitute or enhance human function and capability [1]. In the design of robotic orthoses, both for human performance augmentation and for functional restoring, the most followed route has been that of designing the robot so to replicate as much as possible the kinematic structure of the adjacent, structurally intact human limbs [2], [3], [4]. Robots belonging to this class were thus named *exoskeletons*, according to the definition given in [5]: *"an active mechanical device that is essentially anthropomorphic in nature, is "worn" by an operator and fits closely to his or her body, and works in concert with the operator's movements"*. More recently, a slightly different definition was given in [6] , where exoskeletons are defined as *"wearable robots exhibiting a close cognitive and physical interaction with the human user; these are rigid robotic exoskeletal structures that typically operate alongside human limbs"*, thus eliminating the constraint for an "essentially anthropomorphic" kinematic structure.

Despite of that, in the following of this thesis the first definition provided above will be considered, also considering the Greek etymology of the term, which stands

for "outer skeleton", and consider exoskeletal robot as robot with an anthropomorphic kinematic structure. Exoskeletons are part of a more general category, that of wearable robots, which can also have some degree of non-anthropomorphism. In the design of a robotic exoskeleton, the kinematic synthesis is based on the concept of mimicking the structural component of the adjoining human segments; as such it only depends on the degree of accuracy of a biomechanical model of the human limbs and is then not a free design parameter for the designer. On the contrary, for non anthropomorphic robots the process of kinematic synthesis is open and can be exploited to achieve some design objectives.

In the following sections, an overview of the main features of the mechatronic design of existing wearable robots for the lower limbs will be provided and an analysis of the possible advantages introduced by the adoption of a non anthropomorphic kinematic structure will be done. The analysis will be based on a study of already existing literature and on the analysis of achievements in fields close to wearable robotics, such as biomechanical and robotic studies of bipedal and animal locomotion.

2.1 Mechatronic design of state-of-the-art wearable assistive robots for the lower limbs

Exoskeletons for the lower limbs are usually designed either for human performance augmentation or for providing physical assistance to impaired or weakened persons during walking.

Several different issues are considered for the mechatronic design and optimization of wearable robots for the lower limbs. They include:

- ergonomics of the physical interface with the wearer;
- amount and kind of actively assisted, passively allowed or passively-loaded (e.g. spring-loaded) Degrees of Freedom (DOFs);
- torque applied to the assisted joints to facilitate locomotion;

- power consumption of the device (this parameter is especially crucial for stand-alone exoskeletons);
- overall parameters of locomotory performance, including stability analysis, the level of anthropomorphism obtained and the reduction of metabolic expenditure.

These parameters will be considered in the description of the most relevant wearable assistive robots for the lower limbs be retrieved through an extensive literature study, which will be the basis for the formulation of the objectives of the research described in this thesis.

The developed devices were grouped into three different categories: *i) energetically autonomous exoskeletons for performance augmentation*, *ii) energetically autonomous active orthoses for gait assistance in impaired patients*, *iii) machines for Body-Weight Support Treadmill Training (BSTT)*.

2.1.1 Energetically autonomous exoskeletons for performance augmentation

The first important developments in the field of energetically autonomous exoskeletons come from the program developed under the United States Defense Advanced Research Projects Agency (DARPA) called Exoskeletons for Human Performance Augmentation (EHPA), started in 2001, with the goal to "increase the capabilities of ground soldiers beyond that of a human", in particular during load carrying operations, increasing the weight of the load that can be carried, and reducing the fatigue on the soldier during the task. Three institutions participating to the DARPA program demonstrated working prototypes: the Berkeley Exoskeleton, the Sarcos Exoskeleton and the MIT exoskeleton.

2.1.1.1 Berkeley Exoskeletons

The BLEEX exoskeleton was developed at University of California, Berkeley by the group lead by prof. Kazerooni (Berkeley Robotics and Human Engineering Laboratory). It distinguishes itself for being the first load-bearing and energetically

autonomous exoskeleton [5] [7]. It was designed following a design methodology called by the authors "design by biological analogy", which is basically explained by trying to design an anthropomorphic exoskeleton with similar limb masses and inertias to a human, kinematical properties (DOFs and joints range of motion) determined by analyzing the joints of the human lower limbs who most significantly contribute to locomotion during overground walking, and whose power requirements are determined by biomechanical analyses of human locomotion.

The first prototype of the BLEEX features 3 DOFs at the hip, 1 at the knee and 3 DOFs at the ankle. All three joints in the sagittal plane (hip, knee and ankle Flexion/Extension) are actuated; in addition also the hip adduction/abduction is actuated. Of the unactuated joints, the ankle inversion/eversion and hip intra/extrarotation are spring-loaded, while the ankle rotation is free-spinning [8].

A particular feature of the kinematic design of the device includes a revolute joint that is shared between the two legs of the exoskeleton and allows the whole lower body system to rotate around the vertical axis with respect to the torso, which therefore, does not intersect with the wearer's hip joints. Similarly, the inversion/eversion joint at the ankle is not aligned with the human joint, but is set to the lateral side of the foot. The other five rotational DOFs of the exoskeleton are instead designed to be aligned with the wearer's joints axes.

The exoskeleton is actuated via bidirectional linear hydraulic cylinders mounted in a triangular configuration with the rotary joints, resulting in an effective moment arm that varies with joint angle. BLEEX consumes an average of 1143 W of hydraulic power during level-ground walking, as well as 200 W of electrical power for the electronics and control. In contrast, a similarly sized, 75 kg human consumes around 165 W of metabolic power during level-ground walking.

In order to achieve the goal of being energetically autonomous and to comply with the selection of hydraulic actuators, significant effort was invested in developing a hybrid hydraulic/electric portable power supply [10].

Two different control schemes were proposed and demonstrated for the first BLEEX prototype. The first control scheme, called *sensitivity amplification controller*, implies no direct measurement of human contribution or of interaction forces. The

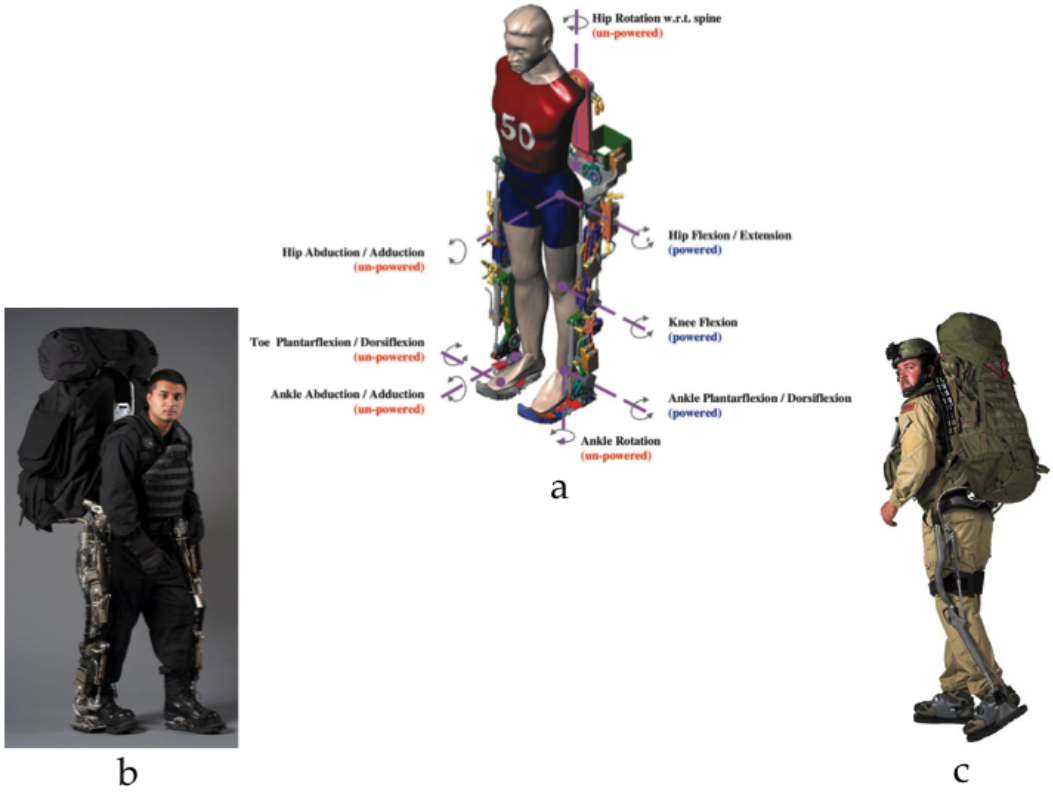

Figure 2.1: Human performance augmentation exoskeletons developed by UCB Robotics and Human Engineering Laboratory and Berkeley Bionics. (a) Schematic showing the degrees of freedom of the first presented Berkeley prototype [9]. (b) First BLEEX prototype worn by a pilot. Successive versions of the BLEEX have been developed by Berkeley Bionics, in (c) is the ExoHiker.

controller, based on the measurements of only the kinematic status of the exoskeleton, is based on positive feedback and was used to increase the closed loop system sensitivity to its wearer's forces and torques without any direct measurement from the wearer. In such way, the exoskeleton aims at shadowing the wearer's movements quickly by amplifying them with high sensitivity. In this control scheme the wearer is actually a pilot and acts in the control scheme as a feedback controller, seeking to reject the perturbations introduced by the robot, which would bring the system out of stability. Despite no interaction measure is considered, the sensing subsystem is still considerable due to the high amount of degrees of freedom to control. It includes 8 encoders and 16 linear accelerometers to determine angle, an-

gular velocity, and angular acceleration of each of the eight actuated joints; a foot switch and load distribution sensor per foot to determine ground contact and force distribution between the feet during double stance, eight single-axis force sensors for use in force control of each of the actuators, and an inclinometer to determine the orientation of the backpack with respect to gravity [8].

An improved version of the control scheme, the hybrid control scheme, was described shortly after [9]. This controller is not as heavily model-based as the previous one (which would require a good model of the BLEEX torso and payload dynamical properties) and adds robustness to changing BLEEX backpack payload. The walking gait cycle is divided into stance and swing phases and different control laws are used during them. Position control is used for the stance leg (including the torso and backpack) and a sensitivity amplification controller is used for the swing leg. The method allows to better grasp the different requirements arising for gait assistance, which requires a stiff support phase during stance (where basically the system helps the subject to be in a stable position), and a high bandwidth amplification control in order to be sensitive to human torques.

After the first prototypal version of the system, a spin-off company from the laboratory, named Berkeley Bionics (Berkeley, CA, USA) worked on new versions of the device for military applications developing the ExoHiker and the ExoClimber systems, tailored for load carrying during overground walking or during slopes ascent. The third generation of their exoskeletal system, the Human Universal Load Carrier (HULC) has reduced bulkiness and weight, since structural parts are titanium made.

The system is now ready for commercialization for military applications. Interestingly, the HULC is claimed in the group webpage [11] to be the first system able to provide a reduction in the order of 5 to 15% of the metabolic cost associated to overground walking. Despite of these claims, no data published in peer-reviewed journals or conference proceedings demonstrating such reduction in metabolic cost could be retrieved at the time of writing this thesis.

2.1.1.2 Sarcos Exoskeleton

The Sarcos Research Corporation (Salt Lake City, UT) has developed a full-body "Wearable Energetically Autonomous Robot" (WEAR). The Sarcos exoskeleton is also energetically autonomous, carrying its own power supply. Actuation is still provided by hydraulic actuators, but, differently to the BLEEX, it features rotary hydraulic actuators co-located with the joints matching the human degrees of freedom. The Sarcos exoskeleton has demonstrated a number of impressive features: structure supporting entire load of 84 kg, wearer standing on one leg while carrying another person on their back, walking at 1.6 m/s while carrying 68 kg on the back and 23 kg on the arms, walking through 23 cm of mud, as well as twisting, squatting, and kneeling [5].

The development of the device continued as a military project and for these reasons many detailed technical information on the device were not published. However, the main features of the current version of the device (dubbed XOS 2) can be extracted from the demonstrations of the device (now developed by Raytheon Company, MA, USA) provided by popular science magazines. The kinematic design of the device can be observed to be a mixed between an end-effector based machine and a real exoskeleton controlling independently human joint's DOF. The upper limb has a pseudo-antrhopomorphic structure, with shoulder, elbow and wrist joints. However, no attachments between the robot and the subject's arm are present apart the hand and the trunk; thus implying that torques are provided to the arm joints through a parallel kinematic configuration, which does not allow to modulate the level of assistance differently for each single human joint. The lower part of the exoskeleton is instead anthropomorphic, at least for what regards the three joints in the sagittal plane. The two hip joints are actuated also in the Adduction/Abduction axis and the same concept used for the BLEEX of shared rotation between the two legs is implemented to allow torso rotation.

2.1.1.3 MIT Exoskeleton

A different concept was developed at the Massachusetts Institute of Technology (MIT) by the group lead by prof. Hugh Herr (Biomechatronics Group, MIT Media

Figure 2.2: Exoskeletons for gait assistance. (a) The Sarcos XOS 2 Exoskeleton, (b) the MIT exoskeleton during a metabolic consumption experiment [5], (c) the HAL-5 exoskeleton, by Cyberdyne, Japan.

Lab). In this project the focus was mainly on energy efficiency of load-carrying during walking. An exoskeleton has been built, according to a design method oriented at replicating in wearable robots the achievements obtained in the field of passive bipedal walkers [12], which demonstrated that a walking machine, whose mechanical structure is designed in order to optimize the exchange of elastic, gravitational and kinetic energy during the gait cycle, has an increased energetic efficiency when compared to conventional walking machine designed through a kinematically anthropomorphic design and controlled via ZMP technique [13, 14].

As for bipedal walkers, the actuation system is simplified to the minimum terms. In particular, no actuators are used to add power to the human joints. The quasi-passive elements in the exoskeleton were chosen based on an analysis of the kinetics and kinematics of human walking.

Hip flexion-extension is supported by a rotary spring, whose elastic constant is

determined by comparison with clinical gait data. Also hip adduction/abduction and rotation joints are spring-loaded, but their elastic constants were determined to provide inherent stability for various admissible backpack loads. Additionally, a cam mechanism was incorporated at the hip to compensate for the relative change in length between the thigh of the exoskeleton and the user due to the joint offset during abduction/adduction. Spring-loaded hip rotation and ankle rotation joints were included to allow non-sagittal plane limb movements.

The knee flexion/extension joint is instead powered by a magneto-rheological variable damper, which is controlled to dissipate energy at desired phases of the walking cycle. It is the only energetically non-conservative element of the exoskeleton. Ankle flexion/extension joint is co-located with human ankle joint and loaded with two springs with different elastic constants to account for the different elasticity requirements for ankle flexion and extension. An additional carbon fiber spring is attached to the heel to reduce impact losses and aids in lifting the heel at the beginning of ankle extension.

The quasi-passive exoskeleton is controlled by using sensory information provided by a set of strain gages on the exoskeleton shin and a potentiometer on the knee joint. These sensors are used to detect the transitions between the different phases of the gait cycle which act as a trigger for a finite-state-machine based controller used to regulate the damping provided to the knee joint.

Without a payload, the exoskeleton weighs 11.7 kg and requires only 2 W of electrical power during loaded walking, power which is mainly used to control the variable damper at the knee.

Experimental work demonstrated a working device that successfully supported a 36 kg load during walking at 1 m/s. It was also shown that the exoskeleton structure transferred on average 80% of the payload weight to the ground. Metabolic studies with the quasi-passive exoskeleton aimed to quantify the amount of energetic efficiency of the whole device by comparing the metabolic cost associated to locomotion at a standardized speed with and without the exoskeleton. Results showed a 10% increase in walking metabolic cost of transport, for a subject carrying the 36 kg load via the quasi-passive exoskeleton versus having only a standard

backpack [3], thus failing to demonstrate that the device provides a metabolic advantage to the wearer.

Further experimental work was carried out to analytically separate the causes of the increased metabolic consumption. A significant reduction in metabolic cost of walking was found when comparing the performance of the described system versus the same exoskeleton without the springs at the hip and ankle and the variable damper at the knee, demonstrating the utility of the quasi-passive elements. Additionally, tests were conducted to determine the effect of the added mass and the inertial loads of the exoskeleton. From these studies, it was concluded that, in addition to the added mass and inertia, dominant causes for the observed cost of transport increase are the additional kinematic constraints inadvertently imposed on the wearer, upsetting the efficient dynamics normally seen during human walking [3].

No further work on the lower-body exoskeleton has even been published by the same group after the first prototype. However, the same group at MIT in later years was successful in demonstrating a leg exoskeleton which, in the specific test of hopping at a self-selected frequency, does instead reduce the metabolic cost. The device has a parallel structure with no intermediate attachment points between the torso and the foot links, and embeds leaf springs to provide intrinsic elastic properties to the structure [15].

2.1.1.4 Hybrid Assistive Limb HAL

The most popular among the lower body exoskeletons described so far, probably due to its futuristic design and the interaction modality based on bioelectrical signals, the HAL-5 system has been developed at the University of Tsukuba by the group lead by prof. Yoshikuyi Sankai. It is targeted both for human performance augmentation and for rehabilitative purposes [2]. The system is the output of a 15 years development process, with many prototypes presented the different years. Since June 2004, a company named Cyberdyne, spin-off of prof. Sankai's laboratory, is in charge of the technological development and marketing. Since then, no paper was published on peer-reviewed journal or conference proceedings; informa-

tion on the characteristics of the device could be retrieved by the author by reading review articles [5], by discussing with students of the lab contributing to the development of the new versions of the device and by assisting to demonstrations given in a technological fair in Naples, Italy [16].

The leg structure of the full-body exoskeleton powers the flexion/extension joints at the hip and knee via a DC motor with harmonic drive placed directly on the joints (see Fig. 5). The ankle flexion/extension DOF was passive in the first HAL 5 version, even though new versions of the device include an actuated ankle joint. The lower limb components interface with the wearer via a number of connections: a special shoe with ground reaction force sensors harnesses on the calf and thigh, and a large waist belt. In distinction to the load-carrying BLEEX, Sarcos, and MIT exoskeletons, the HAL system does not transfer a load to the ground surface, but simply augments joint torques at the hip, knee, and ankle. However, a new model-based mechanical design of the device was presented, which includes a frame transferring the reaction forces to the ground, thus reducing the load of the subject's bones.

The HAL-5 system utilizes a number of sensing modalities for control: skin-surface electromyographic (EMG) electrodes placed below the hip and above the knee on both the front and the back sides of the wearer's body, potentiometers for joint angle measurement, ground reaction force sensors, a gyroscope and accelerometer mounted on the backpack for torso posture estimation. These sensing modalities are used in two control systems that together determine user intent and operate the suit: an EMG-based system and a walking-pattern-based system. A continuous operating time of approximately 160 min is allowed by a battery pack. The total weight of the device amounts to 21 kg, including both upper and lower body (lower body alone weights approximately 15 kg).

The system has been commercialized in the Japanese market with a lease-per-month format, for a price of about 2'200$ per month. A European branch of the company has been reportedly opened in Denmark in 2010, but no evidence of the device being used in Europan rehabilitation centers could be retrieved.

Many demonstrations of the HAL being worn by an able-bodied operator were

provided, both for overground locomotion in everyday contexts and in particular situations such as carrying the load of a human injured subject during a ski-rescue operation.

On the side of providing assistance to physically impaired subjects during locomotion, an algorithm used to estimate human intentions during walking, suitable to be used to control the device when applied to human subjects with unreliable bioelectric signals, was presented in 2006 and tested on a patient with spinal cord injury [17]. Videos demonstrating the process of recovery of subjects with different kinds of neurological disorders undergoing rehabilitation therapy based on the usage of the HAL-5 system or of subsystem of the whole device have been presented in multiple presentations by prof. Sankai. Despite of that, no clinical data demonstrating the effectiveness of such robot-assisted rehabilitation therapy could be retrieved in the literature.

2.1.2 Machines for Body-Weight Support Treadmill Training (BWSTT)

Another class of exoskeleton devices is that of treadmill-based devices designed to deliver therapy to subjects with neurological disorders, such as stroke, Parkinson Disease (PD) or Cerebral Palsy (CP). These devices are well suited to be included in a particularly structured environment. For these reasons the first generations of such devices delivering automated gait therapy to physically impaired patients was represented by treadmill-based systems, with the big advantage of allowing to fix the actuation system and the power source to the ground frame, which do not need to be worn by the human operator. This class of systems allows to automate the Body-Weight Supported Treadmill Training (BWSTT) therapy, which is labour-intensive and requires efforts by two or three human therapists, then allowing to replace the role of the therapist which applies forces to the human limbs during different phases of the gait cycle.

In particular, there is the possibility for the actuation system and the energy source of the device to be supported by a fixed frame thus simplifying the requirement of reducing the weight of the actuator and of the power source, which is a major requirement of energetically autonomous wearable robots.

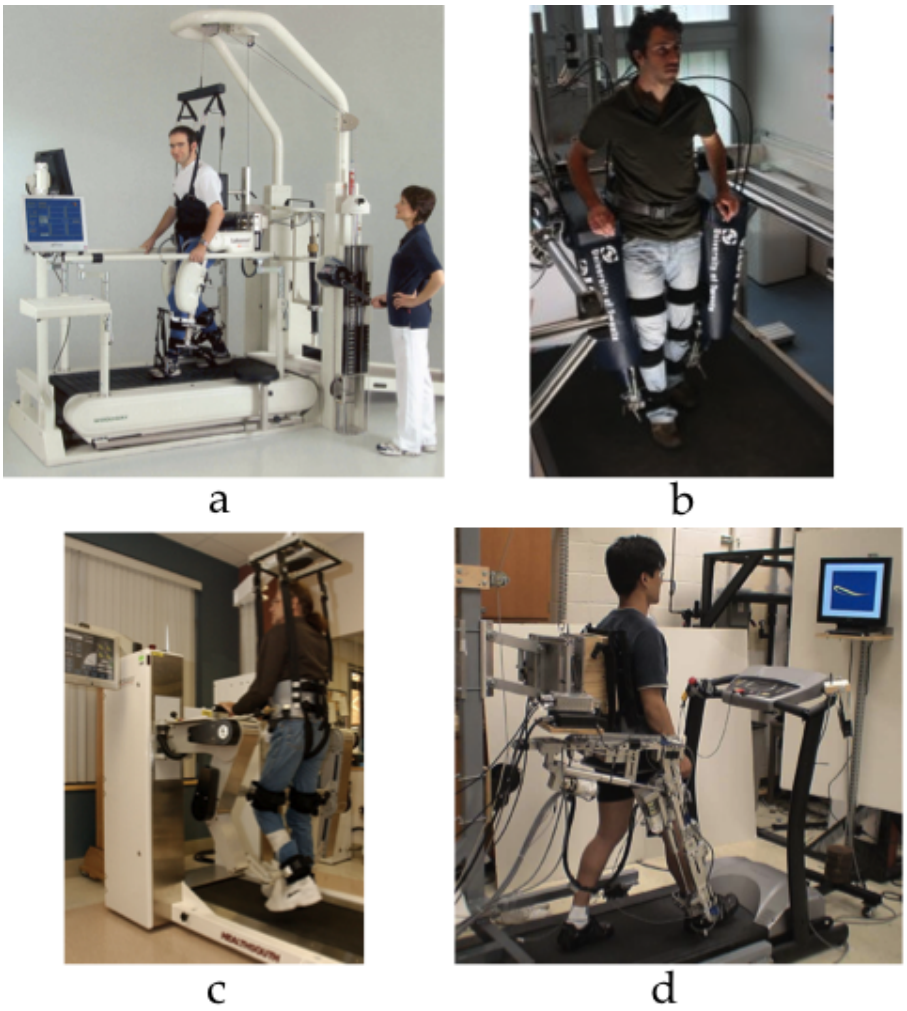

Figure 2.3: Treadmill-based robotic devices for BWSTT: (a) The Lokomat [18]; (b) the LOPES [4]; (c) the Autoambulator [19]; (d) the ALEX [20].

The main implementations of such concept with a exoskeletal device developed so far will be briefly described in the following.

2.1.2.1 Lokomat

The Lokomat (Hocoma Inc., Switzerland) was the first system embedding the concept of BWSTT. It is now commercialized by Hocoma Inc, whose first version underwent the stage of clinical evaluation as rehabilitation tool around year 2001

[18]. The system comprises a tunable weight support system, which supports a fraction of the weight of the subject during locomotion, and a robotic device which supports hip and knee movements only in the sagittal plane, while the ankle joint is not supported. Continuous torque limits for the first prototype are 50 Nm for the hip joint and 30 Nm for the knee joint, both of which are actuated through a DC motor and a ball-and-screw transmission subsystem [21]. A feedback on the kinematic status is provided by potentiometers, which measure the 4 DOFs of the device. The regular patient training with the Lokomat is performed with a fixed gait pattern, which does not take into account the peculiarities of each subject and is implemented by position control of the joint angle trajectories. This control scheme does not allow to follow the *assist-as-needed* approach to robotic-based neurorehabilitation [22][1], which states that the robotic intervention needs to be specifically tailored to the requirements posed by each subject and minimized to only the situations in which the subject really requires it. To accommodate the requirement for patients that have some residual voluntary locomotion capabilities, automatic gait-pattern adaptation algorithms were presented in 2004 [23]. One algorithm is based on inverse-dynamics and uses the estimation of the interaction forces to adapt the angle trajectories so to minimize them. Additionally, also an impedance control scheme, based on the direct measurement of the interaction forces at the human-robot interface is presented and demonstrated. The results show that the impedance controller is the one which allows the best and more comfortable degree of subject adaptability in the gait pattern.

The Lokomat system comprises also an optional pediatric version and has been a huge commercial success in the 2000s. It is diffused in many rehabilitation centers worldwide, being considered the golden standard of robotic assisted BWSTT, despite clinical trials demonstrating its reduced effectiveness when compared to human intervention [24, 25]. Moreover, other studies reporting the alterations in muscle activation patterns and reduced ergonomics provided by the robotic system, whose straps and kinematic structure are reported to be source of discomfort and even pain for some users [26]. It is worth to notice that all published clinical

[1] A description of the general requisites for robot-mediated neurorehabilitation is provided in Chapter 4

trials were based on robotic therapy performed with the control schemes which are really transferred to the clinical market, which do not include any of the adaptive control schemes described above, despite they are presented in the literature as a product of research oriented to developing control schemes to be used in everyday clinical scenarios.

2.1.2.2 LOPES

The LOPES (LOwer-extremity Powered ExoSkeleton) is a treadmill based wearable robotic device for gait training and assessment of motor function in stroke patients [4], developed at University of Twente by the group lead by prof. Herman van der Kooij. It combines a freely translatable and 2-D-actuated pelvis segment with a leg exoskeleton containing three actuated rotational joints: two at the hip (flexion/extension and adduction/abduction) and one at the knee. Motion is generated by electrical motors fixed to the ground frame and a Bowden cable series elastic transmission system is used to transfer torque to the wearer's joints. This system allows to reduce the inertia felt by the wearer during unassisted motion and to implement a force control by only measuring the deflection of the elastic element. The development of the device started in 2001 and since then has been used with healthy subjects as a neuroscientific tool to investigate motor learning [27] and more recently with chronic stroke patients to validate the device as a tool for neurorehabiliation. Preliminary studies were presented to demonstrate the ability of this rehabilitation tool to restore an improved kinematic walking pattern (improved foot clearance during swing) after a period of robot aided gait training [28].

2.1.2.3 Other treadmill-based devices for gait rehabilitation

Other than the two described devices, many other groups developed treadmill-based powered orthoses suitable to be used as tool for rehabilitation therapy.

The AutoAmbulator is a commercial system patented [29] and developed by Healtsouth Corp., AL, USA. Though including a different mechanical design of the weight support subsystem which reduces the weight and overall dimensions of the device, allowing also for faster don and doff times compared to the Lokomat, but it

essentially consists of an electrically actuated anthropomorphic device supporting hip and knee movements in the sagittal plane. Few details on the uses of this system could be retrieved in the peer-reviewed literature.

An interesting device which tries to take advantage from a dynamics-oriented mechanical design is the exoskeleton developed in the Departments of Mechanical Engineering and Physical Therapy at the University of Delaware. A first prototype consists of a passive leg orthosis that is designed to reduce the effect of gravity on the patient during walking and is presented in [30]. This is achieved through a mechanism, which is first used to locate the center of mass of the human limb and the orthosis. Springs are then added so that the system is gravity-balanced in every configuration. The same paper presents experimental work on able-bodied young adults and one individual with paralysis in the right leg due to stroke. Among other things, the results showed that the current implementation of the device, while not affecting required torques at the knee, reduced the average torque required from the patient's hip by 61%.

The same group later developed the ALEX, which is a unilateral treadmill based leg rehabilitation exoskeletons, where hip and knee joints flexion and extension are actuated by linear drives [20]. Other joints, including hip adduction-abduction, and ankle flexion/extension, are spring loaded. A force field controller is implemented in the task-space that displays a position dependent force field acting on the foot, so to guide it through a "virtual tunnel", representing the physiological foot trajectory during overground locomotion.

2.1.3 Energetically autonomous active orthoses for gait assistance in impaired patients

Some of the researches and of the technological developments, started in the field of human augmentation for able-bodied users, have been translated and modified to be useful for physically impaired subjects, both as rehabilitative tool and for assistive technology suitable to be used in everyday environments.

a b c

Figure 2.4: Energetically autonomous active orthoses for gait assistance in physically impaired subjects. (a) The eLegs lower limbs exoskeleton, Berkeley Bionics, CA, USA, used by a paraplegic subject (b); The ReWalk lower limbs exoskeleton, Argon Medical Technologies, Israel, (c) The knee orthosis PK100, Tibion Corporation, CA, USA.

2.1.3.1 Berkeley Bionics eLegs

The eLegs [31, 32] is a system developed by Berkeley Bionics, whose mechanical apparatus is mainly based on the HULC system. The system has a kinematically anthropomorphic structure and includes double-acting hydraulic cylinders to support knee and hip flexion and extension, differently to the HULC system, which only supportes joints flexion using one-way hydraulic cylinders. Hip adduction and abduction are loaded with very stiff elastic components in the use with physically impaired subjects to minimize unnatural postures, and the ankle joint is spring-loaded in the dorsi-plantar flexion direction, reducing the phenomenon of toe-drop. A battery pack and computer are stored on the back, contributing to the

weight of the device, which accounts for a total of 39 kg for the prototypal version described so far. The bracing system includes a torso brace, upper and lower thigh straps, a shank brace and straps for the backpack which carries the batteries and computer and includes a set of crutches or a cart to provide support to the device and patient in the event of a patient fall.

Its sensory apparatus includes heel and toe pressure sensors used as switches to detect foot contact with the ground, a knee potentiometer and hip digital encoder to provide a measure of the actuated joints angle, an accelerometer/gyroscope board in the torso, which measure absolute torso angle in the sagittal plane, in addition to the proprioceptive sensors used for low-level control of the hydraulic actuators.

Testing of the device was performed on four paraplegic patients with complete or incomplete paralysis [32] and on three chronic stroke patients [31].

In the case of the three chronic stroke patients, an hybrid position/force controller similar to that used in [9] was implemented, where a PD controller is used for position control to avoid the overpowering, which can be caused by the kinematic pattern generated by spastic contractions of the impaired leg. Experimental results show an improved degree of anthropomorphism of knee flexion-extension profile and improved stride length and time for the impaired leg.

The testing with paraplegic subjects was performed on three patients with incomplete paralysis and one with complete paralysis [32]. A state machine was implemented with a position control, which tracks a trajectory set whose profile is derived from Clincal Gait Analysis data, and adapted to guarantee a safer clearance from ground during the swing phase, and parametrized in terms of step length and step speed, which could be adjusted according to the subject's and the therapist feeling. During the stance phase, the hip is driven trough a zero-impedance controller, which avoids problems of torso rotation which arise due to the lack of vertical support for the torso link, which is not fixed to a rigid frame as in the case of treadmill-based machines. During stance phase, the momentum of the body, whose center of mass is moving forward, is sufficient to provide motion to the hip during the stance phase. The device was successfully tested on a paraplegic subject, showing that all patients were able to walk using the exoskeleton, which could provide

the necessary lift to the swing leg and to drive it through the desired trajectory.

During a public demonstration of the device, a subject demonstrated her ability to walk using the device, [33] after 18 years of complete paralysis. The system is now (January 2011) in the process of starting the first clinical trials and is expected to be commercialized by mid-2011.

2.1.3.2 Argo Medical ReWalk

The ReWalk system has been developed by Argo Medical Technologies, a company spun-off from Israel Technion. It is a wearable motorized robotic device allowing DOFs of Flexion/Extension for the hip and knee joints, which are actuated by electrical motors co-located with the robot's joints and aligned to the subject's rotation axes. The systems has been demonstrated in conjunction with canes to provide support to the subjects. An intention detection subsystem detects the intention to start motion by evaluating the inclination of the torso, thus implying that a good functionality of the upper body is required to operate the device. A remote control is also used to switch among different control modes. Uses of the device in different daily activities, such as climbing stairs and sitting, have been demonstrated in videos demonstrated by Argo Medical Technology. The control system is based on a position controller to drive the wearer's joints [31]. No evidence of the use of interaction control was retrieved in the literature.

No technological detail of the system has ever been published in the scientific literature; however since 2008 the system has gone through the stages of final engineering and is currently in the process of undergoing the first clinical trials at MossRehab (Philadelphia, PA, USA), to potentially gain FDA approval for clinical use of the device in the US. Pilot clinical trials are also presently starting in Italy, in particular at the Centro Protesi INAIL di Vigorso di Budrio (Bologna, Italy) on 18 paraplegic subjects.

Argo Medical estimates that the device will be marketed by the end of 2011, for a cost of around 100'000 $ [34].

2.1.3.3 Tibion PK100 knee orthosis

The system is a knee orthosis with a carbon fiber structure providing support to the electrical motor, battery and user interface. In order to respond to the heavy power requirements for an actuator to support the weight of a person (the stated design objective was to include paraplegic subjects weighting up to 100 kg), the actuator is connected to the orthosis through a continuously variable transmission system, developed purposively for the project [35]. This provides a controllable trade-off between output torque and velocity in different tasks (sit-to-stand, stairs ascent, and overground walking). During the swing phase, instead, the actuator drive train is completely decoupled from the orthosis to allow a transparent movement. The sensing subsystem includes a force sensor, used for the torque feedback control loop. Rotary encoders provide a reading of the motor and knee brace angles. A foot sensor is inserted inside the shoe to provide the weight-on-foot information used to detect transitions between different gait cycle phases.

Different interaction modes are described in [35], including an assistive mode where motion generated by the subject is amplified, a continuous passive motion mode, implemented through position control to apply repetitive movements to the knee without the subject contribution, and a robotic therapy mode, which is based on the assist-as-needed concept, and as such the robot intervenes only when the subject is not able to complete the movement on his own.

Not any clinical study has yet been reported in the literature. However, a preliminary application of robotic therapy with the device (including several repetition of sit-to-stand movements) has shown encouraging results, demonstrating that the device can be successful in restoring autonomous sit-to-stand motion in chronic stroke patients [36].

2.1.3.4 Other energetically autonomous assistive robots

In addition to the already described devices, other energetically autonomous systems have been demonstrated in the recent years, such as the REX exoskeleton, produced by REX Bionics, New Zealand, an anthropomorphic lower body orthosis designed for sit-to-stand, stair ascend and overground walking, without the use of

Figure 2.5: (a) The Smart Caster Walker Exoskeleton, by Sogang University, Korea, from [37]. (b) The REX Exoskeleton, REX Bionics, New Zealand.

crutches. The system has been demonstrated with healthy subjects, and for sit-to-stand of wheelchair users. It is currently being sold in New Zealand for 150,000$.

An interesting concept meant to bypass some of the design difficulties in creating a portable active orthosis is presented by researchers at Sogang University, Soul, Korea [37]. The device consists of a full lower limb orthosis paired with a specially designed walker that houses the battery, DC motors, and control computer, greatly reducing the weight of the worn structure. A cable drive transmits mechanical power to the joints of the wearer from the actuators in the walker. The orthosis adds power in the flexion/extension directions of the hip and knee, and allows motion in the other DOFs of the leg, except the rotation of the ankle, which is fixed. User intent is sensed by a combination of joint angle sensors and a pressure sensor that gives a rough measure of force being applied by the quadriceps muscle. This design appears to exploit the consideration that most powered orthotic devices for physically impaired persons still require the use of crutches or other additional support methods, and finds a way to reduce the overall weight. Appar-

ently, this system is limited to overground walking since both stairs ascending and sit-to-stand transitions are impeded by the demonstrated design.

2.2 Possible advantages of non-anthropomorphic wearable robots

Despite an expected increase in overall mechanical complexity over traditional anthropomorphic exoskeletons, the possible advantages provided by a free kinematic design of a wearable robot are from an ergonomics and dynamical standpoints and will be separately analyzed in the next sections.

2.2.1 Ergonomics

The design process of any robotic device, especially of those physically interacting with humans, starts with the choice of a suitable kinematic structure. Normally, the kinematic design is carried out in order to fulfill a certain number of design objectives, which include the following [38]:

1. a desired number and type (e.g. revolute, linear, spherical) of DOFs
2. a desired workspace defined in terms of positions and orientations;
3. a certain set of intrinsic dynamical properties (these may be defined differently according to the target application. In the case of neurorehabilitation robots a commonly desired dynamical property is isotropy and transparency during *patient-in-charge* mode);
4. provide structural support for actuators and sensing elements in adequate locations, where they do not deteriorate the dynamical performances of robots.

End-effector based robotic device are those machines whose physical interaction occurs only at one given point of the robot. In this case, the mentioned points are normally the only ones taken into account. In wearable robots there are instead multiple contact points between the user and the robot [39] and thus it is important to guarantee the kinematic compatibility between the robotic structure and the

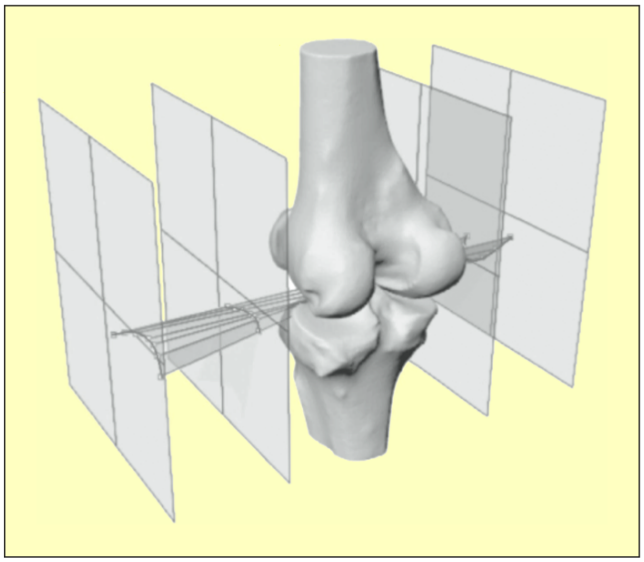

Figure 2.6: Representation of three-dimensional movement of the ICR of a human knee corresponding to a complete flexion-extension movemement. It can be noticed that the relative trajectory dispersion increases as a function of the distance in the lateral direction. This demonstrates the effect of second-order modeling inaccuracies, which for joints modeled as revolute joints in the sagittal plane do not depend only on the inaccuracies in that planes but have a more complex effect in the three dimensional space. From [6].

biological segments addressed by the robot. This means that even before implementing actuation and control of the robot, the purely mechanical structure must enable wearability, ease of use, and operator comfort.

There is only one way for the exoskeletons with an anthropomorphic kinematic structure to be kinematically compatible with the addressed biological structure: the two structures have to be kinematically identical, at least for what regards the DOFs supported by the robot. This implies the need for the perfect alignment of all joints axes.

There are a number of difficulties arising from this problem. Ideally, imagining that an exact kinematic model of the addressed human segment is available for each subject and that it is possible to adapt the mechanical structure of the robot through an continuous set of regulations, the presence of the biological segments poses space constraints to the design of the robot mechanical structure, which needs to be ”external” and cannot interfere with human movements in any allowed pose.

This first design difficulty can be solved by reducing the number of supported DOFs for each target human articulation. A simplified kinematic model of the targeted segments is then considered, so to allow, at least at a modeling stage, the desired properties of "kinematic replication".

Additionally, the schematization of biological joints as ideal kinematic pairs has a limited degree of accuracy, which varies for each articulation. For example, the human knee is replicated in wearable exoskeletons with a revolute joint. Actually, the human knee has a complex three dimensional geometry and its instantaneous centre of rotation (ICR) is not fixed relative to the femoral bone, but instead moves along a trajectory. This trajectory varies as a function of the distance in the lateral direction from the human articulation, as shown in Fig. 2.6. This means that not only is the misalignment between the robot and the human axis responsible for the kinematic incompatibility, but second-order inaccuracies (such as in this case those arising from having modeled the knee joint as a revolute joint) have an effect which can increase also as a function of the lateral misalignment between the human and the robot kinematic chains.

An even more striking case reported in literature is that of the shoulder joint, whose kinematic simplification to a "ball-and-a-socket-joint" is source of misalignments which can be in the order of tens of centimeters. The kinematic approximation is sufficiently accurate only for small rotations and for motions involving only in the glenohumoral articulation [40]. However, when considering large motions of the whole shoulder complex, this approximation looses validity and large shifts of several centimeters are documented [41]. This kind of mis-alignments is a function of the amplitude of supported movements. Although for a very structured task/ environment a limited workspace can be considered to avoid misalignment related problems, this can be a limiting issue when trying to transfer the robotic devices in the everyday life environment. Globally, these errors lead to the so-called macro-misalignments, which essentially define the mismatch (defined in terms of number or type of DOFs) between a robotic and biological structure.

In any case, the kinematic design of a kinematically compatible wearable robot is developed essentially through a process of bio-mimicry, where the target of the

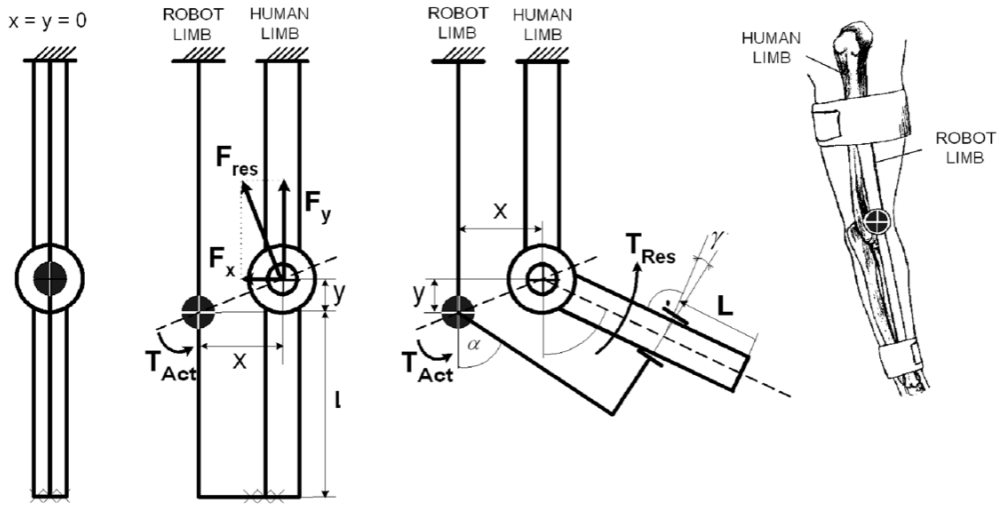

Figure 2.7: Schematization of a 1 DOF human articulation and an attached robot. In (a) the ideal case of perfect alignment is represented. This condition is actually not achievable in reality, or however it is impossible to keep it throughout the whole range of motion. Small misalignments (x, y) in the order of some centimeters, respectively, between human joints and actuated joints cause forces hundreds of Newtons for an actuation torque of some unit of Nm, without allowing any motion, in the case of perfectly rigid coupling. What happens in reality is that the attachment on the soft-tissue of the arm allows the robot to move. The misalignments in Cartesian directions $x = 2cm$ and $y = 1cm$ will cause a skin movement in the order of $L = 4$ cm, at a rotation $\alpha = 45$ deg and $l = 20$ cm. The displacement increases with bigger angles. Also, an angular displacement γ between the axes of the robot and the human segments will be present. This angular displacement is often neglected since the interaction forces arising from this kind of misalignment are smaller. From [42].

design is a more or less accurate kinematic model of the targeted human segments. The reduction in the kinematic compatibility is however determined by the inaccuracies inherent in this model. In addition to the qualitative mismatch defined above as macro-misalignment, it is obvious that inter-subject variability of anatomical structures brings inherent limitations to the degree of achievable alignment between the robot and the human kinematic chains.

A first problem occurs in the definition of the exact location and orientation of human joints axes of rotation, which cannot be measured directly on living subjects, since they are covered by soft tissues. A big number of non-invasive measurement methods are proposed in literature, which can be used to derive a complete quantitative kinematic model of a set of human segments, such as the one described in

[43]. This study describes the use of a 3D magnetic spatial tracking system. The system includes a fixed source of magnetic field and a set of wearable sensors. The induced voltage measured across the loops of these sensors provides an accurate estimation of both the position and the orientation of the sensor relative to the fixed reference frame.

This spatial tracking system has been adapted in the course of this thesis and used to develop a 3D spatial tracking system, which can be used in conjunction with a neurorehabilitation robotic device for the upper limbs, in order to asses possible unnatural postures during the rehabilitation task [44]. The apparatus allows also to quantify the degree of mismatch of the approximation of the shoulder as a spherical joint, defined by the set of parameters reported in Table 2.1.

A schematization of the developed apparatus is reported in FIgure 2.8 which includes also the representation of the profiles measured during a session of robot-mediated rehabilitation therapy.

The method was also adapted to the lower limbs and showed to provide reliable estimates of the Denavit-Hartenberg parameters of the addressed musculo-skeletal system, which can then be employed as a real-time motion tracking system.

Despite the availability of such methods, the process of regulating the parameters of robot kinematic structure to the biological one is still normally accomplished by visual inspection, also because the degree of regulation of the kinematic parameters of the robotic kinematic structure is often discrete and however not sufficiently fine to justify a more complex and cumbersome calibration procedure.

Additionally, the fixation of a robotic device to a human limb is not completely rigid, so that slippage between the device and the limb normally occurs. Furthermore, the contact points are normally above a layer of soft tissue with variable cross section (as it is very well known, a muscle fiber changes its cross section depending on the posture of the articulation(s) supported). This implies that the degree of misalignment depends on the given posture used at the time of tuning the kinematic parameter, and then may be of a modest entity for low-range movements, but it can increase when wide-range motions are desired.

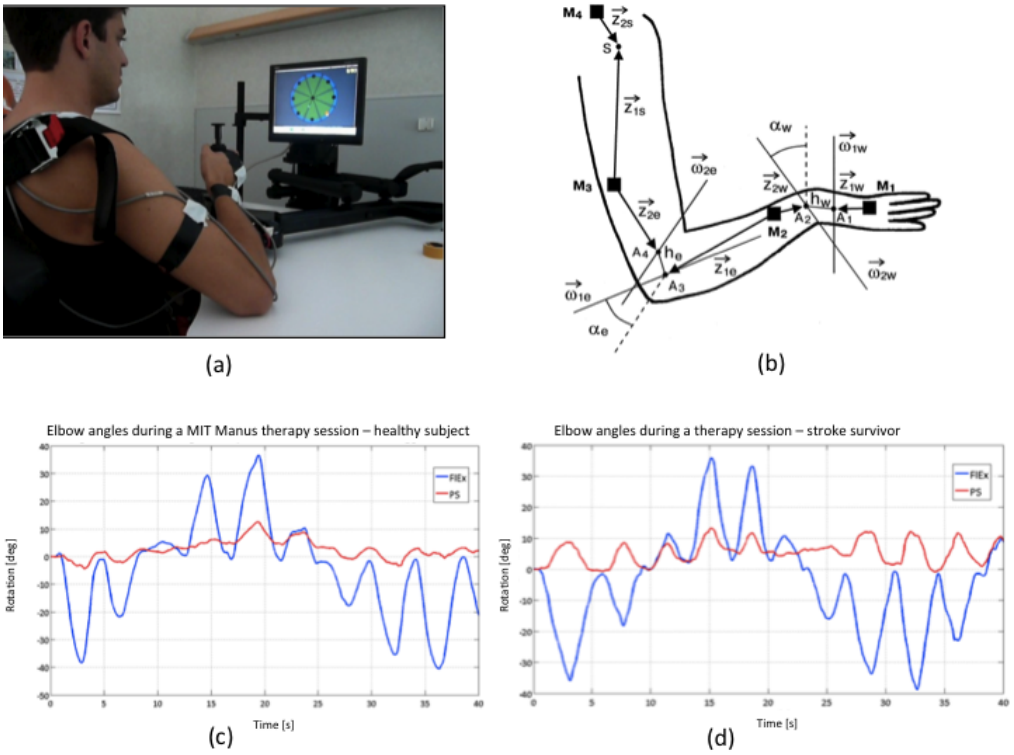

Figure 2.8: 3D spatial tracking apparatus for the reconstruction of the kinematics of the upper limb, used during a session of robot-assisted rehabilitation therapy. (a) experimental setup comprising the spatial tracking system and the IMT3 planar shoulder and elbow robot. (b) 7 DOFs kinematic model of the upper limb used for the calibration and data acquisition phases. The model schematizes the shoulder as a 3 DOF spherical joint, based on the rotation of the upper arm relative to the acromion, the elbow and the wrist as 2DOFs joints. Kinematic profiles of the elbow flexion/extension degree of freedom in a young healthy subject (c) and in a stroke survivor (d) during a typical game of rehabilitation therapy with the robot. From [44].

These facts are likely to cause micro-misalignments between any attached robotic joint and the human joint in the order of a couple of centimeters.

An extremely simplified but insightful model of the effect of misalignments over human articulation is reported in [41]. A figure taken from the cited paper is shown in Fig. 2.7, which takes into consideration the constraint forces arising from a planar misalignment.

In [42], a non-linear analytical model, predicting and interpreting the characteristics of constraint forces generated by misalignment of exoskeleton joints axes,

Table 2.1: Parameters of the kinematic model obtained in the calibration phase, for the nine subjects involved in the experiments. l_1 and l_2, anatomical measurements of upper arm and forearm length, Δr_s, standard error of the measurement of the shoulder center of rotation position, α_e and α_w, elbow and wrist skew angles, h_e and h_w skew distance.

KINEMATIC PARAMETERS	MEAN	MAX	MIN	STD. DEV.
l_1 (mm)	125.5	170.6	103.8	21.1
l_2 (mm)	250.0	267.3	226.6	14.0
Δr_s (mm)	8.1	15.5	5.0	3.7
α_e (°)	92.4	99.2	87.4	3.9
$\lvert h_e \rvert$ (mm)	7.4	11.7	4.6	2.3
α_w (°)	97.4	106.4	86.2	7.3
$\lvert h_w \rvert$ (mm)	2.4	6.6	0.6	1.8

Figure 2.9: The ESA exoskeleton, from [41].

was introduced. The model makes use of force and position measurements to provide a position-dependent estimation of the attachment stiffness and of the real offsets between the human and robotic joints. The soft coupling between human and robot tissues are described by a linear visco-elastic model, whose parameters are estimated by the model, which measures the interaction forces. The measurements also assessed for the first time the amount of reduction in interaction forces introduced by the addition of passive joints allowing for alignment between robot and

biological instantaneous axes of rotation. Results showed a reduction of up to 50 % of interaction forces in extremal regions of the workspace and a reduced deviation of interaction forces.

In [41], a new paradigm for the design of kinematically compatible wearable robots for rehabilitation was proposed, postulating that a WR should not explicitly replicate the kinematic structure of the adjacent human limbs. On the contrary, it should provide a moving system acting in parallel to the human degrees of freedom. Furthermore, it is reported that robotic devices must be able to activate each single human joint, to induce exact ergonomic movements in patients and that robotic actuators should be placed so that each natural degree of freedom of the human limb can be moved with a single or a specified set of actuators. These kinds of wearable robots may possess multiple degrees of redundancy to cope with the interaction with human limbs and joints, without presenting the need of aligning the axes of rotation of artificial joints to those of human joints.

These concepts have been implemented in an exoskeleton for the upper limbs developed to enable in-space force-feedback tele-manipulation with redundant robot arms [41], as shown in Figure 2.9. The kinematic structure of the exoskeleton, which does not mimic upper limbs, offers an alternative kinematic chain bridging over the human joints. Even though the kinematics of the exoskeleton and the human arm are different, any posture of the human joints can be univocally determined by the

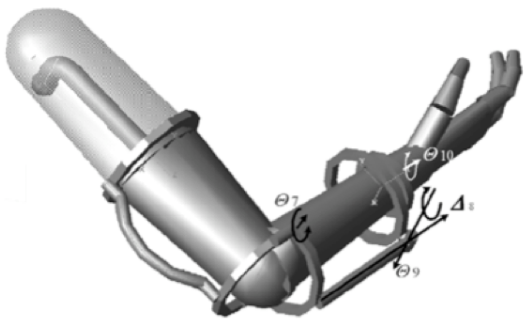

Figure 2.10: CAD model of the non-anthropomorphic elbow exoskeleton, which includes four robotic joints, two of which are actuated to selectively provide elbow Flexion/Extension (joint Θ_7) and forearm prono-supination (joint Θ_{10}) (from [41]).

corresponding posture of the exoskeleton, which allows the complete range of motions of human articulations.

Fig. 2.10 depicts a non-anthropomorphic kinematic structure of a wearable robot acting on a 2 DOF human joint (elbow). The 4 DOF robotic structure is attached in parallel to human upper arm and forearm limbs. Once the operator wears this robot, the resulting kinematic chain is such that only 2 DOF are allowed. These DOF can be controlled by actuating joints Θ_7 (for elbow flexion-extension) and Θ_{10} (for elbow prono-supination), while the two other joints are passive.

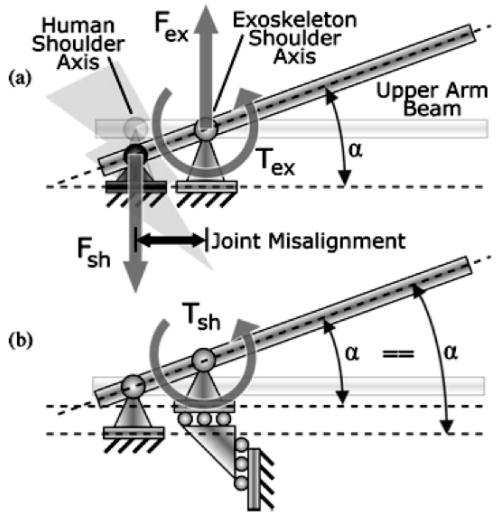

Figure 2.11: Misalignment between human and robot joints axes of rotation. (a) Case of planar anthropomorphic kinematic structures with revolute joints, where a residual force Fsh is applied on the shoulder. (b) Modified kinematic structure of the robot, which include two prismatic joints, which cancel the interaction forces by automatically aligning the axes of rotation until this force goes to zero (from [45]).

The purpose of automatic alignment of exoskeleton axes to human anatomical axes is also pursued in [45], where the unwanted exchange of interaction forces on the skin is avoided by decoupling joints rotations from joints translations. The proposed method consists in adding translational capabilities to the basic kinematic structure of the exoskeleton, thus reducing the interaction forces to only friction and inertia of the prismatic kinematic pairs.

This method is very beneficial from the point of view of axes self-alignment but does not allow converting forces applied by the robot to human limbs into rotation of human articulations, since these forces are absorbed by the translation of moving elements. In order to generate motion of human limbs with the decoupled mechanism it is necessary to apply pairwise forces in order to generate equivalent torques. These forces require two connections per section of the exoskeleton to the corresponding human limb and can be transmitted by adding two extra links to the exoskeleton and using parallelogram-like kinematic chains like that shown in Fig. 2.11.

2.2.2 Dynamical properties

Over the past twenty years studies originally stemming out from the biological investigations on the locomotion of lower animal forms highlighted the intimate connections among intelligence, morphology and performance. As showed in [46], the lowest level of intelligence is actually completely physical, as it consists in the ability of neuro-musculoskeletal systems to present zero-delay, intrinsic responses (preflexes) to a perturbation [47]. Preflexes are useful for performing low-level tasks such as stabilization and feed forward locomotion control.

As an example, the cockroach *Blaberus discoidalis* is able to scramble over randomically distributed obstacles up to three times its body height without significantly slowing down [48]. Such striking performance cannot be achieved by a feedback based, centralized sensory-motor control because of the required quick adaptation to the environment. On the contrary, robust locomotion is achieved mainly through a basic feedforward pattern applied to its properly tuned mechanical system (preflexes). Such principles have been implemented in the development of a highly efficient hexapedal robot capable of sensorless robust locomotion at speeds up to 2.5 body lengths/sec [49].

On a phylogenetically higher level, recent studies on biped robots have shown that even complex tasks, such as walking, may arise from the intrinsic dynamics of a machine during its interaction with the environment. Studies on passive walking show that walking, normally obtained through computationally demanding algo-

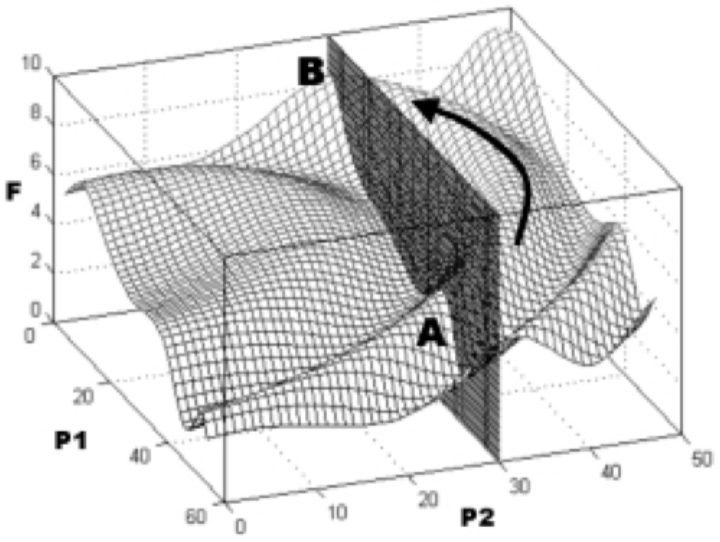

Figure 2.12: Graphical representation of an extradimensional bypass, which can be achieved by a concurrent design of robot morphology and control, from [52].

rithms requiring feedback from several sensors, can emerge from an accurate tuning of the dynamical properties of a purely mechanical system, without any feedback control [50], [51]. The performance obtained through this methodology produces a gait which appears to be more biomimetic under both the energetic and kinematic standpoints. In particular, it has been demonstrated that the energetic efficiency of such mechanisms resembles that of the human body, while existing bipedal walking robots are about 30 times more energy demanding [12].

Moreover, experiments performed on physical simulation environments have shown that it is possible to optimize, via a coupled evolutionary process, both the morphological properties of a robot and its controller, with mutual benefits for both in terms of reduced complexity and enhanced efficiency [52, 53].

In particular, [52] demonstrated in a physics-based simulation environment that a stable bipedal walking could be achieved through a coupled optimization of both the controller and the mass distribution of the structure. Although the size of a search space, which combines both morphological and control parameters, is larger than the one where the two steps are developed in a sequential manner, the au-

thors demonstrated that the combined optimization leads to better results. The authors could argue that the performance increase is attributable to *extradimensional bypasses*, i.e. narrow paths in the fitness landscape that connect otherwise separated, sub-optimal fitness peaks. This process is graphically represented in Fig. 2.12. The demonstration that this kind of fitness profile is descriptive of a complex dynamical process, such as bipedal locomotion, is an extremely interesting result. The generalization of such results allow to highlight the presence of a *morphology and control trade-off* in the design of robots, where an effort in the improvement of the overall performance can be equally split towards modifying the two sub-components of controller and mechanical structure.

The problem of assessing if, how and how much these findings can be transferred to the field of wearable robots for the lower limbs consists of a very tough challenge. Despite of that, the literature suggests that possible improvements of the performances of wearable robots can be provided by "opening" the design of the mechanical subcomponent, and not just focusing on novel control schemes or aspects related to actuators power efficiency or intrinsic safety.

These considerations suggest that wearable robots performances can benefit from a careful design of robot morphology, which is open in the case of non anthropomorphic wearable robots, and can allow to achieve a better dynamical interaction with the human body and with the environment.

2.3 Conclusions and objectives definition

The problem of assessing if, how and how much the findings achieved in the field of pseudo-passive bipedal walking robots can be transferred to the field of wearable robots for the lower limbs consists of an open research challenge. Despite of that, experts in the field of wearable robotics [5] suggests that possible improvements of the performances of wearable robots can be provided by "opening" the design of the mechanical subcomponent, and not just focusing on novel control schemes or aspects related to actuators power efficiency or intrinsic safety. However, the problem of optimal kinematic synthesis of non-anthropomorphic wearable robots may be very difficult to be solved by human intuition and engineering in-

sight alone, due to the large number of open parameters involved in the design. This task can be simplified by automatic tools in support of the designer.

The objective of this thesis is to develop a robust and complete methodology, which can be used for the design of wearable robots. Such methodology which can be employed in fore-coming research in order to answer to the scientific problem of quantifying which advantages to dynamical or ergonomics aspects can be introduced by an open-ended concurrent design of morphology in wearable robots.

Chapter 3

Kinematic synthesis of non-anthropomorphic wearable robots

3.1 Methodologies for the open-ended kinematic design of robots

The idea that machine learning processes inspired by biological evolution can be used to design autonomous machines has its roots in the early days of evolutionary computation and has been implemented several times, starting with the seminal works of Sims [54]. The first approach has been that of evolving robot controllers for fixed legged morphologies, in a simulation environment with a sufficient fidelity to allow replication in the real world of results achievable in simulation. In this context, evolutionary programming [55] and genetic algorithms [56] have been used to evolve controllers for hexapod robots. Genetic algorithms have also been used to evolve recurrent neural networks for bipedal locomotion in simulation environments [57]. However, in all of these approaches, little or no consideration was paid to the mechanical construction of the agent or robot.

Alternatively, Brooks and Stein [58] and Pfeifer and Scheier [59] have pointed to the strong interdependence between the morphology and control of an embod-

ied agent: design decisions regarding either aspect of an agent strongly bias the resulting behavior. One implication of this interdependence is that a good choice of morphology can often lead to a reduction in the size or complexity of the controller. As an extreme case, the study of passive walker dynamics has made clear that a careful choice of morphology can lead to locomotion without any actuation or controller at all [50]. Examples now abound that demonstrate the evolution of both the morphology and control of simulated agents is possible and can give interesting results.

In [53] genetic algorithms have been applied to optimize the design of a pseudo-passive dynamic walker, by evolving both morphology and control parameters. A basic morphology of a 8 DOFs biped robot has been implemented and morphology parameterization was applied on links geometrical and inertial properties, while each joint could be actuated or passive. Active joints dynamical properties were parameterized on the basis of CPG oscillator properties (amplitude, frequency, phase), while passive joints could exert different impedance values. The genetic algorithm was applied to encode morphological and control parameters in a fixed-length genome and to evaluate phenotype performances in a physics-based simulation environment based on the fitness function depending from the distance traveled in a fixed time-length trial. The evolved robot could show a dynamically stable locomotion, with properties of self-regulation and self-stabilization, suggesting that the evolutionary method of design could be an excellent solution for exploiting passive dynamics achieving it mainly with appropriate compliance.

In [60] evolutionary computation has been used for automatically design of robotic structures for achieving locomotion. The design space was made up of bars, ball joints and linear actuators as building blocks for morphology and artificial neurons as building blocks of control. Starting with a population of machines that were composed initially of zero bars and zero neurons, morphology and control co-evolution was performed in simulation, with fitness determined by its locomotion ability (net distance of its centre of mass on an infinite half plane) in a simulation environment supporting quasi-static kinematics. Selected virtual robots with the fittest performances were then automatically converted into physical objects using

rapid prototyping technology without human intervention, with standard linear actuators being subsequently snapped-in and the evolved neural network executed on a micro-controller to activate the motors. The physical machines faithfully reproduced their virtual ancestors' behavior in reality, even though some quantitative differences between real and virtual worlds were present, due to the limitations of the accuracy of the friction model used in the simulation.

The application of evolutionary algorithms to the design of machines connected to the human body requires that a proper biomechanical model of the body is taken into account, where segments can be modeled as a set of properly linked rigid bodies [61] and kinematic constraints may arise from a deep investigation of the bony structure [62]. However, the adoption of kinematically accurate kinematic models of the human body is limited by the necessity of providing a sufficiently fast simulation environment for fitness evaluation. Optimization algorithms require a very high (in the order of 10^6 to 10^9) number of iterations before producing an optimized results, thus implying a necessary trade-off between an accurate simulation

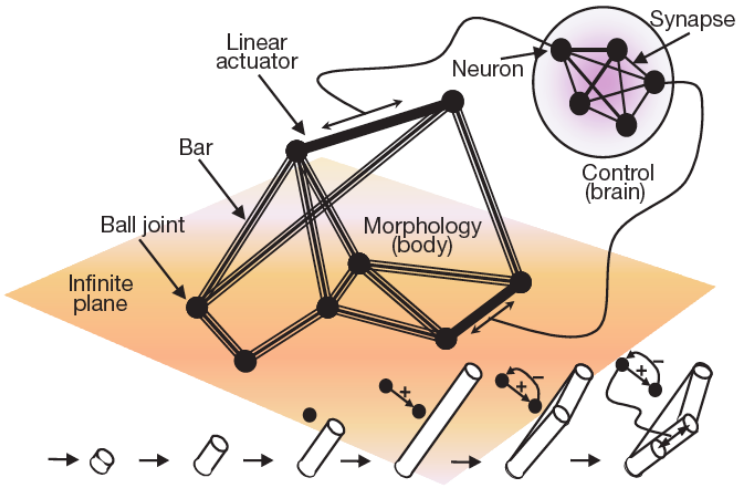

Figure 3.1: Illustration of the building blocks of the evolvable robots used in [60]. Bars connect to each other to form arbitrary trusses; by changing the number of bars and the way they connect, the structural behavior of the truss is modified. Some substructures may become rigid, while others may become articulated. Neurons connect to each other via synapses to form arbitrary recurrent neural networks. The behavior of the network can be modified by changing the synapse weights and the activation threshold of the neuron, or by changing the number of neurons and their connectivity. No sensors were used in the study, then no instance of reactive behaviors could be achieved.

environment and a fast convergence speed of the optimization process.

Concerning the baseline, to the best of the author's knowledge a co-optimization approach for designing together the morphology and the control of a wearable robot has never been taken before.

3.2 Graph-based methodology for the kinematic synthesis of planar WRs for the lower limbs

The mentioned [60] open-ended design methodologies have the advantage that they may lead to interesting and unexpected design solutions. However, such kind of design methods imply that the whole design process is completely demanded to the tool, which can autonomously decide to switch to a more complex structure during the optimization phase so to increase the fitness of the best individuals. These variable parameter space optimization algorithms do not assure that individuals belonging to each interesting family of solutions (i.e. topologies) are evaluated in the evolutionary design phase.

The approach which is being pursued in this thesis work differs from the one shown in [60], since it consists of three different sequential stages. A schematization of the pursued approach is shown in Figure 3.2.

In the first stage a systematic search of all the plausible independent generalized kinematic solutions (i.e. *topologies*) is performed. In the second stage an optimization algorithm acting on a fixed number of parameters (which encode both the mechanics and the control) is used to define the *morphology* providing the best performances in terms of some design objectives. In the final stage, the best morphologies produced by the optimization on each topology are compared with each other, so to define the "fittest" solution. This approach appears more reliable since optimization algorithms acting on a fixed parameter space are simpler and with faster convergence properties. Furthermore, each optimization process is independent from the others and can run in parallel on different computers. Additionally, this approach assures that all interesting generalized solutions (i.e. topologies) are evaluated before producing the final design. However, this approach requires the

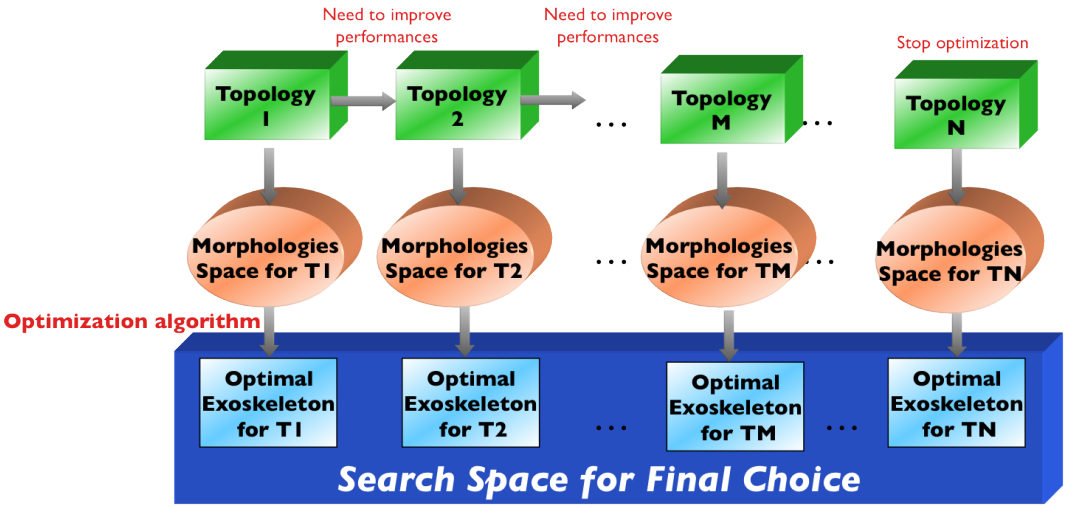

Figure 3.2: Overview of the methodology developed in the context of this thesis. The methodology is based on the multi-objective optimization of a fixed number of parameters, describing robot morphology (kinematic and dynamical properties) and actuation laws (torque applied to the robot joints). This optimization strategy requires the a-priori knowledge of the list of suitable independent solutions (i.e. topologies), which are considered valid if a certain number of kinematic properties of the set constituted by human and robot kinematic chains is respected. The generated topologies can be ordered for increasing complexity (such as number of links and number of DOFs) and the optimization process can be stopped when satisfactory performances are reached.

a-priori knowledge of the list of independent topologies having the basic desired kinematic properties (i.e. maximum number of links and of degrees of freedom (DOFs)) and respecting some basic criteria of kinematic compatibility with the human body.

The following of this chapter describes a graph-based method for the exhaustive enumeration of the topologies of planar non-anthropomorphic wearable robotic orthoses, which represents the first stage of the design methodology described above. The method includes two special tests (i.e. the HR-isomorphism test and the HR-degeneracy test), which have purposively been devised to solve the problem of the enumeration of wearable robots kinematic structures.

With the developed methodology, it was possible to derive the atlas of all the possible independent kinematic structures of a planar wearable robotic orthosis with up to 7 robot links, to assist a human limb modeled as a 4-link/3-joint serial kinematic chain, satisfying a certain set of basic kinematic requirements.

3.2.1 Kinematic structure encoding

Initially, an encoding needs to be defined, in order to represent the kinematic structure of robotic orthoses. Since the aim is obviously to consider in the design also the mobility of the human limbs connected to the robotic orthosis, the whole parallel kinematic chain consisting of both robot links and human limbs is considered. The description of this kinematic chain can be performed at two levels of abstraction: *i) topology*, which defines the number of links and the connections among them and *ii) morphology*, which instantiates a given topology, adding the geometrical properties of links and of joints.

3.2.1.1 Topology

Under some reasonable hypotheses [63], many properties of mechanisms kinematics, such as the number of degrees of freedom, are entirely determined only by the topology of the kinematic chain and unaltered by the geometric properties of its links. At this level of abstraction, the classical analogy between undirected graphs and kinematic chains, as introduced by [64], can be employed, where graph vertexes correspond to the links of the chain and edges correspond to the joints. A graph can then be encoded through the Topology vertex-vertex Adjacency Matrix (TAM), which is a binary symmetric matrix of order n (where n corresponds to the number of links) where the element a_{ij} equals to 1 if link i and link j are connected through a joint, and to 0 otherwise (ref. Fig. 3.3).

As a first assumption, it is decided to focus on planar kinematic chains composed of only revolute joints. It is then unnecessary to discriminate between the kind of joint connecting each link, hence the representation is complete in the description of kinematic chains topology allowing to convert the problem of kinematic synthesis into a problem of graphs enumeration.

The mentioned assumption limits the relevance of the methodology for the design of assistive wearable robots for the lower limbs, since the hip and the ankle joints have spatial movements. However, it can be noticed that most of the power of the lower limbs is provided by actuation of movements in the sagittal plane, which is the dominant plane of motion during human locomotion.

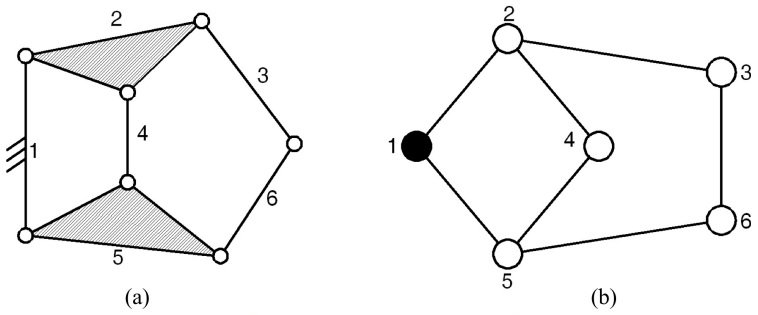

$$\begin{bmatrix} 0 & 1 & 0 & 0 & 1 & 0 \\ 1 & 0 & 1 & 1 & 0 & 0 \\ 0 & 1 & 0 & 0 & 0 & 1 \\ 0 & 1 & 0 & 0 & 1 & 0 \\ 1 & 0 & 0 & 1 & 0 & 1 \\ 0 & 0 & 1 & 0 & 1 & 0 \end{bmatrix}$$

(c)

Figure 3.3: Structural representation (a), graph representation (b) and TAM (c) of a six links kinematic chain. Link 1 is filled in black since it is mechanical ground.

The described representation is then complete in the description of kinematic chains topology and allows converting the problem of kinematic synthesis into a problem of graphs enumeration. However, as it will be more extensively discussed further, the relation between a kinematic structure and a matrix of adjacencies is a one-to-many relation. The same kinematic structure can indeed be achieved by a different matrix of adjacencies (and graph), by just re-labeling links numbers. This implies that any enumeration process based on a matrix-of-adjacencies based representation implies the need for an explicit isomorphism test to assess the real independence of any couple of solutions.

3.2.1.2 Morphology

The previously described representation for the topology of the kinematic chain can be adapted also for describing robot morphology, which gives details on the geometrical properties of links and is necessary to evaluate the possible kinematic configurations of the chain. We restrict our focus on planar kinematic chains containing only revolute joints. Then, the only necessary information to define robot

morphology is the position of joints in a particular configuration. In such a way a binary link is represented by a bar jointed at its extremities, a ternary link by a triangle jointed at its vertices and so on. Under these assumptions we only need to modify the adjacency matrix by adding the information concerning joints coordinates. This can be done by introducing the Morphology Adjacency Matrix (MAM), which is a square matrix of order n containing x-coordinates of joints (if any) in its strictly upper-triangular part and y-coordinates of joints in its strictly lower-triangular part. A "null" value is inserted in the indexes where the TAM contains zeroes, to avoid confusion between the absence of a joint and the superposition of one joint to the x or y axis of the reference frame.

The knowledge of joints position relative to the ground in a given pose of the structure is sufficient to completely define the kinematic properties of the whole structure. However, since the evaluation of each structure will not be based on a quasi-static purely kinematic simulation environment, but on a dynamical one, it is important to provide also all the relevant parameters which are significant to the definition of robot morphology. Other than the kinematic parameters, every link needs to be provided with some dynamical parameters in terms of mass, position of the center of mass and moment of inertia calculated with respect to the center of mass.

The previously cited restriction of the methodology to only consider planar kinematic chains significantly reduces the number of parameters which are required to fully define a link's morphology. The moment of inertia tensor reduces from 6 parameters to only one, representing the moment of inertia relative to the rotation of the link around an axis passing through its center of mass, normal to the sagittal plane where the kinematic chain moves. Some basic structural assessments have been derived [65] so to find the minimum values of links mass for a binary link of a given length. Such parameters can be included in the definition of the parameters boundaries. However, links mass need not to be restricted to the minimum value admissible from structural assessments considered, and then needs to be included as a open parameter which is to be defined during the optimization phase.

For what it concerns the position of the center of mass, it does not necessarily

fall into the same position of the centroid defined by joints position. Since the aim is to provide some desired intrinsic dynamical properties to the robotic structure, it is instead desirable that the optimization can exploit advantages coming from a non-obvious mass distribution. Then, the position of the center of mass can be defined on the basis of a polar representation, relative to the centroid defined by joints positions.

Additionally, the calculation of the moment of inertia can be performed based on the concept of radius of gyration r_g, which for planar links of mass m is such that the moment of inertia I_g is given by the following equation:

$$I_g = m \cdot r_g^2. \tag{3.1}$$

The radius of gyration has the dimensions of a length and can give a more intuitive description of the inertial properties of a planar shape, for example with respect to a circumference of negligible width with a radius R, where r_g=R. Boundaries on the values of the radius of gyration can be provided on the basis of kinematic features, such as joints positions, by setting as a minimum value a percentage of the biggest distance between joints. In particular, the boundaries for I_g were indirectly defined, by setting extremal conditions for r_g. Since it was decided not to consider the possibility of generating structures whose centre of mass is not coincident with the centroid of the convex hull defined by the position of the joints of each link a reasonable approach would be to calculate the moment of inertia by referring to the average and maximum distance between the different joints and the link centroid. Two extremal values for $r_{g,min}$ and $r_{g,max}$ can then be defined as:

$$r_{g,min} = \frac{1}{n}\sum_{i=1}^{n} r_1 \tag{3.2}$$

$$r_{g,max} = \max(r_i), \tag{3.3}$$

where r_i is the distance between the i^{th} joint and llink centroid. Fig. 3.4 shows two possible implementations of a binary link.

Conceptually similar procedures can be derived for defining boundaries for links with a higher order such as ternary or quaternary links. A sketch showing

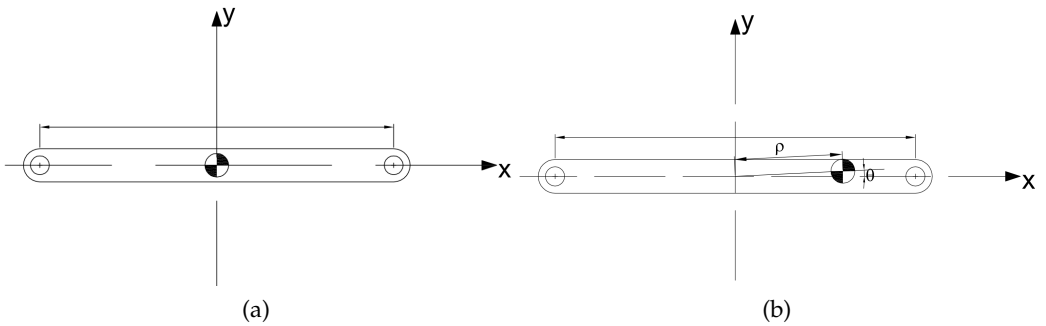

(a) (b)

Figure 3.4: Encoding the morphology of binary links (a) Binary link with a symmetric mass distribution; in this case link center of mass coincides with the centroid defined by the positions of joints A and B (b) Binary link, with an asymmetric distribution of center of mass, in this case the two parameters ρ and θ define the position of the center of mass relative to the link centroid. A similar representation can be provided for the inertia gyrator r_g.

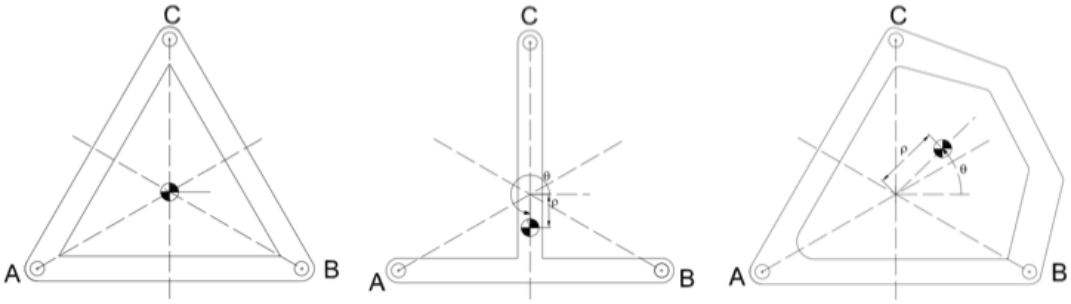

(a) (b) (c)

Figure 3.5: Encoding the morphology of ternary links (a) Ternary link with a symmetric mass distribution; in this case link center of mass coincides with the centroid defined by the positions of joints A, B and C. (b) Ternary link, with an asymmetric distribution of center of mass, in this case the two parameters ρ and θ define the position of the center of mass relative to the link centroid. A similar representation can be provided for the inertia gyrator r_g. (c) An arbitrary situation in which a planar ternary link has non coincident centroid and center of mass; in this case a given value of r_g can be obtained by varying link shape.

possible implementations of ternary links and their representation is provided in Fig. 3.5.

3.2.2 A preliminary step: minimum number of links and joints for given degree of mobility

A preliminary estimation is carried out to derive the minimal number of links and joints which are consistent with the goal of providing a certain number of degrees of mobility. The relevant parameters considered for the mobility of this kinematic structure are the total number of degrees of freedom and the total number of independent subchains.

The kinematic structure has to preserve the range of motion of each human articulation, which is supported/assisted by the robot. For this reason the minimum number of degrees of freedom of the whole kinematic structure is three, one for each of the human joints addressed. More DOFs could enable a better adaptation to the human body, and the achievement of better dynamical properties of the robotic structure, with a consequent increase in the complexity of the mechanical structure. Since we want to investigate only robot kinematic chains constituting parallel chains when attached to the human body (as suggested in [41], we can borrow from graph theory the concept of number of independent circuits (L_{ind}) of a graph (with e edges and v vertexes), which is given by Euler's formula:

$$L_{ind} = e - v + 1 \tag{3.4}$$

Using this formalism we can conclude that we are interested in closed kinematic chains, whose corresponding graphs are such that $L_ind \geq 1$. We finally need to evaluate the mobility of the structure. We assume that Kutzbach-Grubler's criterion is adequate to determine the number of degrees of freedom of the resulting kinematic chain consisting of both robot and human links. By neglecting skin deformations at the exoskeleton attachments points, for a given planar kinematic chain with n links and with f (independent) 1 DOF joints, the total number of degrees of freedom (DOFs) is given by Kutzbach's formula [66]:

$$DOFs = 3 \cdot (n-1) - 2 \cdot f \tag{3.5}$$

This formula can be used to derive the following table, which has as inputs the

number of robot links (from 2 to 10) and joints which are attached to the human limbs model (4 links and 3 joints) and as output the number of independent circuits and of DOFs in the structure. Rows in red represent kinematic chains with insufficient mobility ($DOFs \leq 3$), while combinations representing serial kinematic chains ($L_{ind} \leq 1$) are not reported. In order to be able to control each degree of freedom of the robot one more condition needs to be satisfied, i.e. that the number of robot joints is higher or equal to the total number of DOFs of the structure. The table reports only combinations satisfying also this last condition.

It can be noticed that the minimum number of robot links, which are necessary for a wearable robot satisfying the given properties, is two. The resulting kinematic chain is the simplest one, which can be obtained by modifying the graph reported in by connecting with a revolute joint links 5 and 6. The structural representation of such configuration is shown in Fig. 3.6. This configuration presents 3 robot joints and only two attachments sites with human limbs, one at the pelvis and one at the foot. It is theoretically possible to control each one of the three degrees of freedom of the structure by adding a rotary actuator in each one of the revolute joints of the robot structure.

At this stage it is useful to recall the design goals for ideal human-robot interaction proposed in [41]. According to these principles, a wearable robot should be designed to explicitly not imitate the kinematic structure of a human limb, to avoid the necessity of precise manual alignment between the axes of human and robot joints. Furthermore, it is reported that robotic devices must be able to activate each single joint, to induce exact ergonomic movements in a patient and that actuators are placed such that each natural degree of freedom of the human limb can be agitated with a single or a specified set of actuators. In the above- described example, the concurrent dynamical action of all three actuators is necessary to specify the status of the system, and it is not possible to identify a correspondence between the action of one actuator and the resulting action on one human joint.

This can lead to difficulties in accurately controlling the dynamics of single human joints. This issue can be overcome by considering only kinematic chains with a higher number of independent circuits, starting from those satisfying the condi-

Table 3.1: Number of DOFs of the kinematic structure comprising both human segments and robot links, for the case of a wearable robots for the lower limbs (Human segments=4 (torso, shank, thigh, foot), as a function of the number of robot links and joints added. Red background is for conditions with insufficient mobility ($DOFs < 3$), green background is for assemblies fulfilling both the constraint on DOFs ($DOFs \geq 3$), and the constraint on the minimum number of independent loops (subchains): $L_{ind} \geq 3$
.

Robot links	**Robot joints**	**Total links**	**Total joints**	L_{ind}	**DOFs**
2	3	6	6	1	3
2	4	6	7	2	1
3	4	7	7	1	4
3	5	7	8	2	2
4	5	8	8	1	5
4	6	8	9	2	3
4	7	8	10	3	1
5	6	9	9	1	6
5	7	9	10	2	4
5	8	9	11	3	2
6	7	10	10	1	7
6	8	10	11	2	5
6	9	10	12	3	3
6	10	10	13	4	1
7	8	11	11	1	8
7	9	11	12	2	6
7	10	11	13	3	4
7	11	11	14	4	2
8	9	12	12	1	9
8	10	12	13	2	7
8	11	12	14	3	5
8	12	12	15	4	3
8	13	12	16	5	1
9	10	13	13	1	10
9	11	13	14	2	8
9	12	13	15	3	6
9	13	13	16	4	4
9	14	13	17	5	2
10	11	14	14	1	11
10	12	14	15	2	9
10	13	14	16	3	7
10	14	14	17	4	5
10	15	14	18	5	3
10	16	14	19	6	1

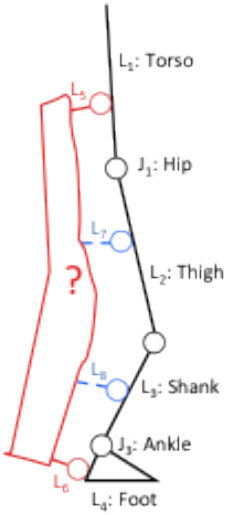

Figure 3.6: Minimal set of links and joints for a wearable robot for the lower limbs assisting the hip, knee and ankle joint. Wearable robot joints and links are in red, attached to a planar model of segments relevant to human walking in the sagittal plane (in black). Links and joints which are not indispensable following the criterion of defining the pose of the lower limb are reported in blue.

tion $L_{ind} \geq DOFs$. These combinations are highlighted in green in Table 3.1, where we see that the minimum number of robots links to be added in the structure is 6, for a total number of 9 robot joints, 3 of which need to be actuated. The simplest kinematic structure corresponding to this configuration is reported in its structural and graph representation in Fig. 3.7.

3.2.3 Enumeration of kinematic chains

After making considerations on the number of additional links and joints provided by the structure, the problem is to derive a methodology which allows to explore all possible assortments of the given number of links and joints which provide a certain desired degree of mobility to the human+robot system. To this aim, the systematic enumeration of the whole set of independent kinematic solutions for the design of a robotic orthosis which can assist the movements of human limbs is provided in this section. The approach is presented for the case of a lower limb, which is schematized here as a serial kinematic chain composed of four links and three joints.

Table 3.2: Parameters of the enumeration algorithm

Robot links (r)	Total links (n)	DOFs	Indep. loops	Total joints (f)	Fixed joints	Add. joints (e)	Open pars (l)	Comb. no. (used method) $\binom{l}{e}$	Total comb. (2^l)	Reduction ratio (%)
4	8	3	2	9	7	2	6	15	64	76.56
5	9	4	2	10	7	3	14	364	$1.64{\cdot}10^4$	97.78
6	10	3	3	12	7	5	23	$3.4 \cdot 10^4$	$8.4{\cdot}10^6$	99.60
6	10	5	2	11	7	4	23	$8.9 \cdot 10^3$	$8.4{\cdot}10^6$	99.89
7	11	4	3	13	7	6	33	$1.11 \cdot 10^6$	$8.6{\cdot}10^9$	99.99

The problem is graphically represented in Fig. 3.8, where the structural representation, the graph representation and the corresponding TAM are reported. The process of enumerating kinematic chains consists of three successive steps: *(A) enumeration of graphs with the desired mobility*, *(B) degeneracy testing*, *(C) isomorphism detection*. These steps will be described separately in the following paragraphs.

3.2.3.1 Enumeration of kinematic chains with the desired mobility

Without loss of generality, each kinematic solution is represented by a graph with $h + r$ vertexes, where h corresponds to the number of body segments (4 in our case) and r corresponds to the number of robot links. A number of constraints need to be defined so to particularize the approach to the situation of a wearable robot. It is worth noting, however, that this approach can be implemented for each schema-

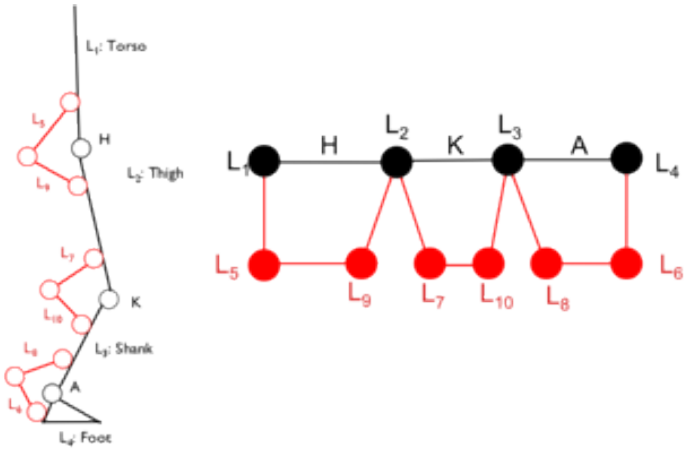

Figure 3.7: Minimal structure allowing the independent control of hip, knee and ankle joints, with 3 DOFs and 3 independent circuits.

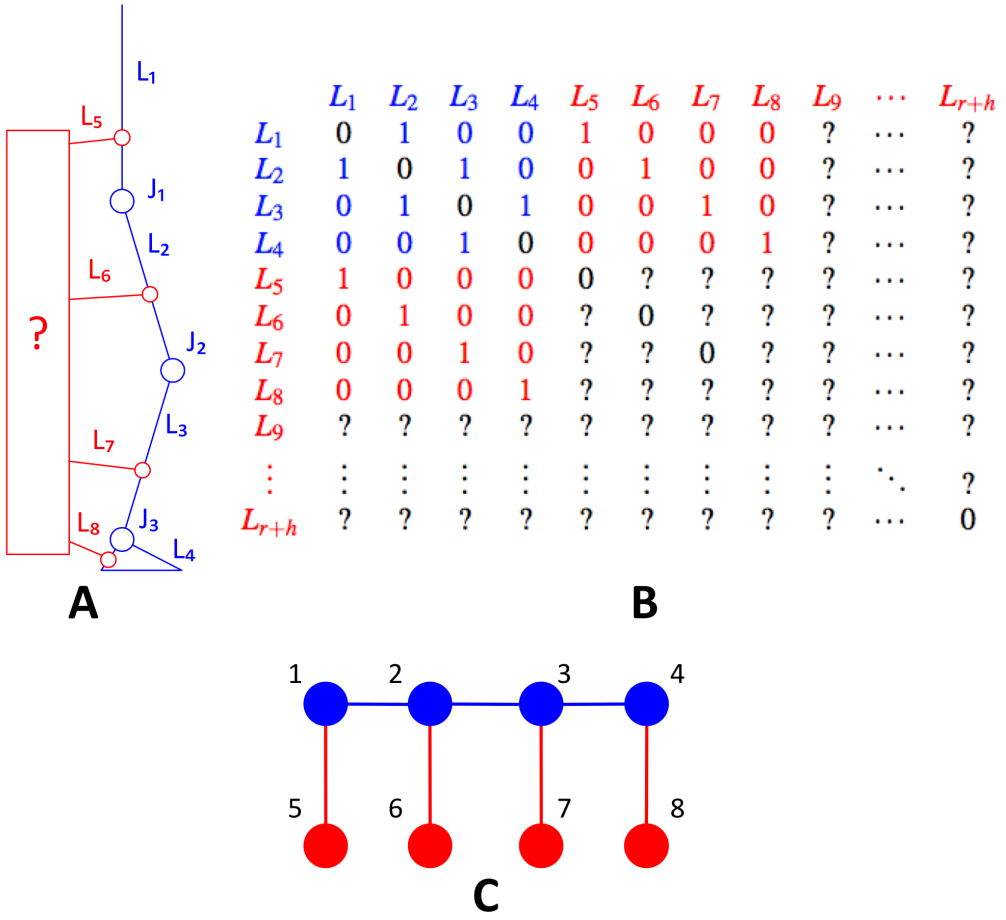

Figure 3.8: Structural representation (A), generalized TAM (B) and graph representation (C) of the problem of structural synthesis of robotic orthoses for a planar wearable robot for the lower limbs. Human articulations and segments are in blue, while robot links and joints are in red. In the adjacency matrix, the blue color is used to represent entries which describe the connectivity of human limbs (condition (1) in paragraph IIIA), while the red color represents fixed entries provided by condition (2), paragraph IIIA.

tization of a biological limb as a planar, serial chain, composed only of revolute joints.

The following general kinematic constraints are imposed in the design

1. the number of DOF of the whole structure (comprising jointly human segments and robot links) is comprised between 3 and 5 DOFs;

2. the robot structure must not impose unnatural constraints between one human joint and another one.

Specifically, the following assumptions are made:

1. links 1 (trunk), 2 (thigh), 3 (shank) and 4 (foot) compose the serial kinematic chain of the human limb supported by the wearable robot;

2. links 5, 6, 7 and 8 are by construction connected to the body segments. The necessity of providing assistance to each human joint implies that each body segment needs to be connected to a robot link. Additionally, each robot link connected to a body segment cannot be attached to another body segment not to reduce mobility of human joints (this would constitute a HR-degenerate subchain (see corresponding paragraph).

The complete list of independent kinematic solutions can be obtained from the basic TAM shown in Fig. 3.8(c). Any topology can be encoded by a binary string of length l, where

$$l = h \cdot (r - h) + \frac{r(r-1)}{2}. \tag{3.6}$$

However, not any combination of parameters is adequate, since we are interested only in kinematic chains with a given number of DOFs, i.e. 3, 4 and 5.

Equation 3.5 implies that given any number of links, the kinematic chain can contain only a fixed number of joints. Since each joint between links i and j corresponds to a 1 in the (i, j) position of the corresponding TAM, the problem of enumeration of all topologies with a desired mobility is converted into the problem of exhaustively listing the binary strings of length l, with a fixed number of ones (e, as shown by Table 3.2).

This problem can be solved by considering all the possible $\binom{l}{e}$combinations of the l integers from 1 to l taken e at a time and using those combinations as suitable locations where "1" values are to be inserted in the binary string which encodes the TAM. This method implies a significant reduction (up to 99,99%) of the number of TAMs to be generated when comparing it to the "brute-force" approach where all 2^l combinations are enumerated. Table 3.2 shows that the number e of additional joints to be added in the kinematic structure takes into account that the basic structure implies the presence of a given set of joints (corresponding to the human

articulations and to the connections with the basic set of robot links shown in Fig. 3.8).

After matrices enumeration, links connectivity is evaluated. The *order* of link i is defined as the number of joints in which link i participates. It can be easily calculated from the TAMs by summing elements in the i^{th} row:

$$order_i = \sum_{k=1}^{n} a_{ik} \tag{3.7}$$

Since only closed kinematic chains are addressed by this enumeration, solutions including links with order lower than 2 must be discarded. Moreover, the upper bound for the order of any link must satisfy the inequality: $\max(order_i) \leq L + 1$, where L represents the maximum number of independent loops.

Since the robotic structure is applied in parallel to three human joints the maximum order of robot links is set to 4.

3.2.3.2 Degeneracy and HR-degeneracy tests

A further selection over the list of enumerated topologies is performed, in order to filter out the kinematic chains which:

- contain rigid or over-constrained subchains;
- correspond to disconnected graphs (i.e. not all graphs vertices are connected by a path);
- impair the simultaneous motion of human joints;

A standard degenerate testing algorithm has been implemented to recognize and discard rigid subchains (such as 3 links-3 joints and 5 links-6 joints subchains).

Degenerate kinematic chains (i.e. those which contain at least one subchain with zero or negative DOFs according to Kutzbach formula, such as 3 links-3 joints and 5 links-6 joints subchains) are then eliminated.

Additionally, disconnected mechanisms (i.e. such that there is not a path connecting each couple of vertices of the corresponding graph) are eliminated with a

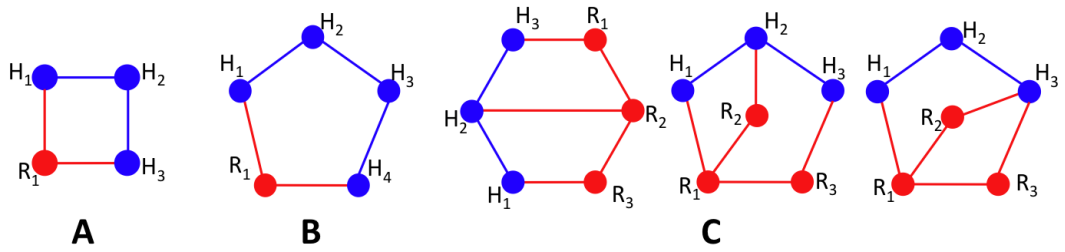

Figure 3.9: HR-degenerate topologies. In A, two adjacent human segments are constrained in a 1-DOF subchain. In B, three adjacent human segments are constrained in a 2-DOF subchain. In 3, all possible assortments of two adjacent human segments involved in a 6 links, 1 DOF subchain are shown.

purposively developed algorithm, which verifies the existence of a path between each couple of vertices.

Furthermore, an additional test was introduced so to exclude those solutions where a subset of p human joints is part of subchain with less than p DOFs. In this case the robot would impair human movements by imposing unnatural kinematic constraints, violating the second kinematic requirement reported above. This test is called *HR-degeneracy test* (*Human-Robot degeneracy* test) since it applies to kinematic chains including both human and robot structures. The test is performed by recognizing the presence of subchains where two adjacent human joints are constrained in a 1-DOF subchain (Fig. 3.9(A) and (C)) or where all three adjacent human joints are constrained in a 2-DOFs subchain (Fig. 3.9(B)). The exhaustive list of such HR-degenerate primitives (reported in Fig. 3.9 could be retrieved from standard atlases of kinematic chains [67] and was re-obtained in a previous work concerning the enumeration of orthoses for a 1-DOF human joint [68].

3.2.4 HR-isomorphism test

Since the chosen method is based on the enumeration of suitable matrices of adjacencies, an explicit isomorphism test is mandatory.

Two kinematic chains K_1 and K_2 are said to be isomorphic if there exists a one-to-one correspondence between links of K_1 and K_2 such that any pair of links of K_1 are jointed if and only if the corresponding pair of links of K_2 are jointed. This means that from the graph corresponding to K_1 one can obtain the graph corresponding

to K_2 by only relabeling link numbers. Many attempts have been proposed to find an accurate and computationally efficient test for detecting isomorphisms. Most computationally efficient methods (as that described in [69]) move around the obstacle of explicit isomorphism detection between pairs of kinematic chains. They are based on group theory applied to graphs and exhaustively generate isomorph-free classes of graphs. These methods would give the exhaustive list of all non-isomorphic graphs and produce as output only one graph for each homomorphic group of graphs. Unfortunately, they are not directly applicable to the described problem since they do not take into consideration the constraints indicated in section IIIA and would not assure that a valid topology (i.e. a topology which respects the constraints imposed in section IIIA) would be obtained, requiring a re-labeling of the obtained graphs and the application of the whole set of inversions of the four serially connected body segments.

For these reasons the method of progressive enumeration of kinematic chains has been adopted. This method is not computationally efficient, but it produces only valid kinematic chains. However, the chosen method implies the need for an isomorphism detection algorithm to avoid the generation of two kinematically identical solutions.

A function defined on a kinematic chain is called an *index of isomorphism* if any given pair of kinematic chains is isomorphic if and only if the corresponding values of the function are identical. The methods for isomorphism detection can be classified into spectral methods and canonical code-based methods [70]. Spectral methods are based on the evaluation of the characteristic polynomial, eigenvalues and eigenvectors of TAM (i.e. properties of their spectrum). Since algorithms used for finding spectral properties can be solved in polynomial time, finding an index of isomorphism based on the spectral properties of matrices of adjacencies implies finding a polynomial-time algorithm for solving the isomorphism problem. Conversely, in canonical code-based methods a unique code is assigned to a kinematic chain, hence there is a unique way of representing it through a TAM. Checking two given kinematic chains for isomorphism reduces to checking the corresponding canonical codes for equality and the canonical code can be an index of isomorphism.

Methods belonging to this family are more reliable but may require an exponential time for creating the canonical code.

The *index of isomorphism* used in the present work is the characteristic polynomial of the Extended Adjacency Matrix (EAM) $A^{(d)}$ of order d, as also suggested in [70], which can be obtained from a TAM (A, of elements a_{ij}), by employing the following formula:

$$A^{(d)} = \begin{pmatrix} s_d(-\mathbf{a_1}) & a_{12} & ... & a_{1n} \\ a_{21} & s_d(-\mathbf{a_2}) & ... & a_{2n} \\ ... & ... & ... & ... \\ a_{n1} & a_{n2} & ... & s_d(-\mathbf{a_n}) \end{pmatrix} \tag{3.8}$$

where the vector $\mathbf{a_i} = (a_{i1}, a_{i2}, ..., a_{in})$ contains elements of the i^{th} row and s_d is the elementary symmetric polinomial of order d in the n variables of vector $\mathbf{a}$, defined as:

$$\begin{aligned} &s_0(\mathbf{a}) = 0 \\ &s_1(\mathbf{a}) = \textstyle\sum_i a_i \\ &\vdots \\ &s_k(\mathbf{a}) = \textstyle\sum_{j_1<j_2<\cdots<j_k} a_{j_1} a_{j_2} \cdots a_{j_k} \end{aligned} \tag{3.9}$$

Said $\mathbf{poly}_i^{(j)}$ the vector containing the normalized coefficients of the characteristic polynomial of matrix $A_i^{(j)}$, our test of isomorphism is such that two matrices A_1 and A_2 are isomorphic if each of the three equations in (3.10) are verified.

$$\mathbf{poly}_1^{(j)} = \mathbf{poly}_2^{(j)}, \text{ for } j = 0, 1, 2 \tag{3.10}$$

In [70] it is demonstrated that the simultaneous evaluation of the characteristic polynomial of both $A^{(0)}$, $A^{(1)}$ and $A^{(2)}$ has a reliability of 100% for kinematic chains consisting of up to 11 links.

For this reason this technique for isomorphism detection has been employed, being a very good compromise between reliability and computational efficiency (since it requires a polynomial time for assessing isomorphism).

However, when applying the isomorphism test to kinematic chains including both human segments and robot links, any isomorphism test produces false-positives

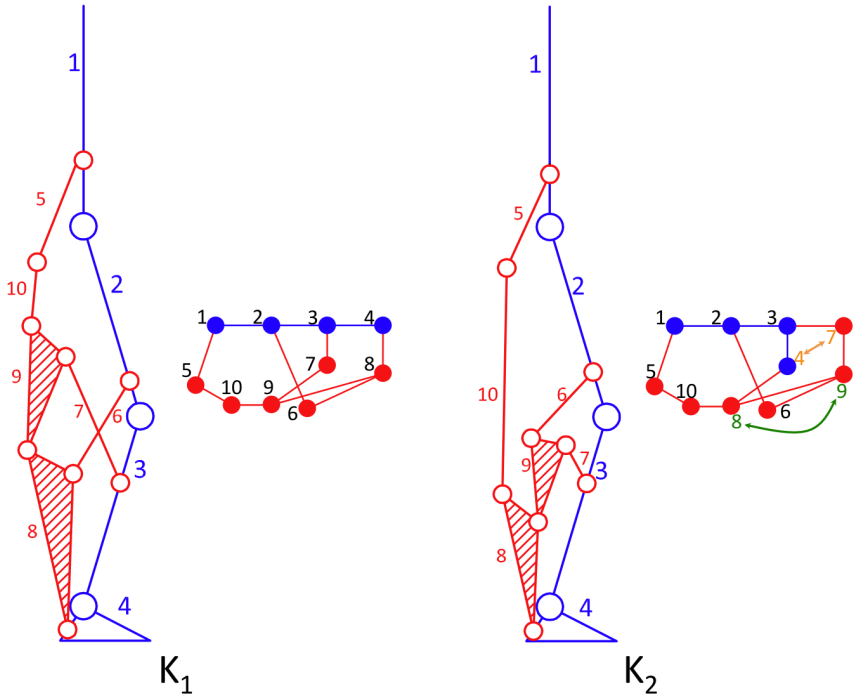

Figure 3.10: Two isomorphic but not HR-isomorphic solutions. The permutation which maps K_1 into K_2 is given by the permutation vector [1 2 3 7 5 6 4 9 8]. This permutation maps link 4 (i.e. foot) into robot link 7. It can be noticed that local kinematic properties around each human joint (for example DOFs of the subchain including each human joint) are different.

because robot and human links would be treated the same way. A false positive happens any time the permutation, which maps one graph into the other, affects any of the human joints. From robot design perspective, such solutions correspond to actual different wearable robots topologies and must not be discarded. An example of two isomorphic but not HR-isomorphic solutions is shown in Fig. 3.10.

To recognize such kind of solutions, a modified version of the isomorphism test has been introduced, the *HR-isomorphism* test (since it applies to kinematic chain including both human and robot structures). This test is described in the flowchart shown in Fig. 3.11 and basically consists on assessing, after a classical characteristic polynomial-based isomorphism test, whether one of the permutations p_{adm} contained in a properly defined set P_{adm} is responsible for mapping one kinematic chain into another. Every permutation vector contained in the P_{adm} set is of the form $p_{adm}(i)$=[1 2 3 4 perms$_i$(5:n)], where the function perms$_i$ provides the ith element of

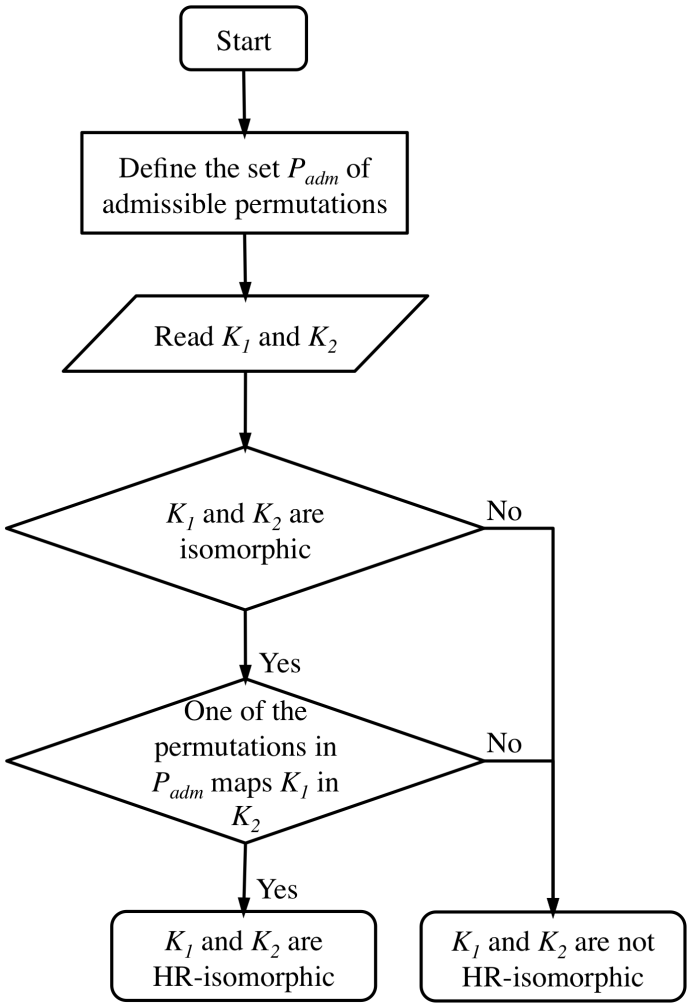

Figure 3.11: Flow chart of the HR-isomorphism test algorithm. The set P_{adm} contains the $r!$ permutations which only act on subgraphs including robot links. They are all defined by a permutation vector of the form $p(i)$=[1 2 3 4 perms$_i$(5:n)], where the function perms$_i$ provides the ith element of the set of permutations of the elements in the input array. These permutations are needed so to verify if one of the permutations in P_{adm} is responsible for mapping K_1 into K_2 thus assessing the *HR-isomorphism* between K_1 and K_2.

the set of permutations of the elements in the input array.

3.3 Results

The described algorithm has been implemented in MATLAB (The MathWorks, Inc.) and allowed to obtain the complete list of topologies describing the kine-

matic chains which consist of both human segments (a serial 4-link, 3-joint kinematic chain) and robot links. We limited our search to the space of robot kinematic chains with up to 7 links, since we expect that a robot with more links would result in a too complex and heavy system. Since in the enumeration process also human kinematic chain is taken into account, the highest order of generated graphs for the case of lower limbs wearable robots is $n_{MAX} = 11$.

3.3.1 Orthosis for a 1-DOF human joint

Preliminarily, the enumeration method has been applied to the simplest case, which consists of an orthosis for supporting a 1-DOF human joint. In this case, there is no reason to make a distinction between human segments and robot links, then the HR-isomorphism test does not need to be taken into account. Additionally, since there are no multiple human joints involved in the design, the HR-degeneracy tests is also expected not to provide any additional insights in the enumeration problem. In other words, it is expected to re-obtain the same results obtained in the general case of mechanism enumeration. The results of the enumeration process are reported in Table 3.3 and are coherent with the results obtained for the general case of mechanism enumeration [63], thus confirming the completeness and technical soundness of the chosen approach.

3.3.2 Four robot links

The simplest solution respecting the constraints defined in section 3.1 is composed of the basic set of 4 robot links, one for each body segment. In order to obtain a structure with 3 DOFs, two additional joints must be added to the basic configuration shown in Fig. 3.8. The two additional joints must involve each of the added robot links, so to avoid the presence of serial chains. Each of the added joint causes the generation of one independent loop. This implies a total number of 2 independent loops in the kinematic chain, which does not allow the robot to independently actuate each of the three human joints. Two independent solutions were found, as listed in Table 3.4, and shown in Fig. 3.12.

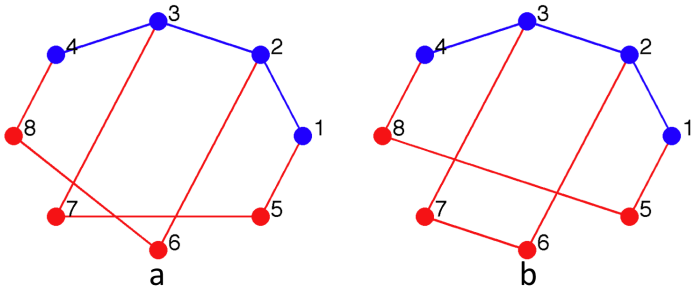

Figure 3.12: The two possible topologies with four robot links.

3.3.3 Five robot links

In this case the design implies the addition of 1 robot link and 3 joints to the basic kinematic structure shown in Fig. 3.8. The resulting kinematic chain has only 2 independent loops, and the total number of DOFs is 4. Four independent solutions exist, two of which are isomorphic but not HR-isomorphic (see Fig. 3.13 (c) and (d)).

3.3.4 Six robot links

The addition of two robot links to the basic kinematic structure shown in Fig. 3.8 implies the possibility of having a structure with either 3 or 5 DOFs (adding five or four joints respectively). In the case of 3 DOFs, 293 independent solutions

Table 3.3: Enumeration of kinematic structures for a planar orthosis assisting a 1-DOF human joint

Number of links (human + robot)	DOFs	Independent topologies
4	1	1
5	2	1
6	1	2
6	3	1
7	4	1
7	2	4
8	5	1
8	3	7
8	1	16

exist, while in the case of 5 DOFs, the number of solutions reduces to 6. In the case of 3 DOFs, there are 3 independent loops, while in the case of 5 DOFs only 2 independent loops are present, which excludes the possibility of independently controlling the motion of each human joint.

3.3.5 Seven robot links

In this case 3 robot links and 6 joints are added, and the compound kinematic chain has a total of 4 DOFs, with 3 independent loops, making it possible to independently control motion of each human articulation. The number of independent enumerated kinematic solutions is 754, as summarized in Table 3.4. The complete list of plausible topologies can be downloaded from the web page linked in the first page.

3.4 Particularization to a hip-knee orthosis

In the context of a collaborative research project funded by the EC commission, the Evryon project [71], the described approach has been particularized to the case of the design of a hip-knee orthosis. This was due to the fact that the problem described in the previous section, the design of a full exoskeleton for the lower body had a large possible number of solutions (a number of 293 topologies needed to be investigated for the minimal configuration respecting both the constraint on the number of DOFs and the constraint on the number of independent loops), which

Table 3.4: Enumeration of independent topologies for wearable robots for the lower limbs

Number of links (human + robot)	DOFs	Independent topologies
8	3	2
9	4	4
10	3	293
10	5	6
11	4	754

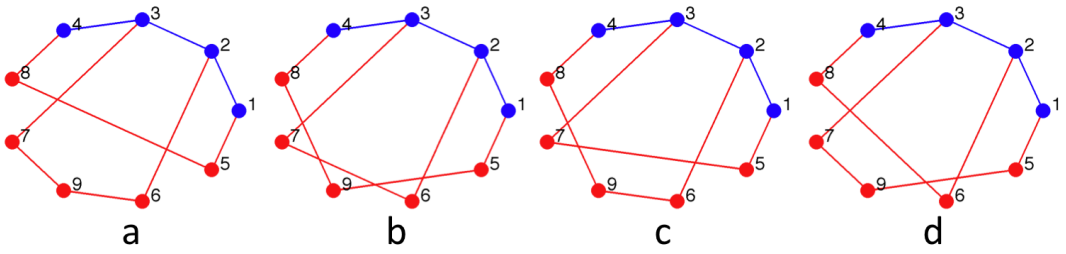

Figure 3.13: Possible topologies including five robot links. In (c) and (d) two isomorphic but not HR-isomorphic solutions are shown. The corresponding permutation is defined by the permutation vector [4 3 2 1 8 7 6 5 9], which basically implies wearing the same robot structure bottom-up. However the two structures are independent from the wearer's standpoint since they impose different kinematic constraints on human joints.

was not possible to exhaustively explore in a simulation-based optimization environment due to the strict timeline of that specific project.

The same steps used for the enumeration of the planar lower body wearable robot could be followed for this new enumeration problem. First the estimation of the minimum number of robot links suitable to provide an adequate mobility to the human+robot kinematic chain is conducted, and its results are shown in Table 3.5.

The problem is graphically represented in Fig. 3.14, where the usual representations are reported.

Table 3.5: Number of DOFs of the kinematic structure comprising both human segments and robot links, for the case of a wearable orthosis to support the hip and the knee joints (Human segments=3 (torso, shank, thigh), as a function of the number of robot links and joints added. Red background is for conditions with insufficient mobility ($DOFs < 2$), green background is for assemblies fulfilling both the constraint on DOFs ($DOFs \geq 2$), and the constraint on the minimum number of independent loops (subchains): $L_{ind} \geq 2$.

Robot links	**Robot joints**	**Total links**	**Total joints**	L_{ind}	**DOFs**
3	4	6	6	1	3
3	5	6	7	2	1
4	5	7	7	1	4
4	6	7	8	2	2
4	7	7	9	3	0
5	6	8	8	1	5
5	7	8	9	2	3
5	8	8	10	3	1

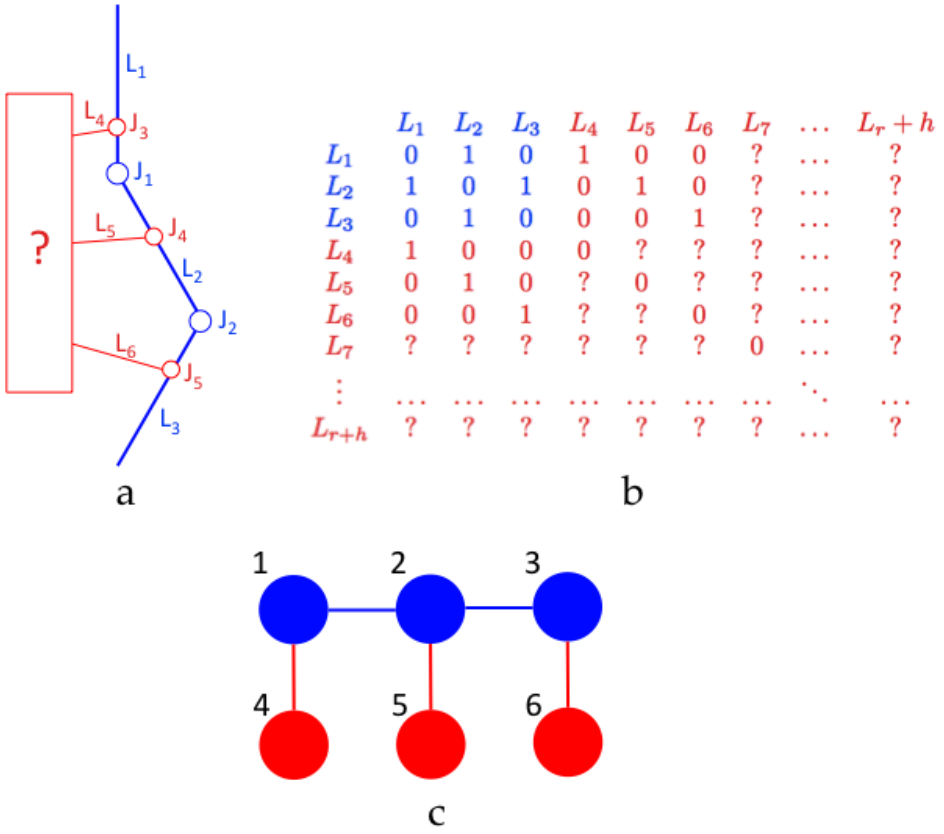

	L_1	L_2	L_3	L_4	L_5	L_6	L_7	...	L_r+h
L_1	0	1	0	1	0	0	?	...	?
L_2	1	0	1	0	1	0	?	...	?
L_3	0	1	0	0	0	1	?	...	?
L_4	1	0	0	0	?	?	?	...	?
L_5	0	1	0	?	0	?	?	...	?
L_6	0	0	1	?	?	0	?	...	?
L_7	?	?	?	?	?	?	0	...	?
⋮	...	...	...	...	...	...	...	⋱	...
L_{r+h}	?	?	?	?	?	?	?	...	?

Figure 3.14: Structural representation (A), generalized TAM (B) and graph representation (C) of the problem of structural synthesis of robotic orthoses assisting the hip and knee Flexion/Extension in the sagittal plane. Human articulations and segments are in blue, while robot links and joints are in red. In the adjacency matrix, the blue color is used to represent entries which describe the connectivity of human limbs (condition (1) in paragraph IIIA), while the red color represents fixed entries of connectivity between robot links or between robot and human links so to avoid situations where one of the human joints is constrained.

The application of the previously described set of functions for the: *(i)* generation of the set of admissible topologies based on the missing entries shown in Fig. 3.14 b; *(ii)* elimination of serial, bio-isomorphic and bio-degenerate solutions lead to the results summarized in Table 3.7, which comprises the cases of four and five robot links, selected from the lines shown in green in Table 3.5. The first configuration is the minimal one verifying the basic constraints imposed on the number of DOFs and on the number of independent loops in the kinematic chain. The second situation, including 5 robot links and 8 additional joints, allows instead to evalu-

Table 3.6: Parameters of the enumeration algorithm, for a hip-knee orthosis

Robot links (r)	Total links (n)	DOFs	Indep. loops	Total joints (f)	Fixed joints	Add. joints (e)	Open pars (l)	Comb. no. (used method) $\binom{l}{e}$	Total comb. (2^l)	Reduction ratio (%)
4	7	2	2	8	5	3	9	84	512	83.59
5	8	3	2	9	5	4	16	1820	65536	97.22

ate the possible improvements provided by introducing one redundant DOF in the kinematic structure of the wearable robot, compared to the number of supported human DOFs. Table 3.6 describes the cardinality of the number of generated solutions, which need to be successively filtered using the described criteria.

In Fig. 3.16 the 10 topologies are reported in their graph representation, while Fig. **??** shows arbitrarily defined morphologies, each of them corresponding to one topology.

3.5 Independent coordinates of the generated solutions

The atlas containing the set of admissible topologies is sufficient to implement a kinematic-based optimization to derive the fittest morphology in terms of some kinematic or kineto-static set of pararmeters. However, the kinematics of a robot is determined by actuators. In the described case, the choice of using only revolute

Table 3.7: Number of topologies generated and filtered for bio-isomorphism and for bio-degeneracy for the case of hip and knee orthosis

	4 robot links 2 DOFs	**5 robot links 3 DOFs**
Total combinations $\binom{l}{e}$	84	1820
Filtered including only closed chains	13	54
Filtered including only not bio-isomorphic	10	22
Filtered including only not bio-degeneracy	10	22

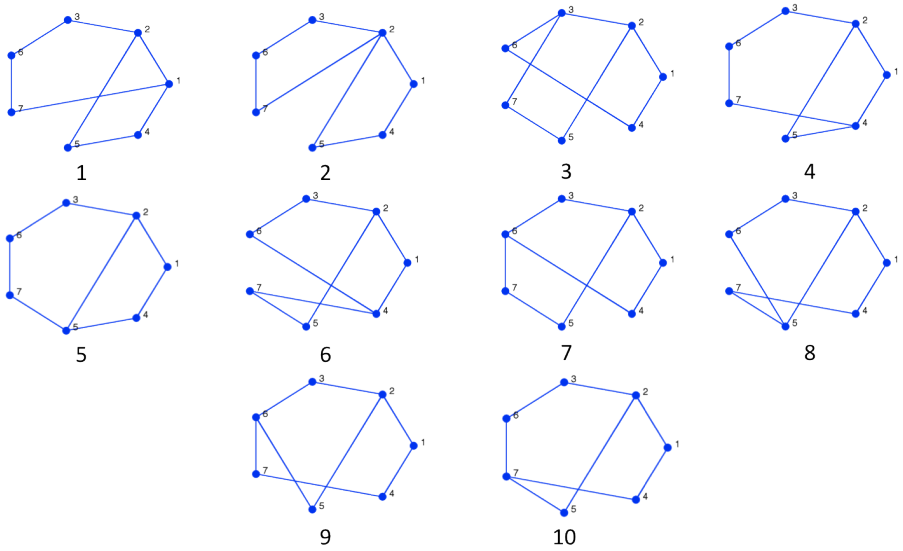

Figure 3.15: Atlas of topologies with 4 robot links, 2 DOFs, for the design of a planar orthosis assisting the hip and the knee Flexion/Extension. The same labeling scheme used in Fig. 3.14b is followed: (torso=link 1, thigh= link 2, shank= link 3); link 4 to 7 are robot links.

joints constrains the design to revolute actuators, co-located with one of the robot joints in the kinematic structures enumerated. However, all enumerated topologies are parallel chains, which imply that the number of joints is higher than the number of DOFs of the structure. It is then necessary to specify which joints to actuate. It is then necessary to specify which joints are actuated and which are instead not. Referring to the topologies enumerated for the case of 4 robot links and 2 DOFs (see Fig. 3.16, since the structure has a total of 2 DOFs, 2 actuators are required to determine the pose of the structure. Since the number of robot links in the solutions is equal to 5, the number of possible couples of actuator which need to be applied so to control the motion of the structure is given by $\binom{6}{2} = 15$.

However, not every one of the ten couples of actuators is able to completely determine the posture of both hip and knee joints. For example, topology no. 2 is composed of two distinct four bar subchains sharing the thigh segment. Each of these subchains has one DOF, contributing to the correct total of 2 DOFs for the whole structure comprising both human and robot links. However, the application of two actuators in two joints belonging to the same subchain (e.g. the one including

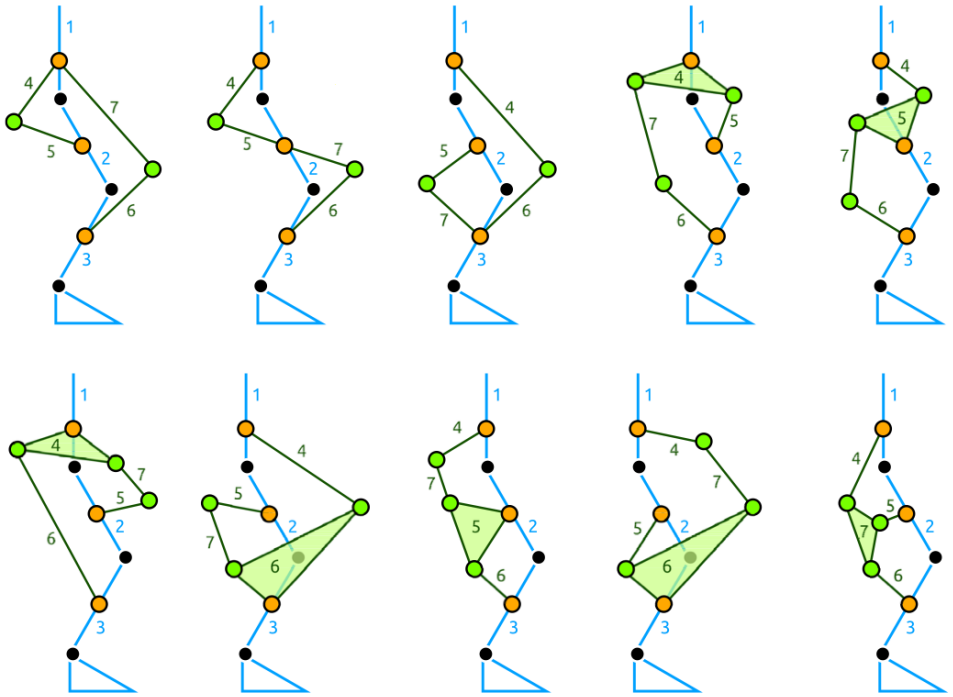

Figure 3.16: Structural representations of morphologies with 4 robot links, 2 DOFs, for the design of a planar orthosis assisting the hip and the knee Flexion/Extension, arbitrarily derived from the atlas shown in Fig. 3.16. In these pictures the same labeling scheme used in Fig. 3.14b is followed: (torso=link 1, thigh= link 2, shank= link 3); link 4 to 7 are robot links. Attachments with human joints are shown in orange, joints between two robot joints are in green.

the hip joint) would imply the impossibility of defining the pose of the other human articulation (in the given example the knee). In other terms, not every couple of joints is an independent coordinate for the kinematic function which maps the input angles with the hip and knee angles. This fact could just be not considered and a variable defining the id (index) of each of the ten couples of actuators used to locate the actuators for each optimization run. However, since the time for evaluating the fitness function is normally very high in optimization algorithms such as genetic algorithms and PSO algorithms, the computational benefits introduced by having the set of couples of actuators for each topology reduced at minimum are very high; for this reason they were calculated beforehand for each of the topologies.

The criterion is to prune the couples of actuators which are not co-located with joints defining independent coordinates. An algorithm was developed which among

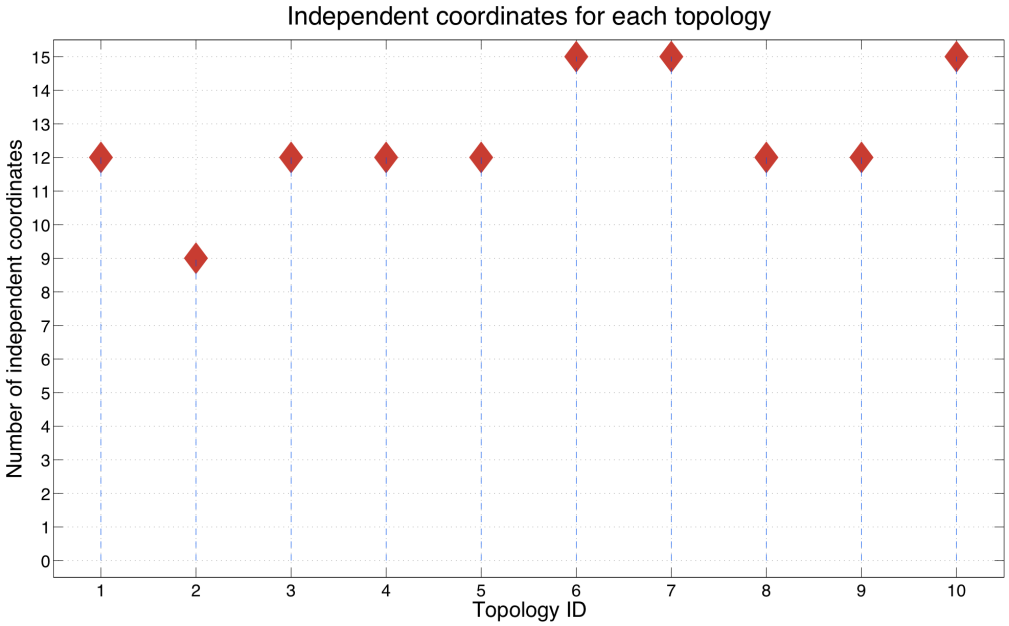

Figure 3.17: Independent coordinates of the topologies obtained for the design of the hip and knee orthosis. Topology IDs are coherent with the graphs shown in Fig. 3.16.

the whole set of 15 admissible couples of robot joints iteratively reduces the links participating in each single joint to a unique link. Then, the mobility analysis is performed using Gruebler's formula. Valid systems are those which after doing two of the described reductions have exactly 0 DOFs left.

The plot in Fig. 3.17 shows the results obtained with such algorithm, which can be verified by visual inspection. A reduction of the 40% of the total number of joints couples is achieved for topology number 2 (case of maximum reduction), while for six topologies the reduction is of the 20% (12 valid possible choices of independent coordinates out of a total of 15). For three topologies, no reduction on the number of couples of independent coordinates is possible.

Part II

Rehabilitation robots for the upper limbs

Chapter 4

Design and evaluation of a novel actuation architecture for upper extremity neurorehabilitation

The second part of this thesis focuses on robotics for post stroke neurorehabilitation for the upper extremity. Currently existing rehabilitation techniques use movement therapy as a tool to promote and strengthen neural plasticity, which is widely considered to be the biological basis underlying the process of recovery. In this perspective, robots provide an ideal platform for objective, reproducible, continuous measurement, control and delivery of movement therapy, and are increasingly being used in this context. However, two factors limit the widespread diffusion of such technology in everyday contexts.

On the one hand, the cost of the first commercially available machines is influenced by the necessity of developing components with a very high mechanical efficiency to guarantee back-driveability and safety in the reversed action mode. This chapter provides the description of the design and of the evaluation of a system including a novel actuation architecture which guarantees a safe and transparent interaction with a simplified and low cost mechanical structure.

On the other hand, many details on the relations between movement therapy, neural plasticity and recovery of motor function after stroke are still largely unknown. This poses substantial difficulties in the definition of a "golden standard" for movement therapy. The

conjunction of robotics technology and brain imaging techniques is potentially a powerful tool to systematically investigate and separate the factors influencing the process of recovery of motor function. In the next chapter, a pilot study conducted to validate the design of an fMRI compatible robotic device, to investigate the neural correlates of motor recovery through robot-mediated rehabilitation therapy after stroke is described.

4.1 Stroke, movement therapy and robotics

Stroke is a growing social problem in the most developed countries all over the world. According to [72], its incidence could grow to become soon the most common cause of death in the well developed world.

In the United States of America, stroke is the third leading cause of death and the leading cause of long-term or permanent disability. Each year about 795,000 people experience a new or recurrent stroke, 50% of them are left with a residual motor deficit. The estimated direct and indirect social cost of stroke amounts to 73.7 billion for 2010 only for US. Currently, a total of 6,400,000 stroke survivors live in the Unites States, accounting for 2,9% of the population more than 20 years old [73]. A common effect of this traumatic neurovascular injury is the loss of voluntary arm movement, with approximately 85 percent of stroke patients incurring acute arm impairment and 40 percent chronic impairment.

No "magic pill" exists for motor rehabilitation after stroke [74]. It is commonly accepted that the process of motor recovery after brain injuries is mainly determined by the biological phenomenon of neural plasticity. However, the contribution of some kind of motor activity to promote the phenomenon of neural plasticity has been disputed for a long time. Thus, it has been difficult to demonstrate convincingly the value of motor therapy for rehabilitation of motor function after neurologic injury. This is due to the fact that spontaneous recovery is occurring while therapy is delivered to patients, and the therapy ethically cannot be withheld from patients to allow for a controlled trial. Additionally, the compromise between variability of initial conditions and practically recruitable number of sample subjects in experimental studies implies that multisite assessment studies are necessary to validate the outcome of one therapy versus another.

However, animal studies on rats and squirrel monkeys provide evidence that active practice is critical to the recovery process [75, 76].

In clinical trials with moderately or mildly impaired human stroke participants, there is evidence that simple repetitive exercise may be superior to other types of therapy. Although the link between restoration of cortical maps and functional recovery is not entirely clear, it is likely that reestablishment of cortical maps for muscle activation is an important component of functional recovery.

In summary, the neurophysiological assumptions for the use of motor therapy in the stroke recovery process can be described as follows:

- Stroke recovery probably depends on neuroplasticity;
- Motor activity has an effect of promoting neural plasticity process;
- The stroke recovery process seems to exhibit the property of specificity, i.e. the benefits conferred to the not treated limbs are weak;
- The process of motor recovery has some common aspects with motor learning, even though the role of abnormal tone, spasticity and other stroke sequelae is unclear.

However, since the details of the neural processes underlying recovery are yet largely unknown, no generally accepted golden standard exists in the strategies of motor recovery after stroke. Several neurological therapeutic approaches are advocated and applied, proponents of each one claiming its superiority in efficacy over the others. hese approaches include:

- Bobath method, incdluding Neuro-Developmental Treatments (NDT) [77];
- Brunnstrom method [78];
- Proprioceptive neuromuscular facilitation (PNF) [79];
- Constraint Induced Therapy (CIT) [80].

Physical and occupational therapeutic programs vary greatly from one facility to another as a result of the adherence to different treatment concepts and philosophies [81, 82]. For example, in the NDT method the emergence of basic synergies is considered as a pathological and undesirable manifestation of spasticity which should be suppressed in order to enable the facilitation of normal physiological movements. Contrary to this concept, Brunnstrom encourages the development of the same basic synergies and related spasticity in the pre-synergic phase of motor recovery, following what is considered to be the natural sequence of motor recovery after stroke as first described by Twitchell [83].

The Bobath concept first explained movement dysfunction in hemiplegia from a neurophysiological perspective stating that the patient must be active while the therapist assists the patient to move using key points of control and reflex-inhibiting patterns. The International Bobath Instructors Training Association (IBITA) defines the current Bobath Concept as a problem-solving approach to the assessment and treatment of individuals with disturbances of function, movement, and postural control due to a lesion of the central nervous system, targeting both impairments and functional activiities. The concept targets both impairments and functional activities; successful goal acquisition in a given task must be practiced to improve efficiency of movement and promote generalization in everyday life. To date the Bobath concept and its related or derived methods are believed to be the most popular and widely applied methods in stroke rehabilitation [84]. Despite of that, recent studies [84] are still trying to systematically evaluate the efficacy and the outcomes of the most commonly employed strategies for the recovery of motor function. It was concluded that the Bobath Concept is not superior to other approaches and that no evidence is available for the superiority of any of the presently available approaches. Many methodological shortcomings are described for the studies reviewed and the need for further high-quality trials advocated. Also, the need to establish generally accepted evidence-based guidelines for the implementation of movement therapy is still advocated as a must for future trends in rehabilitation therapy.

A rehabilitation therapy enjoying an increasing popularity in the last decades

is the Constraint Induced Therapy (CIT). CIT was developed by Dr. Edward Taub of the University of Alabama at Birmingham. The rationale behind this therapy is that, after a stroke, the patient stops using the affected limb because they are discouraged by the difficulty. As a result, a process that Taub calls "learned non-use" sets in, furthering the deterioration, which is exactly what CIT seeks to reverse [80].

In chronic patients, Constraint Induced Therapy has been shown to result in substantial increases in the use of the more affected limb in activities of daily living (ADLs) [80]. Furthermore, CIT results in positive motor cortex reorganization [85] and has advantages relative to Neuro Developmental treatment of equal intensity [86].

Despite the plethora of treatment philosophies that provide different recommendations for the progression of treatment, type of movement and the context of activities, movement based rehabilitation therapy is founded on the interaction between the therapist and patient. This interaction can be classified into three broad categories [87]:

- Passive (or externally imposed) movement, which involves movement of the patient's joints by the therapist as the patient remains relaxed (therapist-in-charge mode.
- Active-assisted movement, which is used when the patient cannot complete a desired movement autonomously (*shared control between patient and therapist*);
- Active-resisted movement, which is mainly used by higher level patients and involves completing movements against resistance from gravity, additional weights, an elastic band, or the therapist.
- Bilateral movement; where the execution of a motor task is mirrored between the healthy and the hemiplegic arm.

The point of whether assisting the subjects during the execution of the motor task is quite crucial and differently interpreted in the several different rehabilitation methods. However, there is a generally accepted consensus that even though

unassisted movement may be the most effective technique in patients with mild to moderate impairments, actively assisted movement may be beneficial in more severely impaired patients.

Active assisted movements may be especially effective in the acute and subacute phases when patients are experiencing spontaneous recovery. If significant movement has yet to return, repeated attempts to use the limb could lead to "learned non-use", because the patients are discouraged by the poor performance of the limb [80]. In this case, active assisted movement may be superior to unassisted movement. The negative conditioning associated with poor performance is avoided, because the attempted movements are completed with external assistance.

A strong clinical evidence for active assistance is a study of 100 acute stroke participants that found significant decreases in arm impairment with an intervention of stereotyped active-assisted movement [88], demonstrating that such treatment was effective in participants with severe motor deficits.

All of the aforementioned therapies rely on repetition as a primary contributor to functional recovery, based on the assumption that the amount of functional recovery can be a function of the number of repetitions of movements in a therapy bout.

4.1.1 Robot-aided neurorehabilitation

In the described context, robots appear as an ideal platform for delivering movement therapy, which can alleviate the labor-intensive aspects of rehabilitation therapy implemented by human therapists and provide an objective and reproducible way to measure and control the evolution of therapy. In this way, the robot becomes a tool for the therapist. The therapist can perform an initial assessment of the patient?s functional level and determine the movement patterns that would be beneficial to practice. The skill of the therapist is then augmented with a device that can repeatedly replicate the movement patterns and free the therapist from this time-consuming activity.

Thus, a potential role for robotic devices is to facilitate highly repetitive, active-assisted movement training for more severely impaired patients, especially in the

acute and subacute phases of recovery. Additionally, robots provide an ideal platform for objective, reproducible, continuous measurement and control of therapy, which can be exploited to reduce the variability associated to the studies aimed at assessing the outcomes of one type of therapy versus another one. Initial research on robotic therapy for post-stroke rehabilitation was successful to provide a strong, objective evidence that nurture has a positive effect on nature: robotic therapy for the paretic limb facilitates motor recovery following stroke, apparently by harnessing and promoting brain plasticity.

The synergy between robotics and life sciences began in the 80s, when several researches started using robotics technologies for neuroscientific purposes. In those years many research groups tried to understand how the CNS plan and perform movements and many studies on human motion control have been carried out by measuring human motion properties through robotic platforms [89, 90, 91].

At the beginning of 90s some of these robots, widely used in neuroscientific studies, have been modified and applied in the rehabilitation field, to assist the patients in motor recovery after cerebral injuries. Since then, the machines for assisted motor therapy have been considerably improved and applied to different fields, such as fitness, sports training, sensory-motor training for maintaining performance of elderly people and physical medicine and rehabilitation, with special attention to neurological pathologies (neurorehabilitation).

An in-depth review of the state of the art of the machines designed for robot-assisted rehabilitation therapy is beyond the scopes of this thesis. However, it is important to highlight the main criteria behind the design of currently available robots, which need to be considered when designing a machine intended for robot-assisted neurorehabilitation. As highlighted in the previous subsection, two interaction modalities need to be guaranteed in movement rehabilitation therapy: the patient needs to be allowed to perform the motor task on his own, if he is capable of doing so; otherwise, the patient, especially in the needs to be guided or supported in the accomplishment of the motor task. The first interaction modality is called in the rehabilitation robotics literature pertaining *patient-in-charge mode*; the second modality is called *robot-in-charge mode*. The main goals behind the develop-

ment of rehabilitation robots are that of replicating the contribution of the therapist; then the described interaction modalities need to be guaranteed.

In this perspective, design criteria with substantial differences with respect to the solutions traditionally followed in industrial robotics need to be followed.

First of all, the minimization of moving masses is a primary requisite imposed as safety measure to minimize the risk of injury due to unexpected collisions. But in such scenarios safety is not the only special concern. The accomplishment of a motor task is always the result of a shared action between the human and the robotic counterparts. The high variability associated to human physiologic and pathologic performance imposes that robot behavior needs to include a high level of adaptability to human contribution. This adaptability is provided through the implementation of interaction controls, requiring the use of exteroceptive sensors and of a high bandwidth mechatronic system. Furthermore, the robotic system is demanded to be transparent to the users's movements during *patient-in-charge mode* so to minimally perturb the spontaneous and correct execution of motor tasks.

The accommodation of all these requirements represents the most generally accepted design difficulties, provided the currently available actuation technologies. Robotic implementations in the last 20 years tried to deal in several different ways with these requirements, given the currently available technologies.

In particular, the approaches pursuing back-driveability and dependability can be categorized in two main groups. The first one comprises high efficiency (i.e. very low friction losses) kinematic structures with low apparent inertia in the back-driven motion [38], [92], [93]. Such systems require accurate mechanical design (e.g. choice of low inertia actuators, minimization of the mass of moving parts, including actuators stators; high efficiency transmissions), precise fabrication of components and accurate system assembly. The second one comprises mini/macro systems, which consist of a large (macro) robot serially linked to a small (micro) robot. The macro-mini approach merges the benefits of a small high bandwidth robot for local operations, while at the same time retaining the versatility, speed and workspace dimension of a larger robot [94], [95]. A dedicated control strategy, exploiting the different dynamical properties of the two sub-systems, allows to achieve good re-

sults in terms of performance and safety/intrinsic compliance.

Other mechatronic solutions take advantages of novel basic components whose added value is to include compliant elements in the actuation architecture, such as Series Elastic Actuators (SEA) and Variable Stifness Actuators (VSA), to provide an intrinsic level of mechanical adaptability which positively influences safety in physical human-robot interaction. Such actuation solutions have been used to provide torque directly to human joints [96] or in implementations where actuators exca mechanical power by means of low efficiency mechanical transmissions [4].

Another category of solutions directly focuses on the development of discontinuous transmissions, based on electrorheological or magnetorheological fluids, such as in [97, 98], which are used in manipulators with multiple DOFs. These transmissions works as clutches, being engaged during *robot-in-charge mode*, when they transmit mechanical power between the actuator and the load, and disengaged during *patient-in-charge mode*, allowing to achieve good back-driveability properties with a relatively simple mechanical design. This provides also the advantage of mechanically decoupling the actuator from the load during *patient-in-charge* operation and to provide a hardware threshold to the maximum value of interaction torque, allowing for a transparent and intrinsically safe system.

4.2 CBM-Motus: PA-DP architecture

The design of robotic systems for assisted motor therapy is centered around some basic principles, which are intended to guarantee a wide set of dependable and effective interaction modalities with the human body, especially because the system is supposed to be applied on motor impaired users. In particular, the design of highly back-driveable mechanisms is a widely pursued approach for the development of dependable robots which allow a safe user-machine interaction in unstructured contexts.

A robotic system has been developed for neurorehabilitation therapies of the upper limb. It is composed of two subsystems: an actuated macro stage and a passive a mini stage, to which the patient is attached during operation. The compound system can work as a robotic neurorehabilitation device device in both interaction

modalities: *(i) patient-in-charge*, where the patient is allowed to move freely and the machine is supposed to be as transparent as possible and *(ii) robot-in-charge*, where the machine applies forces to determine the motion of the end effector.

The macro subsystem is a 2DOFs planar robot with isotropic and homogeneous inertia, which was described in previous work [99], actuated with two brushless motors and a transmission including timing belt and pulleys system. Since the mini subsystem is a passive, lightweight planar mechanism with a low apparent inertia, it is expected that the apparent inertia perceived by the user during the *patient-in-charge* interaction modality is reduced by the presence of this module.

However, despite interacting with a passive device is obviously the best solution in terms of transparency during *patient-in-charge* mode, during *robot-in-charge* mode it is required that the structure can apply forces to the subject's arm. This requirement is satisfied by this actuation architecture, since the passive module is designed so that it has two singular configurations. An adaptive controller drives the actuated system and can switch between the two interaction modalities. In the *patient-in-charge mode* the macro system moves so to compensate for the subject's movements, thus keeping the end-effector of the mini system in the center of its workspace. When it is necessary to switch to the *robot-in-charge* mode, the macro

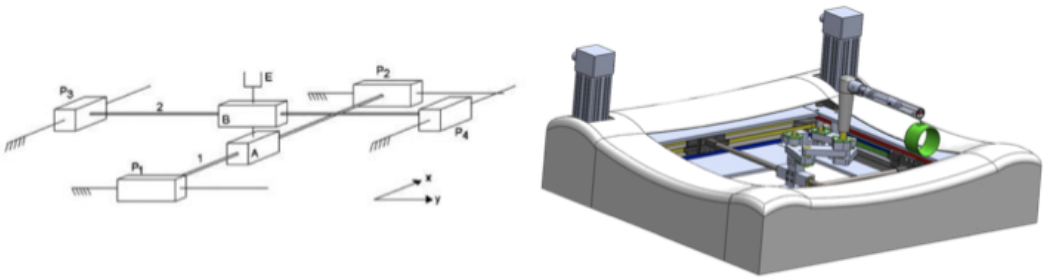

Figure 4.1: (a): Kinematic sketch describing only the macro subsystem, a 2 DOFs kinematic chain with orthogonal co-planar prismatic joints. (b): Mechanical design of the whole machine, including both the macro and the mini part. Rotations and torques applied by the two rotary motors are transferred to the end-effector of the macro-stage by means of eight pulleys and two timing belts. The mini-system (kinematic structure described later) is a passive, 5 bars, 2 DOFs linkage.

system drives the passive module in a singular configuration and that allows the system to apply forces in a semiplane, as shown in the following section.

4.3 Design of the passive module

The mini mechanism was designed in previous work [100]. It is composed of five equally long links (length 80 mm) and has 2 DOFs. Its end effector (point C in figure 4.2) is the handle, which is grasped by the patient. This mechanism has two kinematic singularities at the extremities of its workspace (the cuspidal points shown in figure 4.2). The links of this subsystem are dimensioned so that the workspace of the corresponding passive kinematic chain is wide enough to allow free movements of the patient when the system is in *patient-in-charge* mode, thus avoiding undesired reaching of the workspace boundaries. Links shape is also such that simple constraints are implemented between the joints angles, thus limiting the reachable work-space (WS) to that shown in figure 4.2.

When in *patient-in-charge* mode, the macro system is controlled so to compensate for the motion of the passive module, i.e. moving the position of the ground link of the mini module so that the handle still falls in the center of the workspace of the mini system. To this aim, it is necessary to measure at any time two independent variables, which describe the kinematic status of the mini system. In this case, it was chosen to measure the angles θ_4 and θ_5, through two absolute rotary encoders.

When the system is in *robot-in-charge* mode, it is necessary to drive the mini system to one of the cuspidal points where the machanism has a kinematic singularity. When the mini system is in the top one, the movements of the end-effector in the half-plane (x' ,y': $y' \geq 0$) are not allowed (this is a monolateral constraint), since the boundaries of the workspace are reached and the distal module rigidly holds this configuration until forces in the complementary half-plane are applied. In this configuration, the robot can thus apply force fields $\vec{F} = (F_x, F_y)$ in the same half-plane (such that $F_y \geq 0$). A similar behaviour occurs when the handle is in the bottom cuspidal point. In this case, downwards movements are blocked and downwards forces can be transmitted from the machine to the patient.

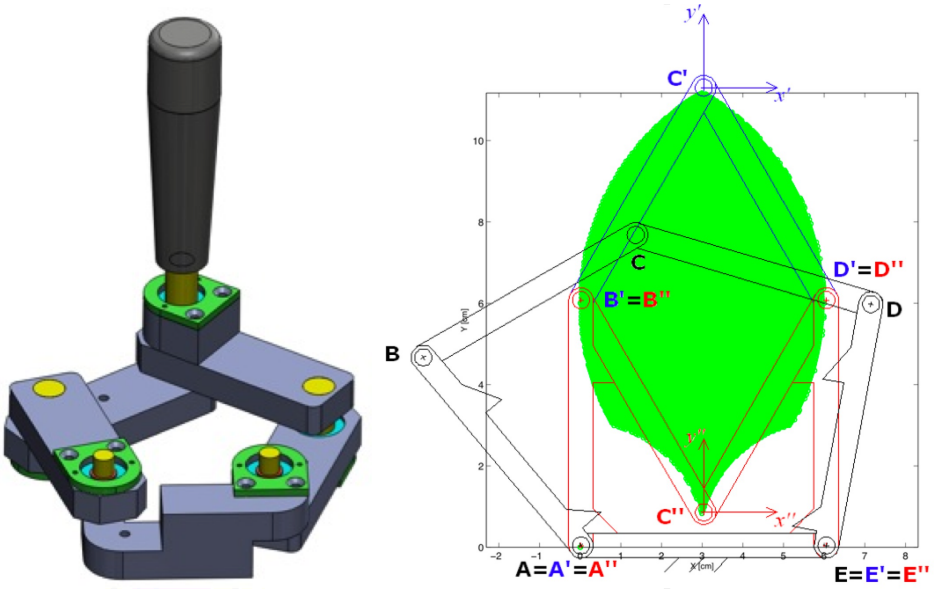

(a) (b)

Figure 4.2: (a) Mechanical drawing of the linkage comprising the Mini subsystem and of the handle. Mechanical stops which allow to obtain the desired workspace are not shown. (b) Sketch showing the Mini subsystem in different configurations: in black a general configuration typical of *patient-in-charge mode* is drawn; in blue and in red the linkage is drawn in both the singular configurations, where it is possible to apply forces to the subject (*robot-in-charge mode*). In the red configuration, the system can only apply forces downwards, and viceversa for the configuration drawn in blue. The green region shows the workspace of the linkage, which is calculated considering the mechanical stops used for safety.

4.4 Transparency during patient-in-charge mode

A major requisite for the design of robots for neuro-motor rehabilitation is transparency during *patient-in-charge* mode, which means that human-robot interaction forces should be minimized as much as possible when the patient is able to move autonomously.

Thus, it is important to estimate the forces applied by the patient, when he is free to move across predetermined trajectories. Maximum transparency would imply that the patient applies a zero force when he is freely moving.

In order to estimate the interaction forces, an inverse-dynamics model of the linkage has been developed, based on the kinematic recordings and on the knowl-

edge of the inertial parameters of the moving parts. The kinematics of the handle are derived by measuring the two independent variables, which describe the kinematic status of the mini system. The measured variables are the angles θ_5 and θ_5 of the five-bar linkage, through two absolute rotary encoders. Considering the equivalent 2 DOFs mechanism for the forward kinematics, it is possible to obtain the position of the end effector (handle) in the absolute reference frame:

$$x_H = x_{G1} + l_{G1} + l_5 \cdot \cos\theta_5 + l_4 \cdot \cos\theta_4 \tag{4.1}$$

$$y_H = y_{G1} + l_5 \cdot \sin\theta_5 + l_4 \cdot \sin\theta_5, \tag{4.2}$$

where x_{G1} and y_{G1} are the planar coordinates representing the position of point O (end effector of the macro system), measured through motors encoders.

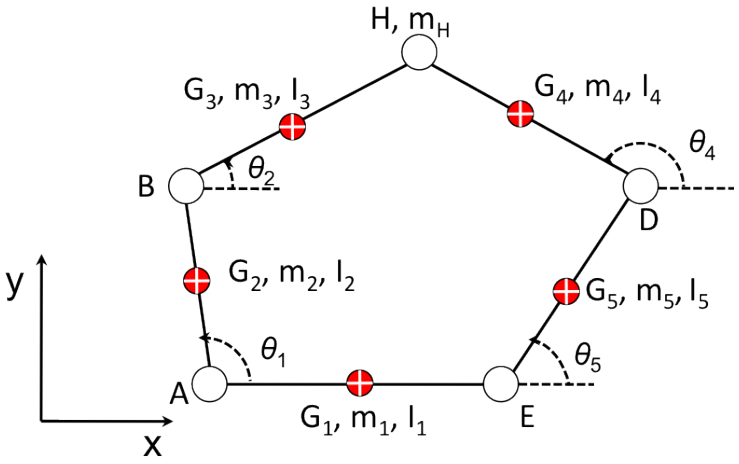

Figure 4.3: Planar kinematic model of the passive system

It is possible then to obtain the coordinates of the center of mass (x_{Gj}) of each of the j moving parts in the kinematic chain, in the absolute (inertial) reference frame. By considering for the sake of simplicity only the open 2-DOF kinematic chain consisting of bodies 4 and 5 (ref. Figure 4.4), it is simple to verify that

$$x_{G5} = x_{G1} + l_{G1} + d_{G5}\cos\theta_5 \tag{4.3}$$

$$y_{G5} = y_{G1} + d_{G5}\sin\theta_5 \tag{4.4}$$

$$x_{G4} = x_{G1} + l_{G1} + l_5\cos\theta_5 + d_{G4}\cos\theta_4 \tag{4.5}$$

$$y_{G4} = y_{G1} + l_5\sin\theta_5 + d_{G4}\sin\theta_4 \tag{4.6}$$

Similar equation stand for bodies 2 and 3, whose angles are calculated using inverse-kinematics.

For each body of the kinematic chain, a free-body diagram was derived and the Newton-Euler equation written as three scalar equations for each moving part of the linkage. By considering the open two-link kinematic chain shown in Figure 4.4, and by denoting as $F_{ij,k}$ the component along the k axis of the force applied by body i to body j, the following system of six equations is to be solved

$$\mathbf{A}(\theta)\mathbf{x} = \mathbf{B} \tag{4.7}$$

where $\mathbf{x} = [F_{05,x}, F_{05,y}, F_{45,x}, F_{45,y}, F_{H4,x}, F_{H4,y}]^T$ is the vector of unknown forces, $\mathbf{B} = [m_5\ddot{x}_{G5}, m_5\ddot{y}_{G5}, I_5\ddot{\theta}_5, m_4\ddot{x}_{G4}, m_4\ddot{y}_{G4}, I_4\ddot{\theta}_4]^T$ is the known vector of inertial forces and

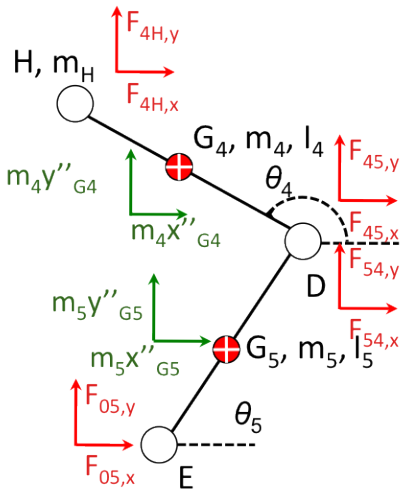

Figure 4.4: 2 DOFs serial chain of the five bar linkage. Absolute angles θ_4 and θ_5 are measured through encoders.

$$A^T = \begin{vmatrix} 1 & 0 & d_{G5}c\theta_5 & 0 & 0 & 0 \\ 0 & 1 & -d_{G5}s\theta_5 & 0 & 0 & 0 \\ 1 & 0 & -(l_5 - d_{G5}c\theta_5 & -1 & 0 & -d_{G4}c\theta_4 \\ 0 & 1 & (l_5 - d_{G5})s\theta_5 & 0 & -1 & d_{G4}s\theta_4 \\ 0 & 0 & 0 & 1 & 0 & -(l_4 - d_{G4})c\theta_4 \\ 0 & 0 & 0 & 0 & 1 & (l_4 - d_{G4})s\theta_4 \end{vmatrix}$$

is the coordinate-dependent matrix. The definition of the transpose of **A** matrix was reported for simplicity of print, as well as the use of the "shorthand" notation where $c\theta$ stands for $\cos\theta$.

Solving the system of equations in 4.7 allows to estimate the forces exchanged by the handle and the adjacent link ($\overrightarrow{F}_{H4}$). A similar system of equations can be simultaneously solved by considering the remaining (left) half-chain of the five-bar linkage, which provides as output the force vector $\overrightarrow{F}_{H2}$. Two equilibrium equations for the translation along the x and y axes can be written:

$$F_H, x = m_h \ddot{x}_H - F_{4H,x} - F_{2H,x} \tag{4.8}$$

$$F_H, y = m_h \ddot{y}_H - F_{4H,y} - F_{2H,y} \tag{4.9}$$

and thus the forces applied to handle by the patient can be estimated.

The described inverse-dynamics model provides an estimation of interaction forces without need of considering any force imposed by the macro (active) module, but only considering the resulting kinematics of the base link. This model was implemented so to estimate forces applied by subjects during free motion.

To this aim 14 young healthy subjects (24.6 $\pm$ 2.8 yo) were asked to perform free planar movements along predetermined directions (i.e. vertical, horizontal and diagonal as shown in Figure 1), at self-selected velocities. The kinematics were recorded at 66 Hz both from the distal (x_{G1} and y_{G1}) and from the proximal (θ_4 and θ_5) modules. Kinematics data were filtered through a 4-order Butterworth filter with a cut-off frequency of 6.6 Hz, before calculating numerically first and second order derivatives. The inertial parameters of the moving parts of the five-bar linkage are completely known since the parts have been custom-designed. The relevant parameters are summarized in table 4.1.

Table 4.1: Model parameters

Parameter	Value
l	80 mm
m_h	260 g
l_{G1}	45 mm
m_1	77 g
I_1	$2.3{\cdot}10^{-4}$ Nm^2
l_{G2}	42 mm
m_2	184 g
I_2	$7.5{\cdot}10^{-4}$ Nm^2
l_{G3}	45 mm
m_3	150 g
I_3	$5.6{\cdot}10^{-4}$ Nm^2
l_{G4}	42 mm
m_4	160 g
I_4	$5.6{\cdot}10^{-4}$ Nm^2
l_{G5}	45 mm
m_5	203 g
I_5	$1{\cdot}10^{-3}$ Nm^2

For each time sample the force applied by the subject was estimated. Along each of the four directions, subjects were asked to move along the same trajectory in both directions (i.e. back and forth). The distance between the starting and the desired point in the plane was set to 300 mm and subjects were asked to move at self-selected speeds. Each acquisition run for a fixed amount of time (10 s) and movements were successively segmented so to consider only the time-window when the user was actually moving. This segmentation was performed by considering as starting point a threshold corresponding to the 5 % of the maximum speed. The target was considered reached when the relative distance between target and current position did not exceed a threshold set to 10 mm for a time interval of least 0.5 s. Fig. 4.5 shows a histogram reporting the mean value of the modulus of applied force during free motion. Interaction forces have low values (around 0.3 N) and no statistically significant difference is noticeable in the averaged histogram across the four directions. Fig. 4.6 reports the values in Fig. 4.5, averaged over each subject, for each direction of motion. No significant dependance on movements direction

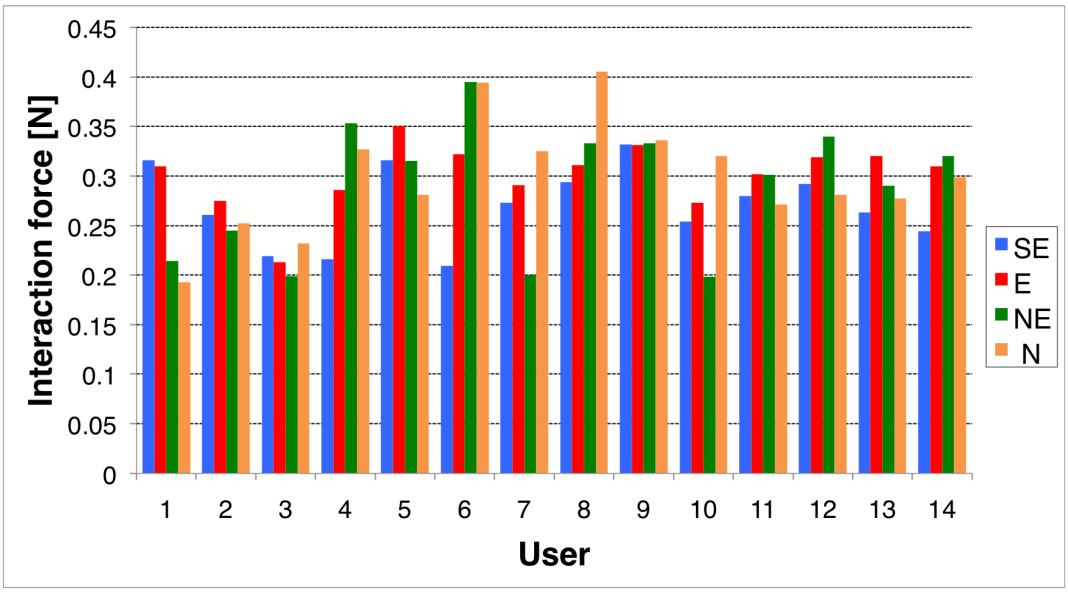

Figure 4.5: Magnitude of interaction force during free motion, for each of the 14 users, as a function of motion direction.

allows to conclude that the system is isotropic in human-robot interaction during the *patient-in-charge* interaction mode.

4.5 Conclusions

A method has been established to analyze the backdriveability of a planar machine intended for neurorehabilitation, which includes a novel macro-mini based actuation architecture: the PA-DP architecture. This architecture complies with the first of the two requirements for human-robot interaction in a neurorehabilitation scenario. The capability of the device to apply forces to the subject's arm guiding the subject in the accomplishment of the reaching task has been demonstrated in other experiments performed at Università Campus Bio-Medico di Roma, which are not reported in this thesis.

The main conclusion which can be derived concerning the backdriveability of the machine is related to its isotropy. The transmission used for the macro system, which includes pulleys and timing belts, has the disadvantage to provide an inher-

ent non-homogeneous resistance to motion emerging from friction present in the device. When reverse motion is applied in the direction of one of the prismatic joints, only half of the moving parts need to be moved, resulting in a reduced perceived resistance to motion. This is not the case of the whole system, which includes the lightweight, passive Mini stage.

Results show that there is not any statistically significant difference in the amount of force applied by the subjects to accomplish a self-paced reaching task between targets where reverse motion is requested only for a half of the kinematic chain (directions N, E and return S and W), when compared to targets where motion by both actuators of the Macro system is required (directions NE and NW and return SW and SE).

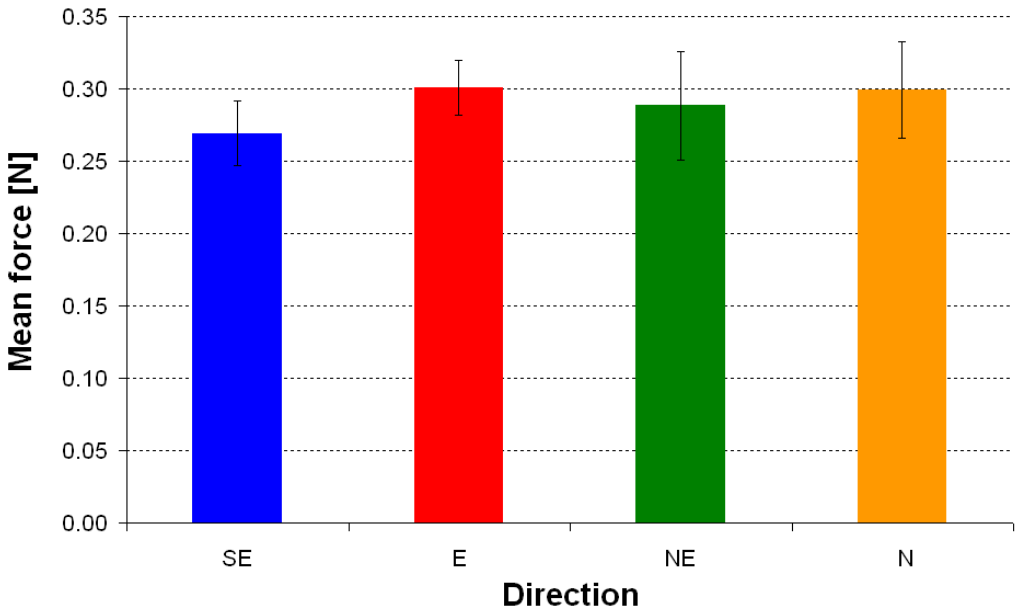

Figure 4.6: Absolute value of interaction force during two consecutive reaching tasks along predefined trajectories, averaged on all subjects. Error bars represent a confidence interval with $p < 0.05$.

Chapter 5

fMRI assessment of the neural correlates of motor recovery through robot-assisted rehabilitation therapy

5.1 Background on the neural correlates of motor recovery after stroke

In the last 15 years non-intrusive imaging techniques such as PET and fMRI have widely been employed to investigate on the neural correlates of motor recovery after stroke. Despite of that, there is still no general consensus on the details of the neural processes determining this recovery.

Studies addressing motor task-related activations highlighted that the process of neuro-recovery involves the restoration of activity in preexisting motor networks, such as the contralateral motor cortex in subcortical strokes and part of the infarct rim for cortical strokes [101, 102].

In patients, the volume of task-related activations was found to increase compared to controls, and shifts of task-related activity to non-motor and contralesional areas consistently documented. A number of studies demonstrated the correlation

between motor recovery and various indexes of brain activation, such as laterality measures [103, 104] or the total amount of additional brain regions activated [105].

These studies support the argument that the more "physiological" is the pattern of activations, the better is the outcome of the motor recovery process. Despite of that, other studies demonstrated that the contralesional hemisphere also plays an important role in the process of motor recovery, depending on the lesion region [106].

Another promising source of information about neural correlates of motor recovery after stroke is provided by functional connectivity MRI (fcMRI). Pioneer fcMRI experiments have demonstrated strong temporal correlations between fMRI time-series measured in spatially distinct but functionally related brain regions during resting state [107]. Such temporal correlations are considered as evidence of mutual exchange of information between different brain regions even during the so-called default mode and can be evaluated to generate functional connectivity maps. Recent experiments on rats have demonstrated that the recovery of sensorimotor function after a surgically-induced stroke correlates with restoration of the resting-state inter-hemispheric connectivity map related to a somatosensory region [108].

In humans some studies started to assess the problem of highlighting the changes in task-related functional connectivity between motor and somatosensory areas and the cerebellum, which are responsible for the process of neuro-recovery after stroke [109]. Functional connectivity analysis during resting-state in stroke patients recently showed that for the somatosensory network the reduction of inter-hemispheric functional connectivity significantly correlates with upper extremity motor impairment [110]. Furthermore, fcMRI experiments have demonstrated that the connectivity within intrinsic functional networks can be modulated by prior experience [111] or by the actual execution of a motor task [112]. The dynamics of these changes differs between patients and controls and can be used as a clinical tool to assess the progress of rehabilitation therapy or even, to predict the amount of recovery.

Most studies involving motor tasks in fMRI consider wrist flexion-extension

[113], single fingers flexion-extension [114] or tapping [115], ankle movement [116]. Many past studies did not employ any kinematic or isometric measurement and thus lack of the possibility to record or standardize the motor performance during the experiment, thus providing to incoherent or difficultly reproducible results.

In recent years various efforts were devoted to finding fMRI compatible solutions to standardize motor performances during fMRI experiments. The use of monoaxial gyroscopes as finger flexion-extension sensors [117]; of optical encoders in conjunction with RF filters [118], and even of EMG sensors with heavily shielded cables [119] has been documented. Also, MRI compatible force transducers were used [120] or custom-designed [118] to measure interaction force in isometric or dynamic tasks. Also MRI compatible robotic systems have been developed to apply forces during a hand gripping task [121], a reaching task in the horizontal [122] and vertical [118] plane, a 1-DOF linear movement involving elbow and wrist rotations [123].

To the best of the author's knowledge, no fMRI study involving stroke patients executing planar point-to-point movements has ever been reported in the literature. In this paper we describe the experimental setup and the preliminary results of a study addressing fMRI analysis of the modulation of the sensorimotor network connectivity of stroke patients during and after the execution of a planar reaching task. An fMRI compatible passive manipulandum was designed and used to measure the kinematics and to provide a real-time visual feedback of the motor task.

5.2 Methods

5.2.1 MRI compatible passive manipulandum and GUI

A planar 2 DOFs parallelogram manipulandum was developed as a passive fMRI-compatible version of the shoulder and elbow module of a robotic device [38], which is clinically employed as a rehabilitation tool for the upper extremity [124].

The structure includes a cylindrical handle, which is grasped by the subject during the experiment. A horizontal bar provides support to the subject's arm, which

is a crucial requisite to perform planar point-to-point experiments with stroke patients. The structure is mostly made of Delrin with a wood base on top of which the subject lies during the experiment providing the necessary stabilization to the system. Manipulandum links are made of Delrin and have a length of 100 mm. Low-friction rotation between links is obtained through low-cost plastic ball and roller bearings with glass balls (McMaster-Carr). The total system has a workspace of around 200 x 200 mm. The weight of the structure and of the subjects? arm is transferred to the horizontal bar by the handle, which is made of Teflon and can slip with low friction over the horizontal surface. The structure reduces the size available for the subject inside the bore. The maximum lateral and vertical measurements at the L3 vertebra level is of 380 and 220 mm, respectively.

Two MRI compatible sensors (S700 ShapeSensorMRI, Measurand Inc) are used to measure the rotation of the two distal links with respect to the mechanical ground. The sensors consist of two plastic boxes and of an optic fiber connecting them, whose light beam is sent over another 10-meter-long optical fiber coming out of the MRI room and then converted in an analogue voltage. No electrical signal is then brought into the MRI scanner by the registration device, thus providing intrinsic fMRI compatibility to the system. The symmetry of the structure allows then to compute the forward kinematics through the simple formula:

$$\begin{cases} x_h = l \cdot \cos(\theta_1) + l \cdot \cos(\theta_2) \\ y_h = l \cdot \sin(\theta_1) + l \cdot \sin(\theta_2) \end{cases} \tag{5.1}$$

The measured position of the handle is recorded at a frequency of 1 kHz. This information is displayed in real-time to the subject through a mirror projection system, in a graphical user interface resembling a "clock" game, which is very similar to the one used during the robotic therapy. In the fMRI experiment, the size of movements is limited to 5 cm from center to periphery and only the proximal half of the clock (including only W, SW, S, SE directions, with a random sequence) are used for the experimental protocol. These solutions are introduced in order to reduce the artifacts due to the distortion of the magnetic field introduced by the moving masses inside the scanner, as already documented in [122], and to facilitate

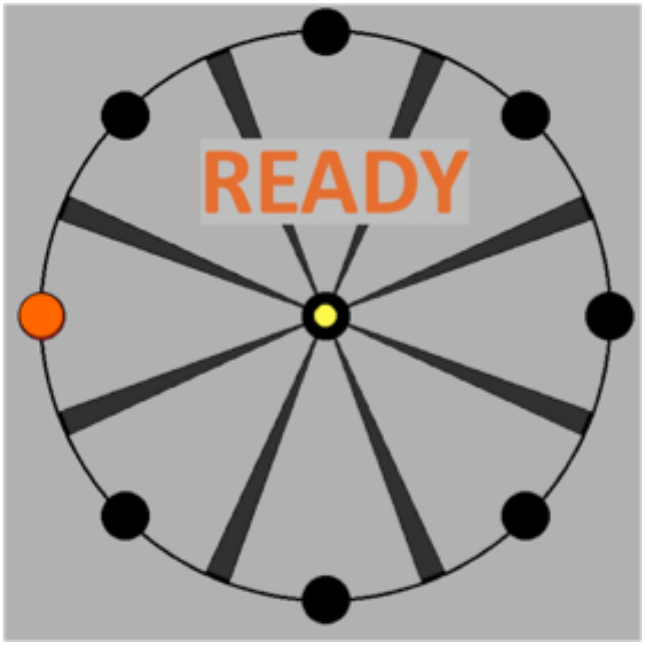

Figure 5.1: GUI used during the experiment. The yellow cursor indicates the current position of the handle; the orange cursor indicates which target to reach. The upper part of the screen is distal to the subject. Only half of the targets shown are used for the point-to-point movements. The READY message clues switching between the passive and the active condition. This clue is used only for the block-design protocol.

the motor task for stroke patients.

The GUI was used to guide the timing and the direction of a movement (when one of the targets was yellow-colored) and to provide feedback on the movement execution. A new target was displayed every 3.2 s, independently of the success or failure of the previous reaching task. Another information was provided by the target color, which changes from yellow to red right at the time by which the movement should be completed. This event took place 1.6 seconds after the display of a new target. The subjects were trained for a few minutes before the experiments. All subjects reported finding the GUI to be intuitive. During the experiment, visual feedback was also used to suggest to switch between active and passive states, as described in more detail in the next section and as shown in Fig. 5.1.

5.2.2 Experimental protocol

Three different scanning protocols were implemented for the study and will be described in distinct sections.

5.2.2.1 Block-design experiment with healthy control subjects

Two healthy control subjects (male, 59 and 63 years old) with right-hand dominance were asked to participate to a block-design experiment where they alternated between a control and an active block. During the control block, the subjects were asked not to move their hand and to visually follow the movements of the cursor in the screen. The cursor was programmed to move towards the target with a straight minimum-jerk trajectory. During the active block, the GUI displayed the current handle position. Visual messages in the screen were used to communicate to switch between these two modes. Five control blocks of 32 s were alternated to four active blocks of the same duration, for a total duration of the experiment of around 5 minutes, as detailed in Fig. 5.2. Each of the control subjects performed the experiment twice, once using their right hand and the other one with their left hand.

5.2.2.2 Functional connectivity experiment with one healthy control subject

A third healthy control subject underwent a different protocol, involving the following types of scan: 1) resting, 2) continuous motor task, 3) continuous control task. During resting, the subject was only asked to fix a black cross over a grey background for 6 minutes. During continuous motor task, the subject was asked to move their upper extremity as prompted by the GUI, i.e. a new point-to-point movement every 3.2 s, for 6 minutes. During the continuous control task, the subject was asked not to move his hand and to visually follow the movements of the cursor in the screen, for 6 minutes. These scans were sequenced as shown in Table 5.1.

5.2.2.3 Experiments with stroke patients

Two chronic stroke patients were enrolled for this study (age: XX). They both had a subcortical stroke in their right-hemisphere (left hemiparesis) and took part

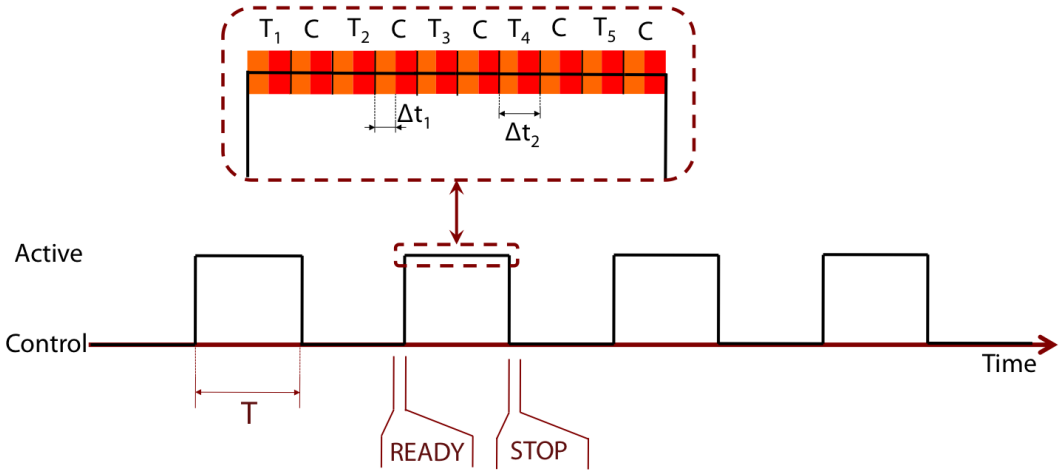

Figure 5.2: Timeline describing the protocol of the block design experiment. The black curve indicates the state of the experiment (control vs. active), the red arrow is the Time axis. The ready and stop messages appear right before and immediately after each active block, whose duration T is 32 s. During an active block, 6 different peripheral targets T_i appear, separated by the return to the center. The target is orange for $\Delta t_1 = 1.6$ s and becomes red immediately after, and stays in this status for the same amount of time Δt_1.

to the experiment a few days before being administered a 12 weeks robot-assisted rehabilitation therapy program. A number of experimental difficulties rose when trying to perform the fMRI experiment with the paretic limb of patients. They had difficulties in grasping the handle, and then, so to allow the execution of the experiment, the dorsal part of their hand was fixed to the handle with a Velcro strap. In this configuration the hand of the subject would be in contact with the horizontal surface and increased the resistance to motion felt by the subject. For this reason a Teflon disc was placed underneath the hand of the patient, to reduce friction and to facilitate a smoother motion. The level of impairment of patients was nevertheless such that they could not successfully perform most of the movements prompted by the GUI in the active phases, but they could just attempt to move their paretic limb in the horizontal plane without much controlling this movement. Hence, the kinematic features of their motor performance are not standardized to those measured in controls. However the two patients performed the various scans as described in Table 5.1.

5.2.3 Analysis of fMRI data

Blood Oxygen Level Dependent (BOLD) images were acquired in a Siemens Trio 3 T scanner in conjunction with a 12-channel Siemens Tim RF coil using a T2-weighted gradient echo, EPI sequence (repetition time [TR]=2 s; echo time [TE]=30 ms, flip angle [α]=90, field-of-view [FOV]=220x220 mm; matrix size= 72x72 voxels, in-plane resolution= 3.125 mm, slice thickness= 4 mm, slice distance= 4.8 mm, number of slices= 32). BOLD image collection was preceded by 5 dummy scans to allow for equilibration of fMRI signal.

Structural volumes were also collected for anatomical localization and surface reconstruction using a T1-weighted magnetization prepared rapid gradient echo (MP-RAGE) sequence (TR=2.53 s, TE= 1.64 ms, α=7, FOV=255x255 mm; matrix size=256x256 voxels, in-plane resolution=1 mm, slice thickness=1 mm, number of slices= 256). In stroke patients a Fluid Attenuated Inversion Recovery (FLAIR) image was acquired to provide anatomical localization of the lesion (TR=9 s, TE= 82 ms, α=120, FOV= 240x240, matrix size= 640x560, in-plane resolution= 0.375 mm, slice thickness= 5 mm, number of slices= 36). A standard fMRI processing stream was employed, using FSL and AFNI software on a CentOS machine. Standard algorithms for slice-timing and motion correction were used to temporally and spatially resample the BOLD data. A Gaussian smoothing filter (FWHM=6 mm) was afterwards applied to match the spatial scale of the hemodynamic process. These preprocessing steps were applied to all BOLD 4D volumes acquired; while depending on the kind of experiment a different set of subsequent processing steps followed.

5.2.3.1 Task-related activations in controls

The smoothed time-series acquired during experiment 1 were normalized to the average value across time and de-noised using an Independent Component Analysis (ICA)-based algorithm to exclude the components of variance recognized as noise [125].

A General Linear Model (GLM) was constructed, using as single regressor a succession of boxcar functions time-shifted around the onset time as defined in the block-design experimental protocol, with a linear offset. The result of such decon-

Table 5.1:
SCANS SEQUENCE FOR THE FIRST EXPERIMENTAL PROTOCOL

Kind	Name	Duration
Resting	R_1	6 min
Continuous motor task	Mvt	6 min
Resting	R_2	6 min
Structural scans		$\simeq$ 30 min
Resting	R_3	6 min
Continuous control task	Cont	6 min
Resting	R_4	6 min

volution is (voxel by voxel) the coefficient of the fit between the measured and a parametric predicted response, corresponding to a selective activation in response to the experimental stimulus (i.e. performing planar horizontal reaching movements). The z-scores corresponding to such correlation were registered to the Montreal Neurological Institute (MNI) 152 template and averaged across the subjects. The resulting averaged z-maps were thresholded (z=5, corresponding to a significance value $p < 0.05$, corrected for multiple comparisons using a highly conservative Bonferroni correction over the whole brain, around 200000 voxels) and afterwards segmented on an anatomical basis, following the definitions in the Juelich Histological Atlas [126] and in the Cerebellum Atlas [127].

Table 5.2 gives an overview of the regions where significant activation was found in control subjects. A view of the activation map found in controls during the planar reaching task is shown in Fig. 5.1.

5.3 Preliminary results

The experiments in controls revealed an extended activation pattern including several different areas within and outside the sensory-motor network. This activation pattern was segmented on a functional-anatomical basis, as shown in Table 5.2, which shows activation corresponding to right upper extremity movement. Activation peaks in the CL $M_1$are more medial when compared to what obtained for a

previous experiment involving only wrist movements. This means that, despite the limited extent of the point-to-point movement, subjects did not rely only on wrist flexion-extension movements, as instructed to do.

Cortical activation is mainly in the contralateral hemisphere ($M_1$and SS), with the exception of PM, SMA, and PP, which show a bilateral activation. Bilateral activation was also found in BA44 (pars opercularis of the inferior frontal gyrus (IFG)) and in the anterior section of the insula, confirming previous findings documenting the involvement of such nonprimary motor areas in motor control and manipulation for different tasks [128], [129].

A representative axial section representing activation in different cortical areas is shown in Figure 5.3a. Task-related activation was also found in the contralateral thalamus and in the ipsilateral cerebellum lobule V, and bilaterally in lobules VI and VIII. A representative coronal section showing task-related activation in the cerebellum is shown in Figure 5.3b.

For each of the seed regions defined as shown in Table 5.2, a 50-voxel region was created starting from the region's centroid and including the most significant contiguous voxels. The defined masks were used as regressors of interest for the functional connectivity analysis during both resting state and continuous motor task.

Functional connectivity to seed region CL_BA4 , (ipsilesional for stroke subjects) and to IL_BA4 was considered both in R_1, in Mvt and in R_2. Figure 5.4 shows the connectivity map and the connectivity difference maps obtained, for the CL_BA4 seed region.

In order to quantify the strength of connectivity (for R_1) and of connectivity difference (for Mvt-R_1 and R_2-R_1), a first measure was introduced: the average value of z-scores within the Sensorimotor Network (SMN, defined from anatomical atlases [126], and split in the two hemispheres, values reported in Table 5.3).

On a more regionally-specific basis, average z-scores values were calculated in medial and lateral portions of M1, in PM and SMA. The same anatomical masks used for the segmentation of task-related activations (Table 5.2) were used to define these regions in MNI space. Connectivity values are reported in Table 5.4.

Table 5.2:
CORTICAL SEED REGIONS FOR RIGHT ARM MOVEMENT (BASED ON $p_{corr} < 0.05$)

Seed Code	**Description**	**Vol [ml]**	**z-weighted centroid coords**
CL_BA4	Contralateral (CL) Primary Motor Cortex (M1)	6.37	(62,50,64)
CL_BA6_med	CL Supplementary Motor Area (SMA)	2.22	(46,60,65)
CL_BA6_lat	CL Pre Motor Cortex (PM), dorsal	5.04	(59,55,69)
IL_BA6_med	Ipsilateral (IL) SMA	0.92	(43,61,68)
IL_BA6_int	IL PM, dorsal	0.32	(35,59,73)
IL_BA6_lat	IL PM, dorsal	0.24	(26,59,66)
CL_BA7	CL Posterior Parietal Cortex (PP)	12.9	(55,33,65)
IL_BA7	IL PP	3.98	(37,29,65)
CL_BA44	CL pars opercularis of IFG (BA44)	1.18	(72,68,48)
IL_BA44	IL BA44	2.02	(18,69,44)
CL_BA1_2	CL Primary Somatosensory (SS)	6.67	(67,48,63)
IL_CB_V	IL Cerebellar (CB) Lobule V	3.98	(38,37,27)
IL_CB_VI	IL CB Lobule VI	5.52	(33,35,24)
CL_CB_VI	CL CB Lobule VI	3.17	(57,34,25)
IL_CB_VIII	IL CB Lobule VIII	1.4	(36,35,10)
CL_CB_VIII	CL CB Lobule VIII	1.42	(56,35,10)
CL_Thalamus	CL Thalamus	0.82	(53,52,39)

The connectivity map in the R1 scan, with seed region in M1, highlights the whole sensorimotor network, with a bilateral connectivity pattern, which includes dorsal BA4 and BA6 (both patients and control), and SMA (with the exception of one patient).

The contrast between connectivity in Mvt and in R1 conditions reveals in the control subject a general decrease of inter-hemispheric connectivity. A significant decrease is concentrated in the lateral portion of (ipsilateral) $M_1$and PM, in accor-

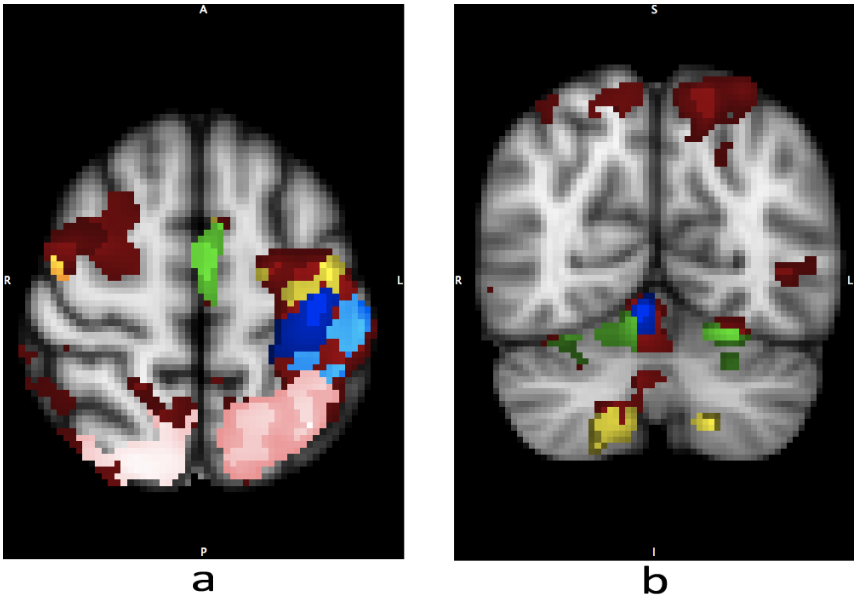

Figure 5.3: (a) Axial slice (z=67 in Talairach space) showing averaged z-scores (lower threshold z=5, $p_{corr} < 0.05$) representing task-related activation in control subjects, for a right upper extremity movement. Region specific (Blue (M1), yellow (PM), green (SM), pink (PP), lightblue (SS)) brightness z-maps (brighter represents a higher level of significance) are superimposed on the red z-map, which represents region aspecific activation. Coronal slice (y=31). Blue: Lobule V, Green: Lobule VI, Yellow: Lobule VIII.

dance with the literature demonstrating this decrease for a different motor task [112]. The same result, but with variable amount of significance, was obtained for both patients. One of the patients (Pt 2) showed also an enhanced connectivity in the lesioned hemisphere, concentrated in the PM cortex and most significantly in

Table 5.3:
CONNECTIVITY TO CL_BA4 IN THE SMN (BASED ON $p < 0.05$, $|z| > 1.65$)

Subject	R_1		Mvt-R_1		R_2-R_1	
	CL	IL	CL	IL	CL	IL
Control	**4.5**	**4.2**	-0.2	-1.1	0.5	**1.8**
Pt 1	**8.4**	**9.1**	-0.1	**-7**	**-6.8**	**-5.4**
Pt 2	**4.5**	**3.8**	**2.3**	**-1.9**	**2.5**	**2.2**

Table 5.4:
CONNECTIVITY TO CL_BA4 IN BA4 AND BA6 (BASED ON $p < 0.05$, $|z| > 1.65$)

Subject	Scan	BA4_lat		BA4_med		BA6_lat		BA6_med	
		CL	IL	CL	IL	CL	IL	CL	IL
Control	R_1	**6.83**	**5.46**	**4.04**	**3.18**	**4.31**	**4.15**	**5.68**	**5.62**
	Mvt-R_1	-0.8	-1.61	0.9	**2.09**	-0.13	**-2.58**	-1.59	-0.81
	R_2-R_1	0.5	0.57	-0.4	0.86	0.01	0.33	**-4.91**	**-3.28**
Pt 1	R_1	**12.42**	**10.83**	**11.66**	**12.75**	**8.99**	**8.01**	**7.53**	**6.39**
	Mvt-R_1	**-2.22**	**-9.58**	-1.62	**-6.37**	-1.2	**-4.9**	-1.56	-0.35
	R_2-R_1	**-6.81**	**-6.97**	**-9.9**	**-10.4**	**-6.18**	**-4.94**	**-5.14**	-1.48
Pt 2	R_1	7.67	**7.17**	**3.23**	**2.28**	**4.39**	**1.8**	0.6	0.91
	Mvt-R_1	1.46	**-3.4**	**4.34**	**3.11**	**4.9**	**1.91**	**8.18**	**6.55**
	R_2-R_1	1.62	-0.91	**3.08**	**4.91**	**3.59**	**3.79**	**4.97**	**5.31**

SMA.

The R_2-R_1 contrast was calculated to assess whether a form of "retainment" in the functional connectivity maps was introduced by the experience of the motor task. No major trend describing the change of connectivity change is consistent across patients. In both patients the decrease of connectivity in ipsilateral motor cortex (lateral part) is slightly retained also in the R_2 task, while this is not the case for the control subject. This trend has different significance in the two subjects (decrease of connectivity changes from -9.58 to -6.97 for Pt 1 and from -3.40 to -0.91 for Pt 2).

5.4 Preliminary design of an actuated device

The results obtained with the passive manipulandum were successful in demonstrating the feasibility of performing experiments in the fMRI scanner having subjects perform planar reaching tasks of limited extent (5 cm). Previous studies [122, 130] involved similar 2 DOF planar reaching movements in fMRI, but their mechanical design was such that they would not be usable with physically impaired

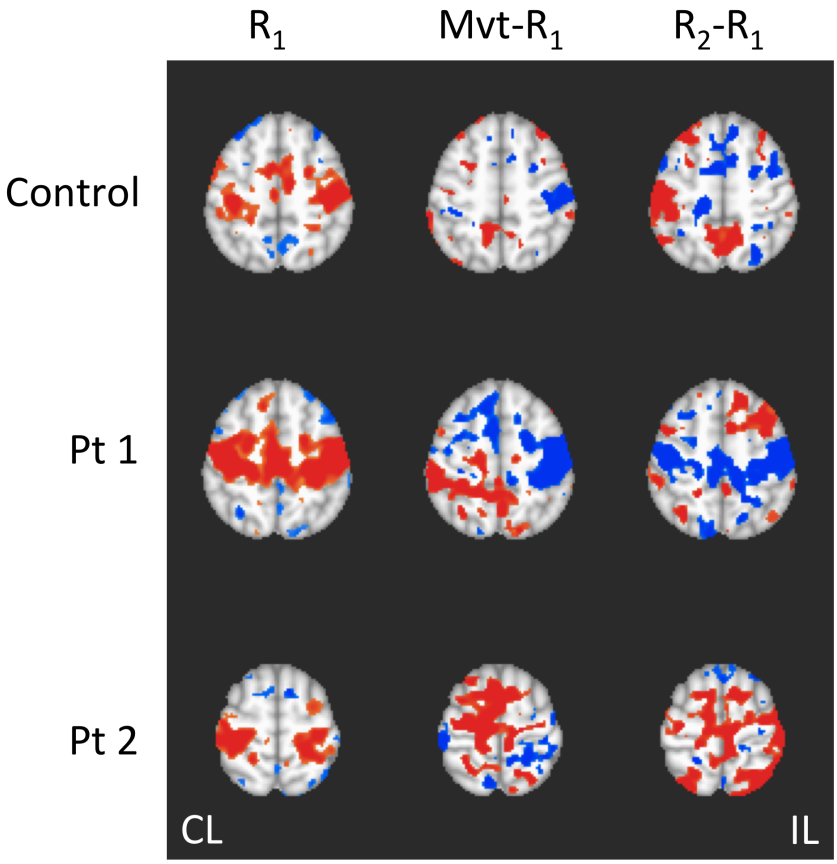

Figure 5.4: Axial slices ($z = 65$ for control and Pt 1, $z = 62$ for Pt 2) showing functional connectivity to CL_BA4. Red darkness scale (darker indicates a higher significance) indicates positive correlation (R1) or increase in connectivity (difference maps), while blue indicates negative correlation (R1) or decrease in connectivity (difference maps). Minimum significance threshold is set to 5 and -5. ($p_{corr} \leq 0.05$). Patients moved paretic, left upper extremity. Control moved right upper extremity (images mirrored, $-x$).

patients. The use of the described device was demonstrated instead also with very severely impaired subjects. However, a common motor deficit in stroke patients with different levels of impairment is represented by an increased difficulty in performing in the distal direction, compared to the proximal direction. This implied that often impaired subjects could move in the south direction, but then would find difficulties in going back to the center and to continue the experiment by starting another reaching movement.

An actuated mechanism would be a novel and interesting tool, both to investi-

gate neural correlates of recovery after neurological injury, like in the clinical study described in the previous part of this chapter, but also to develop force perturbation experiments on healthy subjects, to investigate several hypothesis on the neural mechanisms underlying control of these reaching movements. However, the design of robots suitable to be integrated in fMRI environments is a challenging task, since many of the most widely used elements both to provide actuation and sensing are not MRI compatible.

5.4.1 fMRI compatible mechatronics

The literature generally agrees about the definitions of MR safety and compatibility of an object or device. A device is MR safe when it does not present any additional risk to the patient in the MRI environment. This definition of MR safety does not refer to any potential effects of the device on the MR images, i.e., a MR-safe device may affect the quality of the images. The effect of the device on the MR images is included in the definition of its MR compatibility. A device is MR compatible when, in addition to being MR safe, its presence and/or operation does not significantly affect the quality of the MR images and, inversely, its operation is not affected by the MR scanner.

Materials most often used in the construction of conventional robotic and mechatronic systems are ferromagnetic (e.g., carbon steel) because of their desirable mechanical properties, such as strength, rigidity, and machinability. However, these materials are, in general, not suitable for the construction of MR-compatible devices. Ferromagnetic materials are subject to strong magnetic forces and can become potentially dangerous projectiles if they are placed close to the MR scanner without being securely attached to a fixed structure. Another source of MR-incompatibility is the generation of eddy-currents inside conductive materials, such as aluminum, which may cause image artifacts or unwanted material heating.

Materials suitable for MR-compatible devices are nonmagnetic and nonconductive. Combinations of plastic, ceramic, fiberglass, carbon fiber, and other composites have been extensively used for the development of MR-compatible systems. A main drawback associated with many of these materials is their limited struc-

tural stiffness, with obvious negative effects on the manipulability and accuracy of robotic devices. However, in many mechatronic systems developed for MRI applications, a limited number of metallic parts (such as aluminum, copper, and stainless steel) have often been incorporated into the otherwise MR-compatible structures. MR compatibility studies have demonstrated that small parts, such as screws, bearings, and gears, made of MR-incompatible materials do not present substantial problems or image artifacts as long as they are of small size and appropriately positioned relative to the imaged area. A comprehensive review of the MR compatibility of materials was presented in [131].

MR-compatible mechatronic systems require appropriate forms of actuation. The commonly used electromagnetic actuators are, in general, not compatible with the MRI environment owing to their principle of operation. Therefore, alternative types of actuation have been considered and novel ones have been proposed for MR compatible applications. Hydraulic actuation is intrinsically MRI compatible given the appropriate selection of hydraulic fluid and components. Hydraulic power can be transferred through hoses and produce large forces at distant locations. The main problems reported relevant to that form of actuation were leakages of fluid as well as entrance of air bubbles into the pressurized system. Pneumatics is another form of actuation used with MR devices that eliminates problems associated with hydraulic systems. Pneumatic systems are cleaner and operate at higher speeds compared with hydraulic systems. However, they are suitable only for relatively low-force applications and have limited stiffness owing to the compressibility of the air. Recently, a highly efficient and controllable pneumatic motor called PneuStep [132] was introduced that is suitable for MR applications. PneuStep uses a stepper motor principle to achieve precise motion on the order of 0.050 mm, is simple in design and construction, and its operation is safe and fully MR compatible. This new motor uses pneumatics for actuation and optics for encoding, which are both decoupled from electromagnetism.

Other nonconventional types of MR-compatible actuation include the electrostrictive polymer actuators. The use of electrostatic linear-motion motors for MR applications was theoretically and experimentally studied in [133]. Electrorheological

fluids (ERFs) have provided an alternative way for generating resistive forces inside a MR scanner [121, 134].

With most of the systems developed so far, the favorite actuators have been the ultrasonic, piezoelectric motors (USM). They are suitable for MRI applications because they are magnetically immune and they do not produce any magnetic fields either. Ultrasonic motors are bidirectional with a high torque-to-weight ratio, small size, and compact shape. A special feature of the USM is their high breaking torque, which allows a robotic system to maintain its current position and support its own weight when not actuated. However, this can also be considered a drawback given that the joints of the actuated device cannot be moved manually if necessary, for example, in the case of a medical emergency or failure of the actuation system.

All types of actuators are MR compatible when they are away from the imaging area. To address the compatibility issue in most systems using this form of actuation, the motors remain outside the scanner and a motion transmission system is used to transfer the motion to the distant actuated points [135]. Performance limitations are typically associated with robotic/mechatronic systems with remotely actuated joints that are known to suffer from joint flexibility, backlash, and friction.

The safe and accurate operation of any mechatronic device requires the use of position and/or force feedback signals for closed-loop control. However, the difficulties in such cases are brought by the huge electromagnetic noise present in fMRI environments. To this aim, every principle which does not employ a trasduction of the physical quantity under measurement to the electrical domains is suitable for MRI environments. Custom-designed incremental encoders for translational as well as rotational measurements have been proposed, which use glass grating patterns for detecting motion and fiber-optic cables for the transfer of signals to the remotely placed circuitry [136]. Micronor Inc. has developed both rotary and linear optical encoders based on fiber-optic technology, and without using any metallic part. On the side of exteroceptive measurements, a six-axis force sensor for MRI applications was developed in [137], using fiber optic components and a similar sensor was also used on a MR-compatible haptic device presented in [130]. In both cases, light was transmitted through a fiber cable to the remotely located,

MR-compatible part of the sensor and continued through a returning cable.

5.4.2 Definition of specifications

Pneumatic actuation is chosen for the relative simplicity, compared to hydraulic actuation, and intrinsic backdriveability and safety provided by air compressibility. Also, commercially available pneumatic actuators are available in the market, by Airpot Inc., which consist of a MRI compatible linear cylinder+piston system providing a low static and dynamic friction, whose piston is made of brass. From the side of sensors, the sensors already used for the passive device have an unacceptable accuracy ($\pm$ 1 deg), making them unacceptable for a position feedback control loop. The possibility to use commercially available fully MRI compatible sensors can be pursued, but is not ideal due to the high cost of such sensors. However, other studies documented in the past the use of heavily shielded opto-electronic encoders in fMRI environment, without significant induced noise, as long as the sensors are placed far enough from the scanning region. Under these consideration, the following specification are posed to the design of the active device.

- the structure is made of MRI compatible materials, as in the passive device and should allow the execution of planar 2 DOFs reaching movement, in a circular region with radius $>$ 50 mm;
- the structure should be designed so to have its maximum height in correspondence of the central part of the bore, where the vertical clearance to the bed is maximum;
- the kinematic structure should be a parallel chain, so to exploit the advantages of parallel chains in terms of structural stiffness;
- motion is generated by pneumatically actuated linear cylinders+piston systems. In particular, it would be preferred that cylinders are directly supported by the ground frame, to avoid having to support the weight of the hoses+cylinder assembly by bearings and to avoid reaction forces arising from the elastic behavior of the hoses;

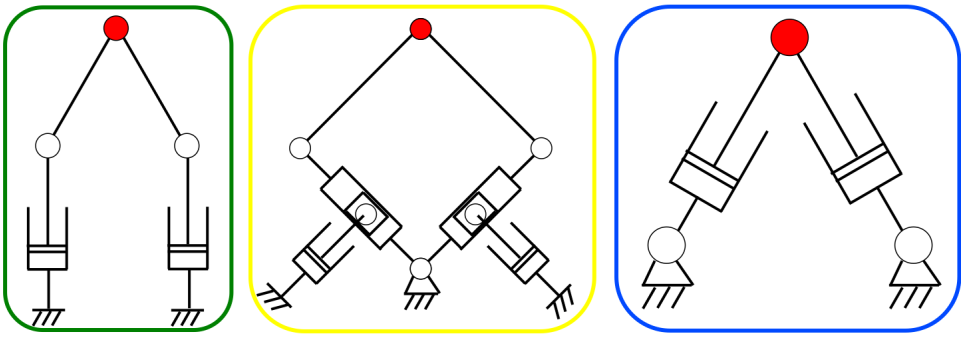

Figure 5.5: Structural representation of three planar 2 DOF kinematic chains for pneumatically assisted reaching movements in fMRI environments. The end-effector (handle) is represented by a red circle.

- forces in the range of 20-30 N are required in both horizontal and vertical directions;
- the structure should include opto-electronic angle sensors, which are easier to mount compared to sensors measuring translational motion, which should be placed as far as possible from the scanning region.

5.4.3 Kinematic model and design

Three different solutions respecting the specifications has been individuated and is shown in Figure 5.5

An analysis of the three solutions can be performed by considering the critical features of each of the designs. In particular, solution (a) has the disadvantage of not allowing a complete calculation of the forward kinematics by measuring only angular quantities; hence linear encoders mounted on the two pistons are required. Moreover, the encoders would be situated in a region very close to the handle and then probably not enough far from the scanning region. Solution (b) respects each single specification, but through a more complex design, which includes a higher number of moving parts, and most importantly a linear guide used to transfer in two rotations the translation of the two pistons. Solution (c) is instead very simple from a mechanical construction standpoint, but has the disadvantage that the

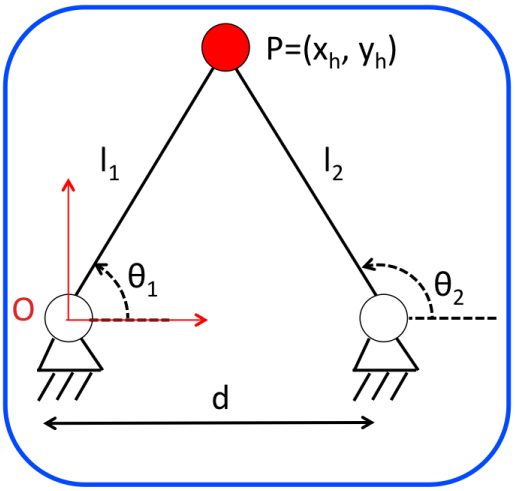

Figure 5.6: Kinematic model of the fMRI-compatible manipulator. l_1 and l_2 are the lengths modulated by the pneumatic actuators, θ_1 and θ_2 are the angles measured by the rotative encoders. The end effector is the red circle, whose planar coordinates x_h y_h are indirectly measured.

cylinder+piston assemblies need to be supported by two bearings. However, the structure allows to measure the forward kinematics by only using rotary encoders to measure the rotation of the two revolute joints between the cylinders and the ground.

The described analysis implied the choice of solution (c), even though before moving to a detailed mechanical design, the accuracy of the measurement of forward kinematics need to be checked.

First, it is necessary to derive the inverse kinematics, which provides a relation to calculate the required acutation parameters l_1 and l_2 which determine a given pose of the end effector, described by the couple (x_h, y_y). From trigonometric calculations, it is possible to verify that the controlled and measured quantities, l_i and θ_i are not mutually independent, but are related by the relation:

$$l_1 = \frac{d \tan\theta_2}{(\tan\theta_2 - \tan\theta_1)\cos\theta_1} \tag{5.2}$$

$$l_2 = \frac{d \tan\theta_1}{(\tan\theta_2 - \tan\theta_1)\cos\theta_2} \tag{5.3}$$

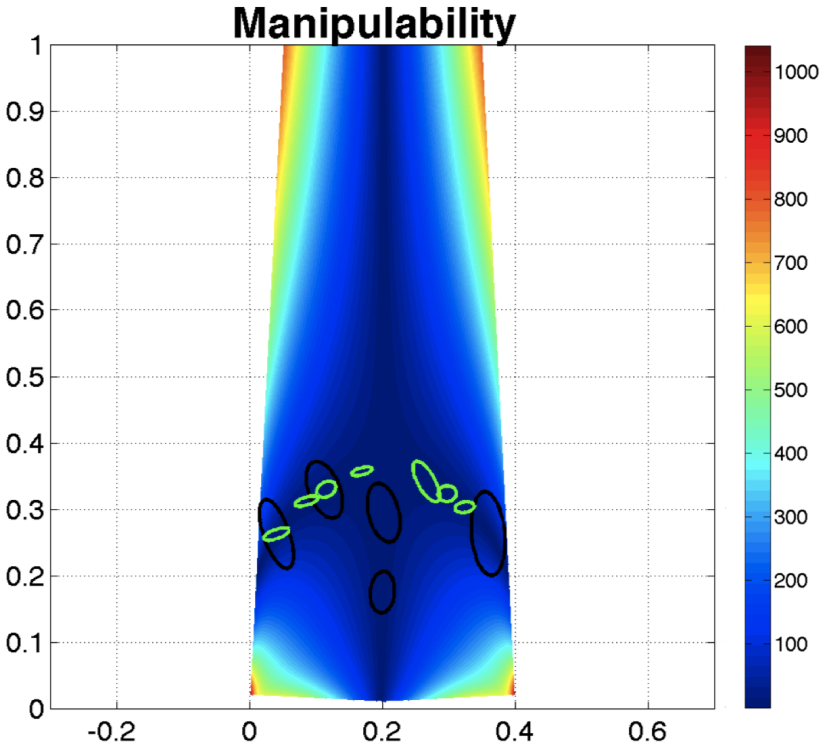

Figure 5.7: Measure of manipulability of the MR compatible robot, calculated according to 5.11. Force ellipsoids are displayed in green; position ellipsoids are displayed in black, both kind of ellipsoids are drawn only around positions with values of isotropy higher than 0.5.

But the required trigonometric functions of the measured angles θ_1 and θ_2 are provided by:

$$\tan\theta_1 = \frac{y_h}{x_h} \tag{5.4}$$

$$\tan\theta_2 = \frac{y_h}{x_h - d} \tag{5.5}$$

The forward kinematics can also be solved straightforwardly, given that the angles θ_1 and θ_2 confine the end-effector in the portion of the plane defined by $(0 \leq x \leq d)$, $(y > 0)$. The forward kinematics is provided by

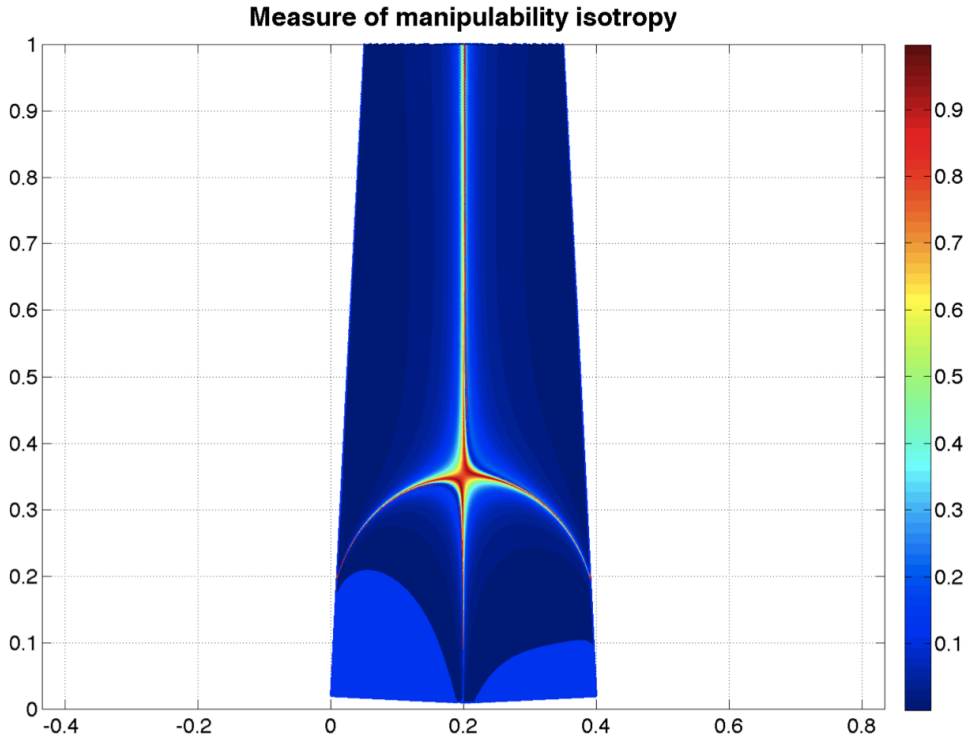

Figure 5.8: Measure of isotropy of manipulability of the MR compatible robot.

$$x_h = l_1 \cos\theta_1 \tag{5.6}$$

$$y_h = l_2 \sin\theta_1. \tag{5.7}$$

However, inverting equations 5.4 and 5.5 is impractical. However, an independent relation can be found for $\cos\theta_1$:

$$\cos\theta_1 = \frac{l_1^2 + d^2 + l_2^2}{2 l_1 d}, \tag{5.8}$$

which imply that

$$x_h = f_1(l_1, l_2) = \frac{l_1^2 + d^2 + l_2^2}{2d} \tag{5.9}$$

$$y_h = f_2(l_1, l_2) = l_1 \sqrt{1 - \frac{(d^2 + l_1^2 - l_2^2)^2}{4 d^2 l_1^2}}. \tag{5.10}$$

The knowledge of the forward kinematics function allows to derive the Jacobean $J(\mathbf{1})$ of the manipulator, which allows to derive the differential kinematics of the manipulator and evaluate the measure of manipulability, defined as

$$w(\mathbf{1}) = \sqrt{\det(J(\mathbf{1})J^T(\mathbf{1}))}. \tag{5.11}$$

Another measure to consider is the isotropy of manipulability, defined as the ratio between the semiaxes of the manipulability ellipsoid (ellipse in our case, since we are dealing with a planar kinematic chain).

Results are shown in Fig. 5.7 and Fig. 5.8, which plot the two described measures as a function of the end-effector position in the plane, having chosen d=400 mm. It can be noticed that the region with acceptable isotropy values higher than 0.5 are included in a circle of the desired radius, centered around the point of coordinates (0.2,0.35).

Finally, the effect of the effect of the indirect measurement of the handle position needs to be quantified. Ideally, sensors should measure directly the position of actuators, according to the most generally followed co-location between sensors and actuators. In the described case, the measured quantities are instead θ_1 and θ_2, which allow to calculate the values of l_1 and l_2 in an indirect way. However, in order to define the range of accuracy in the measurement of θ_1 and θ_2, tolerated to the aims of a feedback position control loop, a model describing the effect of noise in the angular measurements has been developed. Noise has been modeled as an uniform distribution, with variable extent. The behavior of a simple position feedback control loop (J transpose) employing such noisy data has been simulated, giving as desired trajectories a set of straight, minimum jerk trajectories in 8 directions. This simulation was performed in different regions, to assess the compound effect introduced by a different manipulability and different inaccuracies brought by errors in the angular measurements.

An example of the obtained results is shown in Fig. 5.9, which shows the performances of the position control feedback, while tracking trajectories centered around two different regions of the workspace.

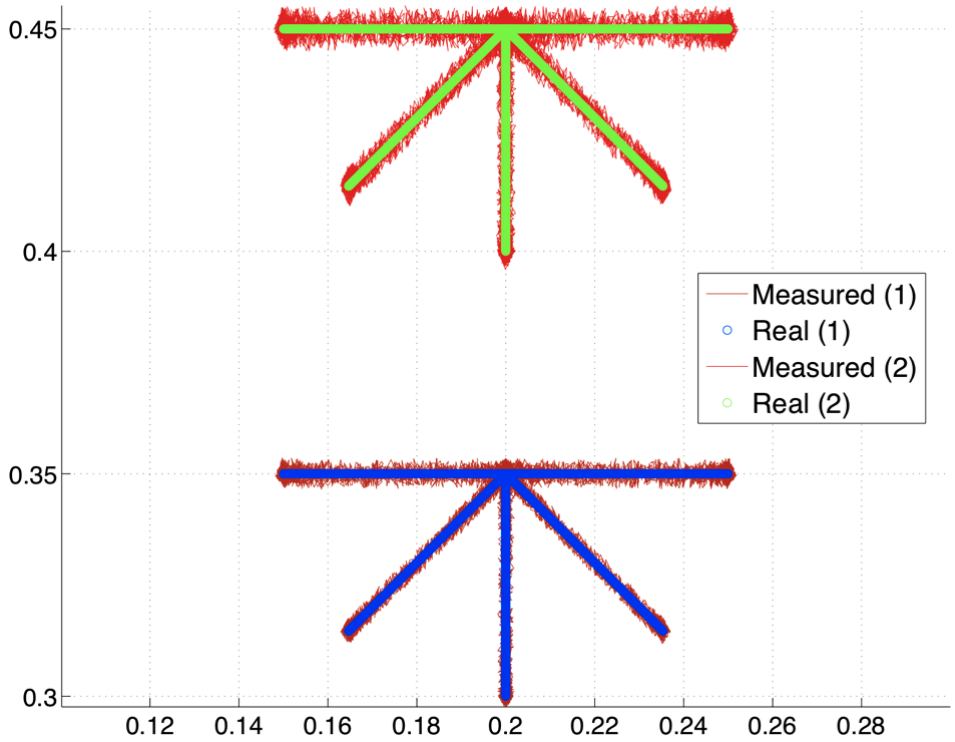

Figure 5.9: Effect of non co-located measurement to the position feedback control loop. The term "measured" refers to the position of the end-effector estimated based on the noisy angular measurements, uniform distribution with amplitude 1 deg centered around the real value, while the term "real" refers to the current position of the end-effector. Robot end-effector is however successfully tracking (maximum errors below 1 mm) the desired trajectory, with the simulated links length and sensors uncertainty. It is visible how the inaccuracy in measuring the end-effector position is higher in the case shown on top of the figure, due to geometrical relations.

5.5 Conclusions

Recovery of motor function after stroke has a high degree of specificity; this demands to perform imaging experiments replicating as much as possible the task performed during the RMT.

The clinical study performed on two chronic stroke subject demonstrated the feasibility to perform planar reaching movements in fMRI environments, both to extract neural activation patterns (in healthy subjects) and to extract functional connectivity maps (both in healthy subjects and in post-stroke patients).

This preliminary study was successful to define a set of measurable parameters which can be used for assessment or even for prediction of the outcomes of rehabilitation therapy after stroke. A quantitative investigation of the accuracy of such indexes need to be performed in future work, testing this hypothesis with a more heterogeneous and bigger population of stroke survivors.

This preliminary study was also successful to validate an experimental setup involving the execution of reaching movements in fMRI environments, providing a set of specifications, which were employed for the preliminary design of a novel fMRI-compatible robotic device.

Chapter 6

Conclusions

The development of efficient robotic systems for rehabilitation and assistive purposes requires the synergistic deployment of advanced solutions from multiple aspects, including the choice of the kinematic structure, actuation systems and from a comprehensive knowledge of relevant biomechanical and neural properties of the human component.

This thesis investigates the application of biomechatronic design methods in two complimentary applications, namely the design of a wearable robotic orthosis for gait assistance and the design of operational robotic device for neurorehabilitation of the upper extremity. In both contexts, the described contributions represented advancements with respect to the current state of the art.

In the context of wearable robotic orthoses for gait assistance, an analysis of the state-of-the-art of currently existing devices allowed to formulate a research hypothesis, which states that the choice of non-anthropomorphic kinematic solutions for wearable robots can provide improvements over the currently available anthropomorphic solutions both from an ergonomics standpoint and from the chance of exploiting the intrinsic dynamics of the system comprising both human and robot.

Despite of the foreseen advantages, it is complex to synthesize an appropriate kinematic structure by relying only on conventional kinematic synthesis methods, due to the large number of open design parameters.

In order to address this design problem, this thesis describes a novel method-

ology, which allows to systematically explore the wide set of solutions provided by non-anthropomorphic wearable robotic orthoses. The described methodology requires the a-priori knowledge of the complete list of independent kinematic solutions with desired properties.

To this aim, this thesis describes a set of algorithms, which allows to solve this problem in a systematic and computationally efficient way. The described methodology also includes two novel tests, specifically devised to solve the problem of enumeration of kinematic structures of wearable robots: the HR-isomorphism and the HR-degeneracy tests.

The complete list of independent solutions with desired kinematic properties, which generalize the set of solutions of the problem of kinematic synthesis of a non-anthropomorphic wearable robot with given kinematic requirements, was obtained. The methodology proved to be adequate to be used for the mechatronic design of a planar wearable robot for the lower limbs, based on optimization techniques aimed at improving a set of design objectives in a physics-based simulations environment.

In the context of the design of robotic devices for neurorehabilitation of the upper limbs, the capability of a novel actuation architecture to guarantee a transparent interaction during *patient-in-charge* mode was demonstrated, based on an inverse dynamical model of the manipulator and on the analysis of experiments performed on 14 healthy subjects. The system allows to reduce the interaction forces when the subject is driving the manipulator, without introducing a significant anisotropy, which is a negative aspect of most currently existing manipulators for planar neurorehabilitation.

Within the same context of neurorehabilitation, it is accepted that the main reason for the limited efficacy of currently existing rehabilitation therapies after stroke is related to the lack of a detailed knowledge on the relations between movement therapy, neural plasticity and recovery of motor function after stroke are still largely unknown.

This thesis describes also a pilot study conducted to validate the design of an fMRI compatible registration device, to investigate the neural correlates of motor

recovery through robot-mediated rehabilitation therapy after stroke. This preliminary study was successful to define a set of measurable parameters, which can be used for assessment or even for prediction of the outcomes of rehabilitation therapy after stroke. A quantitative investigation of the accuracy of such indexes need to be performed in future work, testing this hypothesis with a more heterogeneous and larger population of stroke survivors.

This preliminary study was also successful to validate an experimental setup involving the execution of reaching movements in fMRI environments, providing a set of specifications, which were employed for the preliminary design of a novel fMRI-compatible robotic device.

Chapter 7

List of Publications

Journal papers

1. **F. Sergi**, D. Accoto, N. L. Tagliamonte, G. Carpino, E. Guglielmelli, "A systematic graph-based method for the kinematic synthesis of non-anthropomorphic wearable robots for the lower limbs", *Journal of Frontiers of Mechanical Engineering*, March 2011, in press.

2. A. Benvenuto, **F. Sergi**, G. Di Pino, T. Seidl, D. Campolo, D. Accoto and E. Guglielmelli, "Beyond biomimetics: towards insect/machine hybrid controllers for space applications", *Advanced Robotics*, vol. 23, no. 7-8, pp. 939-953, 2009. (IF: 0.629).

Book chapters

1. G. Di Pino, T. Seidl, A. Benvenuto, **F. Sergi**, D. Campolo, D. Accoto, P. M. Rossini, E. Guglielmelli, "Interfacing insect brain for space applications", in *International Review of Neurobiology*, eds. L. Rossini, D. Izzo and L. Summerer, vol. 86, pp. 39-47, 2009. (IF: 4.017).

Peer-reviewed international conferences

1. G. Carpino, D. Accoto, M. Di Palo, N. L. Tagliamonte, **F. Sergi**, E. Guglielmelli, "Design of a Rotary Passive Viscoelastic Joint for Wearable Robots", Accepted to the *International Conference of Rehabiliation Robotics, ICORR 2011, Zurich, Switzerland*, July 2011.

2. N. L. Tagliamonte, **F. Sergi**, G. Carpino, D. Accoto, E. Guglielmelli, "Design of a Variable Impedance Differential Actuator for Wearable Robotics Applications", *Proceedings of the 2010 IEEE/RSJ International Conference on Intelligent Robots and Systems (IROS 2010), Taipei, Taiwan*, 2010.

3. **F. Sergi**, D. Accoto, N. L. Tagliamonte, G. Carpino, E. Guglielmelli, "Graph-based methodology for the kinematic synthesis of wearable assistive robots for the lower limbs", *32nd International Conference of the IEEE Engineering in Medicine and Biology Society, Buenos Aires, Argentina*, pp. 3682-5, 2010.

4. **F. Sergi**, D. Accoto, N. L. Tagliamonte, G. Carpino, L. Pathiyil, E. Guglielmelli, "A systematic graph- based method for the kinematic synthesis of non anthropomorphic wearable robots", *IEEE International Conference on Robotics, Automation and Mechatronics, Singapore*, pp. 100-105, 2010.

5. I. Gaudiello, D. Caligiore, G. Schiavone, A. Salerno, **F. Sergi**, L. Zollo, E. Guglielmelli, D. Parisi, G. Baldassarre, R. Nicoletti, A. M. Borghi, "Effect on space representation of using a tool and a button", *4th International Conference on Spatial Cognition, Rome, Italy*, September 2009.

6. A. Benvenuto, **F. Sergi**, G. Di Pino, D. Campolo, D. Accoto, E. Guglielmelli and T. Seidl, "Conceptualization of an Insect/Machine Hybrid Controller for Space Applications", *Proceedings of the IEEE International Conference on Biomedical Robotics and Biomechatronics (BIOROB), Scottsdale, AZ, USA*, pp. 306- 310, 2008.

7. **F. Sergi**, D. Accoto, D. Campolo and E. Guglielmelli, "Forearm Orientation Guidance with a Vibrotactile Feedback Bracelet: on the Directionality of Tactile Motor Communication", *Proceedings of the IEEE International Conference on Biomedical Robotics and Biomechatronics (BIOROB), Scottsdale, AZ, USA*, pp. 433-438, 2008.

Abstracts in international conferences

1. J. van den Kieboom, **F. Sergi**, D. Accoto, E. Guglielmelli, R. Ronsse, A. Ijspeert, "Coevolution of Morphology and Control of a Wearable Robot for Locomotion", submitted to the Future and Emerging Conference (FET 11), Budapest, May 2011.

2. G. Carpino, D. Accoto, N. L. Tagliamonte, M. Di Palo, **F. Sergi**, E. Guglielmelli, "Novel Mechatronic Joints for Wearable Robots to Enhance Physical Human-Robot Interaction", submitted to the Future and Emerging Conference (FET 11), Budapest, May 2011.

3. D. Accoto, **F. Sergi**, G. Carpino, N. L. Tagliamonte, E. Guglielmelli, "A design methodology for neurorehabilitative and assistive wearable robots incorporating embodied intelligence", accepted at the *14th European Congress on Clinical Neurophysiology*, Rome, May 2011.

4. **F. Sergi**, J. Schaechter, B. Groisser, A. Rykman, B. T. Volpe, E. Guglielmelli and H. I. Krebs, "A Pilot Study to Investigate the Neural Correlates of Robot-Mediated Motor Recovery Following a Stroke", accepted at the *14th European Congress on Clinical Neurophysiology*, Rome, June 2011.

5. D. Accoto, N. L. Tagliamonte, **F. Sergi**, G. Carpino, E. Guglielmelli, "VIDA: a Variable Impedance Differential Actuator", *Workshop on New variable impedance actuators for the next generation of robots, ICRA 2010, Anchorage, AK, USA.*.

Peer-reviewed national conferences

1. G. Carpino, **F. Sergi**, D. Accoto, E. Fischetti, N. Tagliamonte, E. Guglielmelli, "Design di giunti rotoidali per robot indossabili non antropomorfi", *Neuroriabilitazione Robotica dell'Arto Superiore, Genova, Italy*, December 2009.

2. N. Tagliamonte, **F. Sergi**, D. Accoto, G. Carpino, E. Guglielmelli, "Modellazione e Controllo di Un Attuatore Differenziale ad Impedenza Variabile per Robot Esoscheletrici", *Neuroriabilitazione robotica dell'arto superiore, Genova, Italy*, December 2009.

3. F. Paradisi, **F. Sergi**, L. Zollo, E. Gallotta, D. Accoto, S. Sterzi, E. Guglielmelli, "Ricostruzione cinematica del moto dell'arto superiore durante un compito di riabilitazione robot-mediata", *Neuroriabilitazione robotica dell'arto superiore, Genova, Italy*, December 2009.

Technical reports

1. **F. Sergi**, G. Carpino, N. L. Tagliamonte, D. Accoto and E. Guglielmelli, "Basic contraints on robot design", *Deliverable 5.1 of the Evryon-EEU-Project, FP7-ICT-2007.8.5-231451*, July 2009.

2. A. Benvenuto, G. Di Pino, **F. Sergi**, D. Campolo, D. Accoto, G. Assenza, P. M. Rossini, E. Guglielmelli and T. Seidl, "Machine/Animal Hybrid Controllers for Space Applications", *ESA/Ariadna (07-6301) study*, March 2008.

Bibliography

[1] J L Pons. *Wearable Robots: Biomechatronic Exoskeletons*. 2008.

[2] H Kawamoto and Y Sankai. Power assist system HAL-3 for gait disorder person. *Lecture Notes in Computer Science, Springer-Verlag*, (2398):196–203, Jan 2002.

[3] CH Walsh, K Endo, and H Herr. A quasi-passive leg exoskeleton for load-carrying augmentation. *International Journal of Humanoid Robotics*, 4(3):487–506, Jan 2007.

[4] J Veneman, R Kruidhof, E Hekman, R Ekkelenkamp, E Van Asseldonk, and H van der Kooij. Design and evaluation of the lopes exoskeleton robot for interactive gait rehabilitation. *Neural Systems and Rehabilitation Engineering, IEEE Transactions on*, 15(3):379 – 386, 2007.

[5] A Dollar and H Herr. Lower extremity exoskeletons and active orthoses: Challenges and state-of-the-art. *Robotics, IEEE Transactions on*, 24(1):144 – 158, 2008.

[6] J Pons. The promise of an emerging field. *IEEE Engineering in Medicine and Biology Magazine*, 29(3):57–63, 2010.

[7] H Kazerooni and R Steger. The Berkeley lower extremity exoskeleton. *Journal of Dynamic Systems, Measurement, and Control*, 128:14–25, 2006.

[8] A B Zoss, H Kazerooni, and A Chu. Biomechanical design of the berkeley lower extremity exoskeleton (bleex). *Mechatronics, IEEE/ASME Transactions on*, 11(2):128–138, 2006.

[9] H Kazerooni, R Steger, and L Huang. Hybrid control of the berkeley lower extremity exoskeleton (BLEEX). *The International Journal of Robotics Research*, 25(5-6):561–573, May 2006.

[10] K Amundson, J Raade, N Harding, and H Kazerooni. Hybrid hydraulic-electric power unit for field and service robots. *Intelligent Robots and Systems, 2005. (IROS 2005). 2005 IEEE/RSJ International Conference on*, pages 3453 – 3458, 2005.

[11] University of Berkeley Robotics and Human Engineeering Laboratory website http://bleex.me.berkeley.edu/research/exoskeleton/hulc/, retrieved on January 2011.

[12] S Collins, A Ruina, R Tedrake, and M Wisse. Efficient bipedal robots based on passive-dynamic walkers. *Science*, 307(5712):1082–1085, Jan 2005.

[13] M Vukobratovic and D Juricic. Contribution to the synthesis of biped gait. *Biomedical Engineering, IEEE Transactions on*, BME-16(1):1 – 6, 1969.

[14] M Vukobratovic and B Borovac. Zero-moment point - thirty five years of its life. *International Journal of Humanoid Robots*, 1(1):157–173, 2004.

[15] A M Grabowski and H Herr. Leg exoskeleton reduces the metabolic cost of human hopping. *Journal of applied physiology*, 107(3):670–8, Sep 2009.

[16] Technological Fair "Futuro remoto 2009", Città della scienza, Napoli, November 2009.

[17] K Suzuki, Y Kawamura, T Hayashi, T Sakurai, Y Hasegawa, and Y Sankai. Intention-based walking support for paraplegia patient. *Systems, Man and Cybernetics, 2005 IEEE International Conference on*, 3:2707–2713, 2006.

[18] Hocoma inc. website http://www.hocoma.con, visited in january 2011.

[19] Healthsouth inc. website http://www.healthsouth.com, visited on january 2011.

[20] S Banala, Seok Hun Kim, S Agrawal, and J Scholz. Robot Assisted Gait Training With Active Leg Exoskeleton (ALEX). *Neural Systems and Rehabilitation Engineering, IEEE Transactions on*, 17(1):2 – 8, 2009.

[21] G Colombo, M Joerg, R Schreier, and V Dietz. Treadmill training of paraplegic patients using a robotic orthosis. *Journal of Rehabilitation Research and Development*, 37(6):693–700, May 2000.

[22] L. L Cai, A. J Fong, C. K Otoshi, Y Liang, J. W Burdick, R. R Roy, and V. R Edgerton. Implications of assist-as-needed robotic step training after a complete spinal cord injury on intrinsic strategies of motor learning. *Journal of Neuroscience*, 26(41):10564–10568, Oct 2006.

[23] S Jezernik, G Colombo, and M Morari. Automatic gait-pattern adaptation algorithms for rehabilitation with a 4-DOF robotic orthosis. *Robotics and Automation, IEEE Transactions on*, 20(3):574 – 582, 2004.

[24] T. G Hornby, D. D Campbell, J. H Kahn, T Demott, J. L Moore, and H. R Roth. Enhanced gait-related improvements after therapist- versus robotic-assisted locomotor training in subjects with chronic stroke: A randomized controlled study. *Stroke*, 39(6):1786–1792, Jun 2008.

[25] J Hidler, D Nichols, M Pelliccio, K Brady, D D Campbell, J H Kahn, and T G Hornby. Multicenter randomized clinical trial evaluating the effectiveness of the Lokomat in subacute stroke. *Neurorehabil Neural Repair*, 23(1):5–13, Jan 2009.

[26] Joseph M Hidler and Anji E Wall. Alterations in muscle activation patterns during robotic-assisted walking. *Clin Biomech (Bristol, Avon)*, 20(2):184–93, Feb 2005.

[27] E Van Asseldonk, M Wessels, A H Stienen, F C van der Helm, and H van der Kooij. Influence of haptic guidance in learning a novel visuomotor task. *Journal of physiology, Paris*, 103:276–285, 2009.

[28] E Van Asseldonk and et al. Robot aided gait training according to the assist-as-needed principle in chronic stroke survivors. *Neuroscience Conference, Chicago, IL, USA, 2009*.

[29] R G West. Powereed gait orthosis and method of utilizing same. *US Patent 7041069*, Jan 2006.

[30] S Banala, S Agrawal, A Fattah, V Krishnamoorthy, W L Hsu, J Scholz, and K Rudolph. Gravity-balancing leg orthosis and its performance evaluation. *IEEE Transactions on Robotics*, 22(6):1228–1239, Nov 2006.

[31] K A Strausser, T A Swift, A B Zoss, and H Kazerooni. Prototype medical exoskeleton for paraplegic mobility: First experimental results. *3rd Annual Dynamic Systems and Control Conference, September 13-15, 2010, Cambridge, MA, USA*, Jul 2010.

[32] T A Swift, K A Strausser, A B Zoss, and H Kazerooni. Control and experimental results for post stroke gait rehabilitation with a prototype mobile medical exoskeleton. *3rd Annual Dynamic Systems and Control Conference, September 13-15, 2010, Cambridge, MA, USA*, Jul 2010.

[33] Berkeley Bionics website, Reflections After Walking in eLEGS the First Time http://berkeleybionics.com/2011/reflections-after-walking-in-elegs-the-first-time/.

[34] Gizmag, "ReWalk robotic exoskeleton to go on sale in 2011 " http://www.gizmag.com/rewalk-robotic-exoskeleton/17197/, visited on January 2011.

[35] R Horst and R Marcus. FlexCVA: A continuously variable actuator for active orthotics. *Engineering in Medicine and Biology Society, 2006. EMBS '06. 28th Annual International Conference of the IEEE*, pages 2425 – 2428, 2006.

[36] R Horst. A bio-robotic leg orthosis for rehabilitation and mobility enhancement. *Engineering in Medicine and Biology Society, 2009. EMBC 2009. Annual International Conference of the IEEE*, pages 5030 – 5033, 2009.

[37] K Kong and J Doyoung. Design and control of an exoskeleton for the elderly and patients. *Mechatronics, IEEE/ASME Transactions on*, 11(4):428 – 432, 2006.

[38] HI Krebs, N Hogan, ML Aisen, and BT Volpe. Robot-aided neurorehabilitation. *IEEE Transactions on Rehabilitation Engineering*, 6(1):75–87, 1998.

[39] E Guglielmelli, M Johnson, and T Shibata. Guest editorial special issue on rehabilitation robotics. *Robotics, IEEE Transactions on*, 25(3):477 – 480, 2009.

[40] G Wu, FCT Van der Helm, HEJ Veeger, M Makhsous, P Van Roy, C Anglin, J Nagels, AR Karduna, and K McQuade. ISB recommendation on definitions of joint coordinate systems of various joints for the reporting of human joint motion– Part II: shoulder, elbow, wrist and hand. *Journal of Biomechanics*, 38(5):981–992, 2005.

[41] A Schiele and F C van der Helm. Kinematic design to improve ergonomics in human machine interaction. *IEEE Trans Neural Syst Rehabil Eng*, 14(4):456–69, Dec 2006.

[42] A Schiele. An explicit model to predict and interpret constraint force creation in pHRI with exoskeletons. *Robotics and Automation, 2008. ICRA 2008. IEEE International Conference on*, pages 1324 – 1330, 2008.

[43] EV Biryukova, A Roby-Brami, AA Frolov, and M Mokhtari. Kinematics of human arm reconstructed from spatial tracking system recordings. *Journal of Biomechanics*, 33(8):985–995, 2000.

[44] F Paradisi, F Sergi, L Zollo, E Gallotta, D Accoto, S Sterzi, and E Guglielmelli. Ricostruzione cinematica del moto dell'arto superiore durante un compito di riabilitazione robot-mediata. *Neuroriabilitazione robotica dell'arto superiore*, Dec 2009.

[45] A Stienen, E Hekman, F van der Helm, and H van der Kooij. Self-aligning exoskeleton axes through decoupling of joint rotations and translations. *Robotics, IEEE Transactions on*, 25(3):628 – 633, 2009.

[46] T Kubow and RJ Full. The role of the mechanical system in control: a hypothesis of self-stabilization in hexapedal runners. *Philosophical Transactions of the Royal Society, Part B*, 354(1385):849–861, Jan 1999.

[47] IE Brown and GE Loeb. *Biomechanics and Neuro-Control of Posture and Movement*, chapter A reductionist approach to creating and using neuromusculoskeletal movement. 2000.

[48] R J Full and M S Tu. Mechanics of six-legged runners. *Journal of Experimental Biology*, 148:129–46, Jan 1990.

[49] JG Cham, JK Karpick, and MR Cutkosky. Stride period adaptation of a biomimetic running hexapod, Jan 2004.

[50] T McGeer. Passive dynamic walking. *The International Journal of Robotics Research*, 9(2):62–82, 1990.

[51] Steve Collins, Martijn Wisse, and Andy Ruina. A three-dimensional passive-dynamic walking robots with two legs and knees. *The International Journal of Robotics Research*, 20(7):607–615, Jul 2001.

[52] JC Bongard and C Paul. Making evolution an offer it can't refuse: Morphology and the extradimensional bypass, 2001.

[53] K Matsushita, H Yokoi, and T Arai. Pseudo-passive dynamic walkers designed by coupled evolution of the controller and morphology. *Robotics and Autonomous Systems*, 54(8):674–685, 2006.

[54] K Sims. Evolving virtual creatures. *Computer Graphics, Annual Conference Series*, pages 15–22, 1994.

[55] F Gruau and K Quatramaran. Cellular encoding for interactive evolutionary robotics. *Fourth European Conference on Artificial Life*, pages 368–377, Jan 1997.

[56] JC Gallagher, RD Beer, KS Espenschied, and RD Quinn. Application of evolved locomotion controllers to a hexapod robot. *Robotics and Autonomous Systems*, 19(1):95–103, Jan 1996.

[57] T Fukuda, Y Komata, and T Arakawa. Stabilization control of biped locomotion robot based learning with GAs having self-adaptive mutation and recurrent neural networks. *Robotics and Automation, 1997. Proceedings., 1997 IEEE International Conference on*, 1:217 – 222 vol.1, 1997.

[58] RA Brooks and L A Stein. Building brains for bodies. *Autonomous Robots*, 1:7–25, Jan 1994.

[59] R Pfeifer and C Scheier. Understanding intelligence. *Understanding Intelligence*, Sep 2001.

[60] H Lipson and JB Pollack. Automatic design and manufacture of robotic lifeforms. *Nature*, 406(6799):974–978, 2000.

[61] J Z Li, S H N Tan, C H Cheong, and P V S Lee. Multi body solid dynamic model and its application in human kinematic analysis. pages 48–51, 2007.

[62] D Andreescu, F Ionescu, and H Riehle. Modelling and simulation of human body by considering the skeleton's bones. *BioMech '07: Proceedings of the Fifth IASTED International Conference on Biomechanics*, Aug 2007.

[63] T S Mruthyunjaya. Kinematic structure of mechanisms revisited. *Mechanism and Machine Theory*, 38(4):279–320, Jan 2003.

[64] L Dobrjanskyj and F Freudenstein. Some applications of graph theory to structural analysis of mechanisms. *Journal of Engineering for Industry-Transactions of the ASME, Series B*, 89:153–158, 1967.

[65] F Sergi, G Carpino, N L Tagliamonte, D Accoto, and E Guglielmelli. Basic constraints on robot design, deliverable 5.1 of the evryon EU-Project, FP7-ICT-2007.8.5-231451. Technical report, 2009.

[66] K Kutzbach. Mechanische leitungsverzweigung. *Maschinenbau, der Betrieb*, 8:710–716, 1929.

[67] H Ding and Z Huang. A unique representation of the kinematic chain and the atlas database. *Mech Mach Theory*, 42(6):637–651, Jan 2007.

[68] F Sergi, D Accoto, N Tagliamonte, G Carpino, L Pathiyil, and E Guglielmelli. A systematic graph-based method for the kinematic synthesis of non-anthropomorphic

wearable robots. *Robotics Automation and Mechatronics (RAM), 2010 IEEE Conference on*, pages 100 – 105, 2010.

[69] B D McKay. Isomorph-free exhaustive generation. *J Algorithm*, 26:306–324, Feb 1998.

[70] R P Sunkari. *Structural synthesis and analysis of planar and spatial mechanisms satisfying Gruebler's degrees of freedom equation*. PhD thesis, 2006.

[71] Evryon website, http://www.evryon.eu.

[72] CJL Murray and AD Lopez. Mortality by cause for eight regions of the world: Global burden of disease study. *Lancet*, 349(9061):1269–1276, Jan 1997.

[73] D Lloyd-Jones, RJ Adams, TM Brown, M Carnethon, S Dai, G De Simone, TB Ferguson, E Ford, K Furie, and C Gillespie. Heart disease and stroke statistics–2010 update. a report from the american heart association. *Circulation*, 2009.

[74] H I Krebs, B T Volpe, M Ferraro, S Fasoli, J Palazzolo, B Rohrer, L Edelstein, and N Hogan. Robot-aided neurorehabilitation: From evidence-based to science-based rehabilitation. *Topics in Stroke Rehabilitation*, 8(4):54–70, Mar 2002.

[75] D M Feeney, A Gonzalez, and W A Law. Amphetamine, haloperidol, and experience interact to affect rate of recovery after motor cortex injury. *Science*, 217(4562):855–857, 1982.

[76] R J Nudo, B M Wise, F SiFuentes, and G W Milliken. Neural substrates for the effects of rehabilitative training on motor recovery after ischemic infarct. *Science*, 272(5269):1791–4, 1996.

[77] B Bobath. Adult hemiplegia: Evaluation and treatment. *Heinnemann, London*, 1978.

[78] S Brunnstrom. Movement therapy in hemiplegia: A neurophysiological approach. *Harper and Row, Hargestown*, 1970.

[79] M Knott and D E Voss. Proprioceptive neuromuscular facilitation. *Harper and Row, New York*, 1968.

[80] E Taub, G Uswatte, and R Pidikiti. Constraint-induced movement therapy: A new family of techniques with broad application to physical rehabilitation–a clinical review. *Journal of Rehabilitation Research and Development*, 36(n):1–21, Jul 1999.

[81] R C Wagenaar, O G Meijer, P C van Wieringen, D J Kuik, G J Hazenberg, J Lindeboom, F Wichers, and H Rijswijk. The functional recovery of stroke: A comparison between neurodevelopment treatment and the brunnstrom method. *Scandinavian Journal of Rehabilitation Medicine*, 22(1):1–8, 1990.

[82] M J Reding and F H McDowell. Focused stroke rehabilitation programmes improve focused stroke rehabilitation programmes improve outcome. *Archives of Neurology*, 46:700–701, 1989.

[83] T E Twitchell. The restoration of motor function following hemiplegia in man. *Brain*, 74:443–480, 1951.

[84] B J Kollen, S Lennon, B Lyons, L Weathley-Smith, M Scheper, J H Buurke, J Halfens, A C Geurts, and G Kwakkel. The effectiveness of the bobath concept in stroke rehabilitation: what is the evidence? *Stroke*, 40(4):89–97, 2009.

[85] J Liepert, H Bauder, H R Wolfgang, W H Miltner, E Taub, and C Weiller. Treatment-induced cortical reorganization after stroke in humans. *Stroke*, 31(6):1210–1216, 2000.

[86] J H van der Lee, D H Wagenaar, G J Lankhorst, T W Vogelaar, W L Deville, and L M Bouter. Forced use of the upper extremity in chronic stroke patients: Results from a single-blind randomized clinical trial. *Stroke*, 30(11):2369–2375, 1999.

[87] P Lum, D Reinkesmeyer, R Mahoney, W Z Rymer, and C Burgar. Robotic devices for movement therapy after stroke: Current status and challenges to clinical acceptance. *Topics in Stroke Rehabilitation*, 8(4):40–53, 2002.

[88] H M Feys, W J De Weerdt, and B E Selz. Effect of a therapeutic intervention for the hemiplegic upper limb in the acute phase after stroke: A single-blind, randomized, controlled multicenter trial. *Stroke*, 29(4):785–792, 1998.

[89] T Flash and N Hogan. The coordination of arm movements: an experimentally confirmed mathematical model. *Journal of Neuroscience*, 5(7):1688–1703, Sep 1985.

[90] F A Mussa-Ivaldi, N Hogan, and E Bizzi. Neural, mechanical, and geometric factors subserving arm posture in humans. *Journal of Neuroscience*, 5(10):2732–2743, Sep 1985.

[91] Y Uno, M Kawato, and R Suzuki. Formation and control of optimal trajectory in human multijoint arm movement. *Biological Cybernetics*, 61(2):89–101, 1989.

[92] SH Scott. Apparatus for measuring and perturbing shoulder and elbow joint positions and torques during reaching. *Journal of neuroscience methods*, 89:119–127, Jan 1999.

[93] I Howard, JN Ingram, and DM Wolpert. A modular planar robotic manipulandum with end-point torque control. *Journal of neuroscience methods*, 181:199–211, Jan 2009.

[94] A Sharon, N Hogan, and D E Hardt. The macro/micro manipulator: An improved architecture for robot control. *Robotics and Computer-Integrated Manufacturing*, 10(3):209–222, Jan 1993.

[95] M Zinn, B Roth, O Khatib, and JK Salisbury. A new actuation approach for human friendly robot design. *The International Journal of Robotics Research*, 23(4-5):379–398, Jan 2004.

[96] A M Dollar and H Herr. Design of a quasi-passive knee exoskeleton to assist running. *2008 IEEE/RSJ International Conference on Intelligent Robots and Systems*, pages 747–754, Oct 2008.

[97] T Kikuchi, T Ozawa, H Akai, and J Furusho. "hybrid-PLEMO", rehabilitation system for upper limbs with active/passive force feedback, and its application for facilitation techniques. *Rehabilitation Robotics, 2009. ICORR 2009. IEEE International Conference on*, pages 781–786, 2009.

[98] T Kikuchi, K Otsuki, J Furusho, H Abe, J Noma, M Naito, and N Lauzier. Development of a compact magnetorheological fluid clutch for human-friendly actuator. *Advanced Robotics*, 24:1489–1502, Jan 2010.

[99] L Zollo, D Accoto, F Torchiani, D Formica, and E Guglielmelli. Design of a planar robotic machine for neuro-rehabilitation. *Robotics and Automation, 2008. ICRA 2008. IEEE International Conference on*, pages 2031 – 2036, 2008.

[100] D. Accoto, N. Simeone, E. Guglielmelli, E. Cecchini, "Modulo d'interfaccia aptica" Italian patent application no. RM2010A000122, March 18, 2010.

[101] C Calautti and J C Baron. Functional neuroimaging studies of motor recovery after stroke in adults: A review. *Stroke*, 34:1553–1556, 2003.

[102] J Schaechter. Motor rehabilitation and brain plasticity after hemiparetic stroke. *Progress in neurobiology*, Jan 2004.

[103] S C Cramer, G Nelles, R R Benson, J D Kaplan, R A Parker, K K Kwong, D N Kennedy, S P Finklestein, and B R Rosen. A functional MRI study of subjects recovered from hemiparetic stroke. *Stroke*, 28(12):2518–2527, Dec 1997.

[104] C Calautti, M Naccarato, PS Jones, N Sharma, DD Day, AT Carpenter, ET Bullmore, EA Warburton, and JC Baron. The relationship between motor deficit and hemisphere activation balance after stroke: a 3T fMRI study. *NeuroImage*, 34(1):322–331, 2007.

[105] N S Ward, M M Brown, A J Thompson, and R S J Frackowiak. Neural correlates of motor recovery after stroke: a longitudinal fMRI study. *Brain*, 126(Pt 11):2476–2496, Nov 2003.

[106] A Feydy, R Carlier, A Roby-Brami, B Bussel, F Cazalis, L Pierot, Y Burnod, and M A Maier. Longitudinal study of motor recovery after stroke: recruitment and focusing of brain activation. *Stroke*, Jan 2002.

[107] B Biswal and F Z Yetkin. Functional connectivity in the motor cortex of resting human brain using echo-planar MRI. *Magnetic Resonance ...*, Jan 1995.

[108] M. P. A Van Meer, K Van Der Marel, K Wang, W. M Otte, S El Bouazati, T. A. P Roeling, M. A Viergever, J. W Berkelbach Van Der Sprenkel, and R. M Dijkhuizen. Recovery of sensorimotor function after experimental stroke correlates with restoration of resting-state interhemispheric functional connectivity. *Journal of Neuroscience*, 30(11):3964–3972, Mar 2010.

[109] D Mintzopoulos, LG Astrakas, A Khanicheh, AA Konstas, A Singhal, MA Moskowitz, BR Rosen, and AA Tzika. Connectivity alterations assessed by combining fMRI and MR-compatible hand robots in chronic stroke. *Neuroimage*, 47:T90–T97, 2009.

[110] A R Carter, S V Astafiev, CE Lang, L T Connor, J Rengachary, M J Strube, D L W Pope, G L Shulman, and M Corbetta. Resting state inter-hemispheric fMRI connectivity predicts performance after stroke. *Ann Neurol.*, 67:365–375, Jan 2009.

[111] A B Waites, A Stanislavsky, D F Abbot, and G D Jackson. Effect of prior cognitive state on resting state networks measured with functional connectivity. *Human Brain Mapping*, 24(1):59–68, Jan 2005.

[112] M Amann, J G Hirsch, and A Gass. A serial functional connectivity MRI study in healthy individuals assessing the variability of connectivity measures: reduced in-

terhemispheric connectivity in the motor network during continuous performance. *Magn Reson Imaging*, 27(10):1347–1359, Dec 2009.

[113] P Lindberg, C Schmitz, H Forssberg, M Engardt, and J Borg. Effects of passive-active movement training on upper limb motor function and cortical activation in chronic patients with stroke: A pilot study. *J Rehabil Med*, 36(3):117–123, Jan 2004.

[114] H Johansen-Berg, H Dawes, C Guy, S M Smith, D T Wade, and P M Matthews. Correlation between motor improvements and altered fMRI activity after rehabilitative therapy. *Brain*, 125:2731–2742, 2002.

[115] C E Levy, D S Nichols, P M Schmalbrock, P Keller, and D W Chakeres. Functional MRI evidence of cortical reorganization in upper-limb stroke hemiplegia treated with constraint-induced movement therapy. *Am J Phys Med Rehabil*, 80(1):4–12, Jan 2001.

[116] JR Carey, KM Anderson, TJ Kimberley, SM Lewis, EJ Auerbach, and K Ugurbil. fMRI analysis of ankle movement tracking training in subject with stroke. *Experimental Brain Research*, 154(3):281–290, Jan 2004.

[117] J D Schaechter, C Stokes, B D Connell, K Perdue, and G Bonmassar. Finger motion sensors for fMRI motor studies. *Neuroimage*, 31(4):1549–59, Jul 2006.

[118] R Gassert, D Chapuis, N Roach, A Wing, and H Bleuler. 2-dof fmri-compatible haptic interface for bimanual motor tasks with grip/load force measurement. *The Sense of Touch and its Rendering*, pages 109–129, 2008.

[119] J Z Liu, T H Dai, T H Elster, V Sahgal, R W Brown, and G H Yue. Simultaneous measurement of human joint force, surface electromyograms, and functional mri-measured brain activation. *J Neurosci Methods*, 101(1):49–57, Aug 2000.

[120] J Hidler, T Hodics, B Xu, B Dobkin, and L H Cohen. MR compatible force sensing system for real-time monitoring of wrist moments during fMRI testing. *J Neurosci Methods*, 155(2):300–7, Sep 2006.

[121] A Khanicheh, A Muto, C Triantafyllou, B Weinberg, L Astrakas, A Tzika, and C Mavroidis. fMRI-compatible rehabilitation hand device. *Journal of NeuroEngineering and Rehabilitation*, 3(1):24, 2006.

[122] J Diedrichsen, Y Hashambhoy, T Rane, and R Shadmer. Neural correlates of reach errors. *J Neurosci*, 25(43):9919–31, Oct 2005.

[123] N Yu, N Estévez, M C Hepp-Reymond, S S Kollias, and R Riener. fMRI assessment of upper extremity related brain activation with an MRI-compatible manipulandum. *International Journal of Computer Assisted Radiology and Surgery*, Aug 2010.

[124] A C Lo, P D Guarino, L G Richards, J K Haselkorn, G F Wittenberg, D G Federman, R J Ringer, T H Wagner, H I Krebs, B T Volpe, C T Bever, D M Bravata, P W Duncan, B H Corn, A D Maffucci, S E Nadeau, S S Conroy, J M Powell, G D Huang, and P Peduzzi. Robot-assisted therapy for long-term upper-limb impairment after stroke. *N Engl J Med*, 362(19):1772–83, May 2010.

[125] J Tohka, K Foerde, A R Aron, S M Tom, A W Toga, and R A Poldrack. Automatic independent component labeling for artifact removal in fMRI. *Neuroimage*, 39(3):1227–45, Feb 2008.

[126] S B Eickhoff, K E Stephan, H Mohlberg, C Grefkes, G R Fink, K Amunts, and K Zilles. A new SPM toolbox for combining probabilistic cytoarchitectonic maps and functional imaging data. *Neuroimage*, 25(4):1325–35, May 2005.

[127] J Diedrichsen, J H Balsters, J Flavell, E Cussans, and N Ramnani. A probabilistic MR atlas of the human cerebellum. *Neuroimage*, 46(1):39–46, May 2009.

[128] F Lacquaniti, D Perani, E Guigon, V Bettinardi, M Carrozzo, F Grassi, Y Rossetti, and F Fazio. Visuomotor transformations for reaching to memorized targets: A PET study. *Neuroimage*, 5(2):129–146, 1997.

[129] GR Fink, RSJ Frackowiak, U Pietrzyk, and RE Passingham. Multiple nonprimary motor areas in the human cortex. *Journal of neurophysiology*, 77(4):2164–2174, Jan 1997.

[130] R Gassert, L Dovat, O Lambercy, Y Ruffieux, D Chapuis, G Ganesh, E Burdet, and H Bleuler. A 2-DOF fMRI compatible haptic interface to investigate the neural control of arm movements. pages 3825–3831, May 2006.

[131] John F Schenck. The role of magnetic susceptibility in magnetic resonance imaging: MRI magnetic compatibility of the first and second kinds. *Medical Physics*, 23(6):815–850, 1996.

[132] Dan Stoianovici, Alexandru Patriciu, Doru Petrisor, Dumitru Mazilu, and Louis Kavoussi. A new type of motor: Pneumatic step motor. *IEEE/ASME TRANSACTIONS ON MECHATRONICS*, 12(1):98–107, Feb 2007.

[133] A Yamamoto, K Ichiyanagi, T Higuchi, H Imamizu, R Gassert, M Ingold, L Sache, and H Bleuler. Evaluation of mr-compatibility of electrostatic linear motor. *Robotics and Automation, 2005. ICRA 2005. Proceedings of the 2005 IEEE International Conference on*, pages 3658 – 3663, 2005.

[134] A Khanicheh, D Mintzopoulos, B Weinberg, A A Tzika, and C Mavroidis. MR_CHIROD v.2: Magnetic resonance compatible smart hand rehabilitation device for brain imaging. *IEEE Transactions on Neural Systems and Rehabilitation Engineering*, 16(1):91–98, 2008.

[135] A Hribar and M Munih. Development and testing of fMRI-compatible haptic interface. *Robotica*, 28(02):259–265, 2010.

[136] K Chinzei, N Hata, F Jolesz, and R Kikinis. MR compatible surgical assist robot: System integration and preliminary feasibility study. *Proc. Med. Image Comput. Comput.-Assisted Intervention*, pages 921–30, Jul 2000.

[137] N Takahashi, M Tada, J Ueda, Y Matsumoto, and T Ogasawara. An optical 6-axis force sensor for brain function analysis using fmri. *Sensors, 2003. Proceedings of IEEE*, 1:253 – 258 Vol.1, 2003.